Surface Functionalization of Metal Chalcogenide (MQ_2, M = Mo, W, Re, Ti, Zr; Q= S, O) Nanoparticles

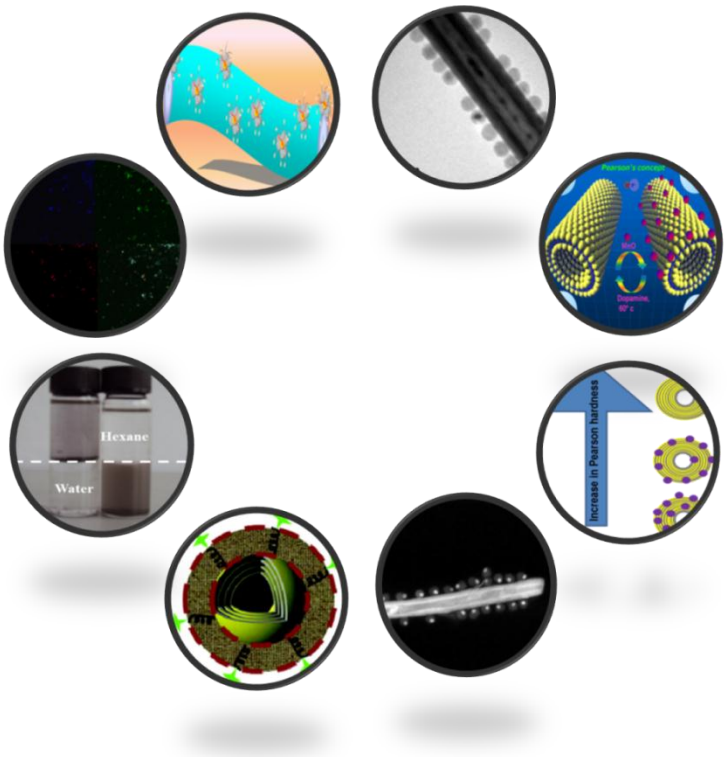

Dissertation zur Erlangung des Grades

"Doktor der Naturwissenschaften"

am Fachbereich Chemie, Pharmazie und Geowissenschaften
der Johannes-Gutenberg-Universität in Mainz
vorgelegt von

Jugal Kishore Sahoo, M.Sc.
geb. am 14th July 1983, Nua Bhuban, Orissa, India

Mainz 2011.

PUBLICATIONS

[1] "Reversible Self Assembly Of Metal Chalcogenide/Metal Oxide Nanostructures Based On Pearson Hardness", **Jugal Kishore Sahoo**,Muhammad Nawaz Tahir, Aswani Yella, Thomas D Schladt, Enrico Mugnaioli, Ute Kolb, W. Tremel. ***Angew. Chem. Int. Ed 2010, 49, 7578-7582***. ***Highlighted in Cover Page of the Journal.***

[2] "Soluble IF-ReS_2 Nanoparticles By Surface Functionalization With Terpyridine Ligands", **Jugal Kishore Sahoo**, Muhammad Nawaz Tahir, Aswani Yella, Robert Branscheid, Ute Kolb, W. Tremel, ***Langmuir, 2011, 27 (1), 385-391***.

[3] "Self-Assembly Of Metal Chalcogenide/Metal Oxide Nanostructures Based On degree of Pearson Hardness." **Jugal Kishore Sahoo**, Muhammad Nawaz Tahir, Aswani Yella, Thomas D Schladt, Steffen Pfeifer, Bahar Nakhjavan, Enrico Mugnaioli, Ute Kolb, Wolfgang Tremel. ***Chemistry Of Materials (accepted, 2011).***

[4] "Synthesis and functionalization of metal chalcogenide nanotubes. Muhammad Nawaz Tahir, Aswani Yella, **Jugal Kishore Sahoo**, Helen Anal Therese, Nicole Zink and Wolfgang Tremel. ***Phys. Status. Solidi. B, 247, No 10, 2338-2363 (2010).***

[5] "IF-ReS_2 With Covalently linked Porphyrin Antennae.'' Muhammad Nawaz Tahir, Aswani Yella, **Jugal Kishore Sahoo**, Filipe Natalio, Ute Kolb, Florian Jochum, Patrick Theato, Wolfgang Tremel. ***Isr. J. Chem. 2010, 50, 500-505***.

[6] "Hydrogen Peroxide Sensors Based on TiO_2 Nanorods Covalently Functionalized with Horseradish Peroxidase". Muhammad Nawaz Tahir, Rute Andre, **Jugal Kishore Sahoo,** Florian Jochum, Filipe Natalio, Patrick theato and Wolfgang Tremel. ***Nanoscale (accepted, 2011).***

[7] "Molecular Camouflage: Making use of Protection Group Chemistry to Control the Self-Assembly of Inorganic Janus Particles on Metal Chalcogenide Nanotubes by Pearson Hardness". **Jugal Kishore Sahoo**, Muhammad Nawaz Tahir, Faegheh Hoshyargar, Bahar Nakhjavan, Robert Branscheid, Ute Kolb, Wolfgang Tremel. ***Angewandte Chemie, (2011) Submitted.***

[8] "Metal Affinity based Biomolecular Recognition inside Synthetic Nanopores Modified with Iron-Terpyridine Complex". Mubarak Ali, Saima Nasir, Quoc Hung Nguyen, **Jugal Kishore Sahoo**, Muhammad Nawaz Tahir, Wolfgang Tremel, Christina Trautmann, and Wolfgang Ensinger. ***J. Am. Chem. Soc. (2011) Submitted.***

[9] "Synthesis of $Nb_xW_{1-x}S_2$ Graphene Sheets". Faegheh Hoshyargar, **Jugal Kishore Sahoo**, Muhammad Nawaz Tahir, Aswani Yella, Filipe Natalio, Martin Panthöfer, Robert Branscheid, Ute Kolb And Wolfgang Tremel. ***Manuscript under Preparation (2011).***

[10] "Rational Assembly and Selective Dual Functionalization of Au@MnO Nanoflowers onto TiO_2 Nanowires". **Jugal Kishore Sahoo**, Muhammad Nawaz Tahir, Mohammad Ibrahim Shukoor, Thomas D Schladt, Filipe Natalio, Enrico Mugnaioli, Ute Kolb and Wolfgang Tremel. ***Manuscript under preparation (2011).***

[11] "Biocompatible Amine Functionalized ZrO_2 Nanoparticles as Multi-Color Luminiscence Agents". **Jugal Kishore sahoo**, Filipe Natalio, Muhammad Nawaz Tahir, Anubha Kashyap, Dennis Strand, Wolfgang Tremel. ***Manuscript under preparation (2011).***

Conference Proceedings

[1] "New Synthetic Approaches to Functionalized Chalcogenide Nanostructures." Wolfgang Tremel, Aswani Yella, Martin Panthöfer, M. Nawaz Tahir, **Jugal Sahoo**, Enrico Mugnaioli, Ute Kolb. ***Proceedings of the twentieth (2010) international offshore and polar engineering conference. Beijing, China. June 20-25.***

[2] "From Single Molecule to nanoscopically Structured Materials: Rational reversible Self Assembly of Metal Chalcogenide/metal Oxide Nanostructures Based On Pearson Hardness". **Jugal Kishore Sahoo**, Muhammad Nawaz Tahir, Aswani Yella, Thomas D. Schladt, Enrico Mugnaioli, Wolfgang Tremel. ***Abstract of Papers, 240th ACS national Meeting, Boston, MA, United States, August 22-26, 2010. INOR-754***.

POSTERS

[1] "Surface Functionalization Of Metal Chalcogenide Nanostructures." **Jugal Kishore Sahoo**, Muhammad Nawaz Tahir, Aswani Yella and Wolfgang Tremel. **Minerva Symposium, Israel, 2008.**

[2] "From Single Molecule to Nanoscopically Structured Materials ; Rational Reversible Self-Assembly of Metal Chalcogenide/Metal Oxide Nanostructures Based on Pearson Hardness." **Jugal Kishore Sahoo**, Muhammad Nawaz Tahir, Aswani Yella, Thomas D Schladt, Enrico Mugnaioli, Wolfgang Tremel. **240th ACS National Meetings, 2010, August 22-26, Boston, MA.**

[3] **"**Overcoming the Wetting Mismatch of Surfaces: Hierarchical Assembly of Metal Oxides@Metal Chalcogenides Nanotubes Achieved Through Surface Functionalization" Muhammad Nawaz Tahir, **Jugal Kishore Sahoo**, Aswani Yella, Wolfgang Tremel. **EuCheMs 2010 Nürenberg, Germany**.

[4] "Synthesis Of $Nb_xW_{1-x}S_2$ Graphene like Sheets.' Faegheh Hoshyargar, **Jugal Kishore Sahoo**, Muhammad Nawaz Tahir, Aswani Yella, Martin Panthöfer, Robert Branscheid, Wolfgang Tremel. **IWEPNM 2011, Austria.**

ORAL PRESENTATIONS

[1]"Surface Functionalization Of Metal Chalcogenide Nanostructures." **Jugal Kishore Sahoo**, Muhammad Nawaz Tahir, Aswani Yella and Wolfgang Tremel. Minerva Symposium, Israel, 2008.

Abstract

The work, presented in the doctoral thesis, is a compilation of different methods of functionalization of layered transition metal dichalcogenide (LTMC) nanostructures. The layered metal chalcogenide NT-MQ_2 (MQ_2; M= Mo, W, Re, Nb, Q= S, Se), NT-MQ_2 and IF-MQ_2 are the pure inorganic congeners of carbon nanotubes and fullerenes, that exhibit analogous mechanical and electrical properties. They consist of metal atoms sandwiched between two inert chalcogen layers. The MQ_2 layers are stacked with only vanderwaal's force of interaction in between the layers whereas within the layers, the metal and the chalcogen atoms are bonded to each other with covalent interaction. The steric shielding of the metal atom by the chalcogen surface layer makes it difficult for nucleophilic attack by oxygen or organic ligand, hence making it highly inert and notoriously difficult to functionalize.

One method of tailoring the surface of these highly inert nanostructures could be by exploring its intrinsic structures. Sulfur, which is present outside each MQ_2 layer, is intrinsically soft. Hence the soft sulfur layer will have the tendency to bind to other nanoparticles (metal oxide, metal) that have soft acid cations, according to Pearson HSAB principle, which states 'hard acid prefers to bind to hard base where as soft acid prefers to bind soft base'. The method has been employed to achieve functionalization of LTMCs with a number of metal and metal oxide nanostructures (e.g. Au, MnO, Fe_3O_4, Pt-Fe_3O_4), that have soft or boarderline metal cations. The functionalization has been found to be reversible at elevated temperature in presence of catecholate ligand. This emphasizes the fact that, the recycled metal chalcogenide nanostructures can be used again for functionalization. However at room temperature, the metal oxides can further be tailored for suitable applications. The degree of functionalization depends on the Pearson hardness of the metal cation. Harder the metal cation, lower is the degree of binding, softer the metal cation, higher is degree of binding, e.g. TiO_2 and Fe_2O_3 doesn't bind at all to the metal chalcogenide surface because of its high pearson hardness. Similarly it has also been observed that the binding of soft metal (Au) is irreversible, whereas that of borderline metal cations (Mn^{+2}, Zn^{+2}) are reversible.

Similar principle has been employed to adhere Janus nanostructures onto the LTMCs. Both face of Janus nanoparticle (Pt, Fe_3O_4) being prone to bind the LTMCs. It has been observed that, it's possible to bind selectively one face of the Janus nanostructure, by camouflaging the other face and vice versa.

Another method of functionalization of LTMCs could be by employing chalcophilic transition metal in combination with a multidentate surface ligand. The 3d metals "wet" the sulfur surface of the chalcogenide nanoparticles whirlst the multidentate surface ligands partially block one hemisphere of the metal thereby preventing an aggregation of the chalcogenide nanoparticles through crosslinking. We have used iron as the transition metal and terpyridine as the tridentate surface ligand. Where iron binds to the surface of LTMCs at one end, the other coordination vacancies of the iron is fulfilled by tridentate terpyridine ligand. Through this coordinate covalent functionalization, the solubility of LTMCs in different solvents (hydrophilic and hydrophobic) can be enhanced by incorporating PEG (poly ethylene glycol) and hydrophobic long alkane chain onto terpyridine respectively.

In addition, we have used facile chemical route to achieve the functionalization of TiO_2 nanowire with Au@MnO magnetic nanoflowers and been able to bring three different unique surfaces to a common platform. The modification strategy is based on the chelating affinity of dopamine to metal oxide nanoparticles, as well as the affinity of amine to bind to gold domain of nanoflowers. The surface bound nanoflowers are still amenable to functionalization with anchor groups such as thiol that readily binds gold surface. The different surfaces can be addressed by selectively conjugating a thiol tagged SS-DNA to gold domain whereas NBD dye can be conjugated to TiO_2 surface by free amine present in the polymeric ligand.

To compile it all, we described an easy, versatile synthetic method to prepare water soluble photoluminescent ZrO_2 nanoparticles. The nanoparticles retain their morphology and monodispersity after functionalization. The functionalized ZrO_2 nanoparticles showed multi-color luminiscnece in 1-photon microscopy. The facile synthesis, the long-term aqueous stability, and the extreme robustness of the photophysical properties make the zirconia nanoparticle, an excellent candidate for biomedical applications, both for *in vivo* and *in vitro* studies.

1. Introduction.

1.1. Nanotechnology

Richard Feynman's speech with title 'There is plenty of room at the bottom' in 1959 emphasised this concept - if our small minds, for some convenience, divide this universe into parts, physics, biology, geology, astronomy, psychology and so on – remember that Nature does not know it [1-2]. Nanotechnology, one of 21st century's most promising technologies, is viewed as a critical driver of future technologies, and to address some of humanity's most vexing challenges e.g. energy, environment and health. The science of nanoscale structures deals with creation, investigation, manipulation and utilization of system those are 1000 times smaller than the components currently used in microelectronics. A nanometer is a billionth of a meter, that is, about 1/80,000 of the diameter of a human hair [Figure 1.1], or ten times the diameter of a hydrogen atom. It manipulates the chemical and physical properties of a substance on molecular level. Nanotechnology alters the way we think, it blurs the boundaries between physics, chemistry and biology, thus making it completely interdisciplinary in nature.

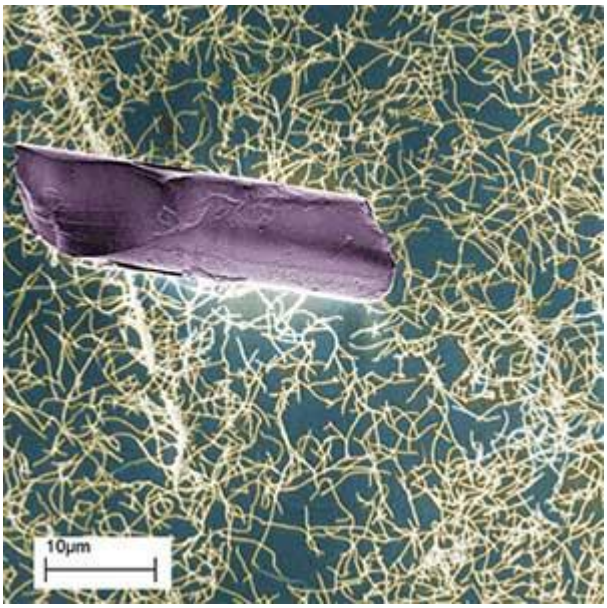

Figure 1.1. *Human hair fragment and a network of single-walled carbon nanotubes (courtesy. Nanowerk).*

Nanotechnology expresses itself in a wide range of materials, such as nanoparticles, nanotubes, nanowires, fullerenes, quantum dots, nanorods, micelles, liposomes, etc and finds

applications in different fields [3]. Almost all of these materials have a modified or designed surfaces to hook onto different ligands or biomolecules that can add additional functionality to the nanostructure for applications in different arena such as biosensing [4-6], drug delivery [7-8], imaging [9], tomography [10], cancer nanotechnology [11] etc. Hence surface tailoring imparts multifunctionality to nanostructures to enhance its applications in different scientific horizon.

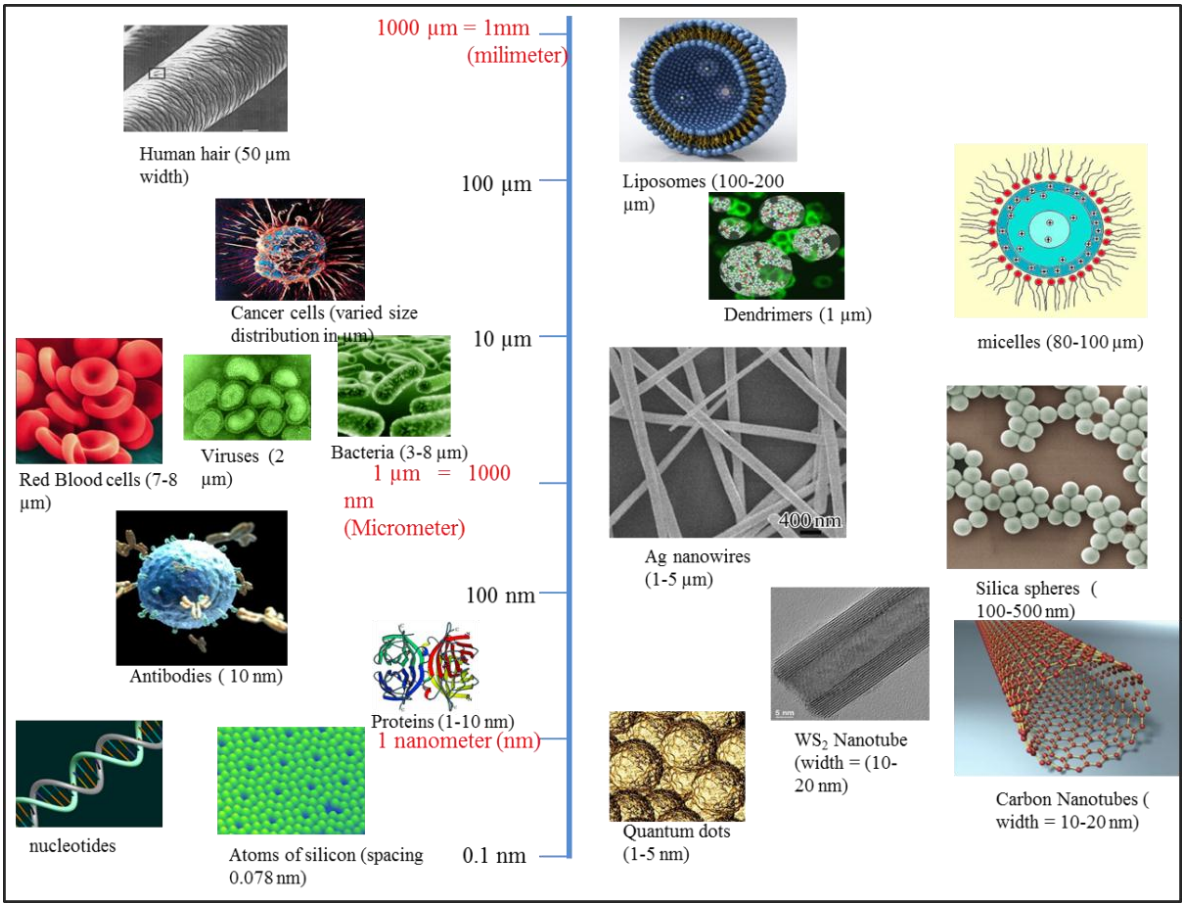

Figure 1.2. *Size comparison between naturally occurring biomolecules in humans with artificial man-made structures in micro and nano scale.*

One unique type of nanostructure is layered metal chalcogenide nanostructures. The present doctoral thesis is a compilation of novel surface functionalization of this layered metal dichalcogenide (LTMC) nanostructures. In the following sequel, a brief illustration of LTMC will be provided which includes its history, different morphologies, their intrinsic properties and application in various fields of sciences.

1.2. Layered Metal Dichalcogenide Nanostructures (LTMC)

1.2.1. Preliminaries.

The discovery of fullerenes in 1985 by Kroto, smalley and Curl [12] and carbon nanotubes in 1991 [13] establishes a new paradigm in nanochemistry and led to the birth of a new field in inorganic chemistry i.e. nanoparticles with polyhedral (closed hollow) structures.

However, this discovery also triggered scientist across the globe to investigate the virtue of formation of fullerenes and nanotubes are not only limited to carbon. In 1992, R. Tenne from Weizmann institute of Science discovered that the formation of such polyhedral structure is not limited to only carbon system, but can also be possible for other systems as well. In a letter to *Nature*, he reported an equivalent stable structure in layered semiconductor tungsten disulfide [14].

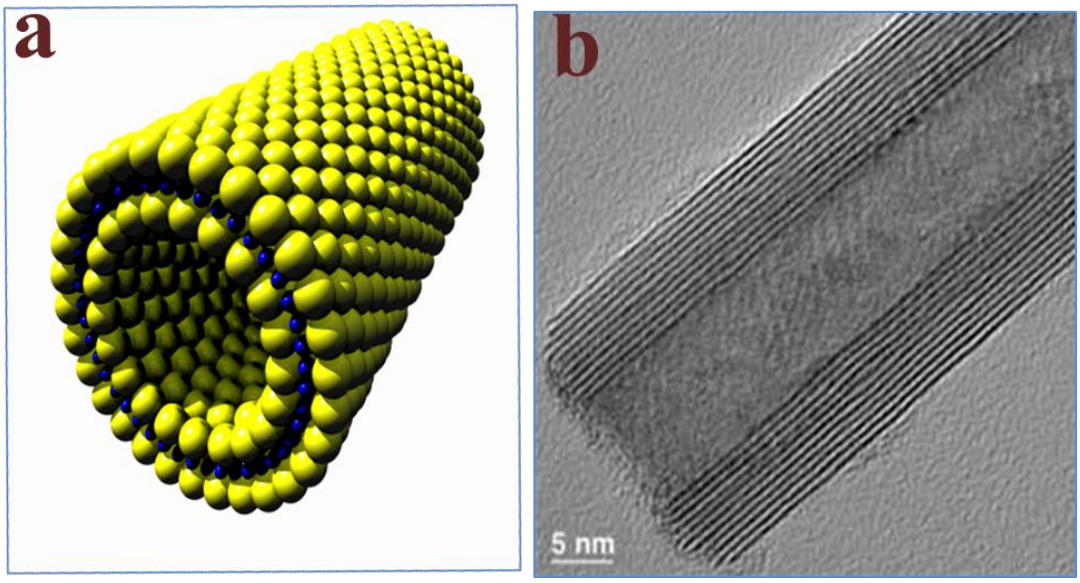

Figure 1.3. *Representation of a tentative WS_2 Nanotube. (a) Schematic drawing of a single walled WS_2 nanotube, where Blue and yellow atom denotes tungsten and sulfur atom respectively. (b) A TEM image of a portion of a multiwalled WS_2 nanotube.*

The discovery of analogous MoS_2 was soon followed [15, 16]. Since the observation of single nanotube, significant progress has been made and today, gram quantity of some metal chalcogenides is obtained in pure form. During the past few years, various strategies have

been developed to synthesize nanostructured metal sulfides and selenides and have witnessed enormous growth [17-24] in recent years. Different approaches to other nanotubes such as $NiCl_2$ [25], VS_2 [26], TiS_2 [27], InS [28] have also been reported which implies that layered chalcogenide nanomaterials can form fullerenes or nanotubes under suitable conditions. A variety of methods including arc discharge [29,30], sulfurization/ selenization of metal oxides [31–41], chlorides [42, 43], carbonyls [44], decomposition of ammonium thiometalates [45–47], chemical vapor transport [48, 49], laser ablation [50–53], microwave plasma [54, 55], atmospheric pressure chemical vapor deposition (APCVD) [56], or spray pyrolysis [57] were utilized for the synthesis of inorganic fullerene-(IF) or nanotube-like (NT) structures.

1.2.2. Structure of LTMCs.

In this section, focus will be given to the class of nanomaterials, which are prone to form fullerenes and nanotubes i.e. layered transition metal chalcogenides**,** as a major part of this particular doctoral work deals with the surface functionalization of such nanostructures. Several layered transition metal chalcogenides (sulphides, selenides and tellurides) possess structures comparable with the structure of graphite. The metal dichalcogenides MQ_2 (M = Mo, W, Re, Nb; Q = S, Se) contains a metal layer sandwiched between two chalcogen layer, with the metal in a trigonal pyramidal or octahedral coordination. The MQ_2 layers are stacked along the c-direction in an ABAB fashion, making them analogous to the single graphene sheets in the graphite structure (Figure 1.4). However, unlike that of graphite, each molecular sheet consists of multiple layers of different atoms chemically bonded together.

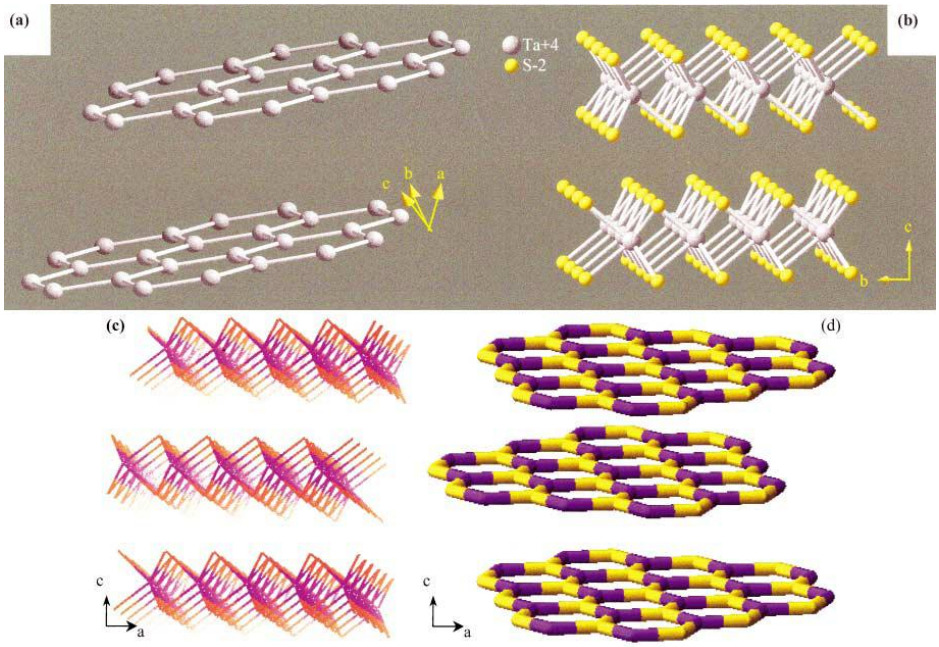

Figure 1.4. *Comparison of the structures of (a) Graphite and layered metal dichalcogenide compound (b) NbS_2/TaS_2, (c) MoS_2, (d) BN. (ref. 17).*

However at the edges, MoS_2 sheets contain unsaturated Mo and S atoms. These atoms have so called 'dangling bonds' which are energetically unfavorable. The presence of dangling bonds can be attributed to the absence of a M or Q atom at the edges. While the metal atom in the bulk of MQ_2 layer is six fold coordinated to the chalcogen atoms, it is only fourfold coordinated at the edges. Similarly the chalcogen atom at the rim is twofold coordinated to the metal atoms instead of being threefold coordinated in the bulk. In bulk, the energy gain by interlayer interaction compensates the energy loss by dangling bonds. When size of the molecular sheet shrinks, the relative number of rim atoms with dangling bond increases, compared to that of fully bonded bulk atoms. The ratio of surface to volume increases upon size reduction, subsequently the effect of dangling bonds exceeds that of interlayer interaction in bulk. Therefore the dichalcogenide layers become unstable towards bending and have high tendency to roll into curved structures, in order to minimize the number of dangling bonds. The curvature, thus generated form hollow closed structures designated as inorganic fullerene-like (IF) structures.

1.2.3. Applications of LTMCs.

Layered transition metal dichalcogenides possess a wide range of interesting physical properties**.** They are widely used in catalysis and in tribology.

1.2.3.1 Tribological Applications.

MQ_2 nanotubes and fullerenes find excellent lubrications properties due to low surface energy, high chemical stability, nanometric size and weak interlayer bonding. The tribological efficacy of these nanomaterials has been investigated, and it was shown that only small amounts of these materials in lubrications oil enhance the lubricating properties significantly. Earlier it was assumed that the spherical IF-MQ_2 nanoparticles would behave like nanoball bearings thereby providing superior solid lubrication to the existing technology [58-59]. The mechanistic studies showed [58] that the lubricating properties of the IF nanoparticles are attributed to a gradual exfoliation of the external sheets of the particles during friction process leading to their transfer onto the asperities of the reciprocating surfaces and a shearing of the basal planes. The beneficial effect of the IF nanoparticle powder as an additive to lubricating fluid has been studies in quite some detail. These phenomena are summarized in refs [59-60]. More recently, IF-WS_2 nanoparticles were integrated into metal and polymer films, endowing them with a self-lubricating [61-63] character and offering a very large number of applications. Rolling and sliding friction of this nanoparticle is not possible in this case unless they are gradually released from metal/polymer/ceramic matrix onto the surface. However, some of the beneficial effect of IF nanoparticles can be attributed to the gradual exfoliation and the transfer of WS_2 nano sheets onto the asperities of the mating metal surfaces. Furthermore, the bare metal surface is shown to oxidize during the test, leading to a gradual increase in the friction coefficient to a very high value (0.3-0.6). In contrast, the metal surface impregnated with IF nanoparticles suffers less or no oxidation during tribological test, although the coverage of the metal surface by the nanoparticles doesn't exceed 20-30 %. This observation indicates that the temperature of the IF-WS_2 impregnated interface is lower than that of the pure metal surface during the tribological test. Recent investigations have demonstrated that a transfer film is incorporated into the iron oxide surface layer. A tribo chemical reaction between the 2H-MoS_2 nanolayers and the iron/iron oxide was proposed as an explanation for the adhesion of this tribofilm. This technology offers numerous applications, among them various medical devices, like improved orthodontic practice. In a related study by Dassenoy et al., $Mo_6S_3I_6$ nanowires were also proclaimed as an excellent

solid state lubricant [64a]. It is suggested that iodine loss during the test leads to a decomposition of the nanowires and an in situ formation of lubricating MoS_2 nanosheets.

A new type of composite metal-nanoparticle coating that significantly reduces the friction force of various surfaces, particularly archwires in orthodontic applications, was demonstrated by Tenne et al. [64b, c]. The coating is based on electrodeposited Ni film impregnated with inorganic fullerene like nanospheres of WS_2 [64d]. The test has shown reduction of up to 60 % of the friction force between coated rectangular archwires and also maintains this low value of friction for the duration of the test. Due to these excellent lubrication properties, layered metal chalcogenide also find place in nanobiotechnology i. e. for the coating of stents and artificial joints.

These applications make metal chalcogenide nanoparticles interesting targets for bio functionalization or drug delivery through controlled release of small molecules or proteins. A first medical application, the decrease of friction in orthodontic wires and braces was recently demonstrated [64b, c]. Furthermore the applications of MoS_2 based anti-friction medical coating e.g. for guide wires in catheters for use in invasive treatment such as cardiac catheterization and coating for artificial joints and hips have been advertised.

1.2.3.2 Catalysis.

Layered metal chalcogenides are known to be very potent catalysts for hydrodesulfurization [65]. These nanoparticles were used for the first time, in catalysis for the hydrodesulfurisation of thiopene. In the first report, $Mo(CO)_6$ was reacted with sulfur in an aprotic solvent using an ultrasonic probe and silica nanoparticles, which served as a template, and was removed by HF etching to result hollow nanoparticles of MoS_2 [66a]. Although these nanoparticles were not well crystalline but revealed high reactivity and selectivity towards the hydrodesulfurization of thiopene.

In another study, Ni nanoparticles were deposited onto a MoS_2 nanotube support. This nanocomposite was found to serve as a very potent and selective catalyst for hydrodesulfurisation of thiopene and a few of its derivatives. These few examples demonstrate the remarkable potential of inorganic nanotubes and fullerene-like nanoparticles in eliminating the environmental impact of sulfur-rich gasoline and in green chemistry [66b, c].

1.2.3.3. High Strength Nanocomposite.

The mechanical robustness of the NT-WS_2 and MoS_2 and the other IF nanoparticles were studied recently documented [67-68]. Furthermore, Raman measurements of these nanoparticles indicate no degradation under hydrostatic pressures of 20GPa, which confirmed their high pressure resilience [69]. IF-WS_2 and MoS_2 nanoparticles were shown to withstand shockwaves of up to 25 and 30GPa, respectively, with temperature of 1000 °C [70]. Significantly, the structural integrity of the nanoparticles was also confirmed by TEM, making these materials probably the strongest cage molecules known today and offering them a plethora of applications for the shielding of vehicles and in the future as an additive to strengthen construction materials. This work propelled interest in fabricating nanocomposites with enhanced mechanical properties based on the IF and NT-MoS_2, etc. Tenne et al. [71] also studied the effect of nanoparticles on the toughening and mechanical properties of low and high temperature curing epoxy systems using IF-WS_2 nanoparticles and Functionalized nano-POSS (Polyhedral-Oligomeric-Sil-Sesquioxane). The results indicated that IF-WS_2 increased the fracture toughness by more than 10 fold in both epoxy systems at very low concentrations (0.3-0.5 wt. %) while increasing its storage modulus and preserving its glass transition temperature. Epoxy functionalized POSS demonstrated an increase in toughness in addition to preserving rigidity and thermal properties at higher concentrations (3 wt. %). They have concluded that chemical interaction between sulfide and the epoxy matrix and the inherent properties of WS_2 were the decisive factor for the outstanding nano-effect in the case of IF-WS_2.

1.3. Surface Functionalization of Nanomaterials.

Surface functionalization or surface engineering is a sub discipline of materials science which deals with the surface of solid matter. It introduces different chemical functionality onto the surface of nanomaterials in order to make it robust and versatile and applicable in different fields. Properties and performance of nanomaterials depend strongly on their surface characteristics. The application of nanomaterials in different fields and technology is limited owing to their restricted behavior in different protic and aprotic solvents. Molecular tailoring on the surface of the nanomaterials helps them to tune their properties, charge, functionality and reactivity which play a pivotal role in exploring, augmenting and developing integrated

system for demanding applications in different fields of nanoscience and technology [72]. The surface properties of nanoparticles determine the interactions between the components, as well as the solubility and agglomeration behavior in different polar and non-polar solvents and thus decide whether individual nanoparticles are stable as nano-building blocks for the design of nanocomposites or for self organizing devices. Surface engineering techniques are being used in automotive, aerospace, power, electronic, biomedical, chemical industries. Furthermore surface tailoring can be used as a tool for enhancing and developing a wide range of functional properties including physical, chemical, electronic, magnetic, and mechanical properties at the required substrate surfaces.

A model functionalized nanoparticles can be designed as shown in Fig 1.5. which contains

(a) Nanoparticles form the core of the design, that can either be solid (e.g. quantum dots, metal, metal oxide, layered metal chalcogenide nanoparticles) or liquid (liposomes, micelles, dendrimers) depending on desired applications.

(b) An anchor group (Ni^{+2}, Fe^{+2} in case of layered metal chalcogenide nanomaterials, dopamine (metal oxides such as TiO_2, Fe_2O_3, Fe_3O_4, etc), thiol (SH) (coinage nanoparticles e.g. Au, Ag and quantum dots, e.g. CdS, CdSe etc).

(c) A spacer group which can be PEG sub units to improve solubility in hydrophilic solvents or a long alkane chain to improve solubility in different hydrophobic solvents.

(d) A flourophore (NBD, pyrene, Texas red) which can act as an optical tracer.

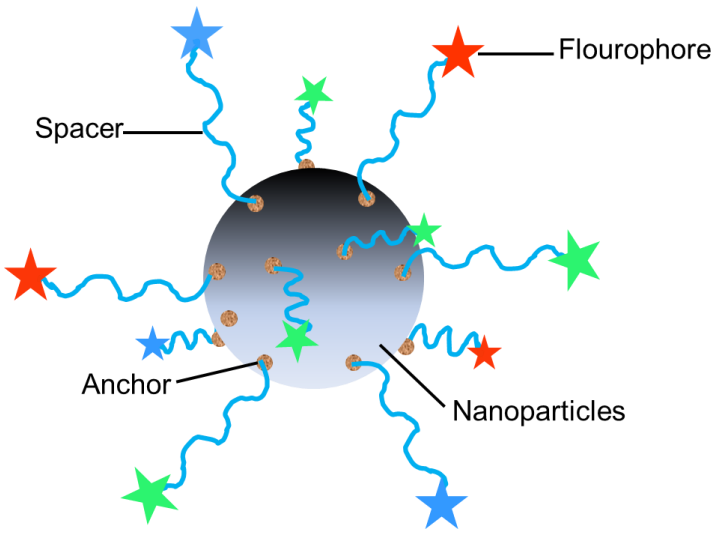

Figure 1.5. *A model scheme of surface functionalization.*

There are different approaches of tailoring the surface of inorganic nanomaterials to make organic-inorganic hybrid nanocomposites. The simplest approach is to entrap an inorganic nanoparticle into organic host and vice versa. To connect the inorganic nanomaterials with the organic moiety in hybrid nanocomposites by strong covalent or ionic interactions, reactive organic groups or polymers having suitable functionality have to be attached to the surface of inorganic nanomaterials. There are two major strategies of synthesizing organic inorganic nanocomposites.

(a) **Post-Synthesis Functionalization**; in this method, the organic groups grafted to the inorganic nanoparticles after its synthesis.

(b) **In-situ Functionalization**; in this method, the organic groups or ligands are introduced during the synthesis of nanoparticles.

Post synthesis functionalization has the advantage of changing the interfacial properties of the surface, without affecting the bulk properties, whereas in in-situ functionalization, the organic ligand controls the size, crystalinity and growth of nanomaterials. Surface functionalization is used as a tool for application of nanomaterials in various disciplines of nanoscience and nanotechnology e.g. nanobiotechnology, drug delivery and tissue engineering [73-75], nanolithography [76-79], catalysis [80], sensors [81], nanophotonics [82] etc. (Figure 1.6)

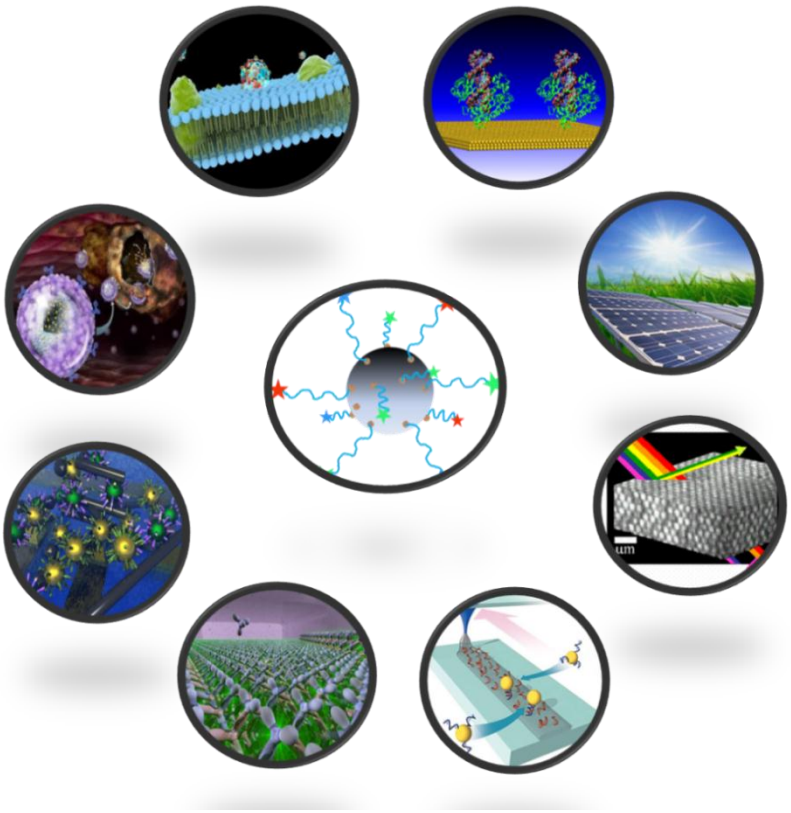

Figure 1.6. *Use of functionalized nanostructures in different fields of nanoscience and technology.*

1.4. Surface Functionalization of Layered Metal Dichalcogenide Nanostructures.

As described before, LTMC nanostructures are the inorganic congeners of carbon nanotubes and fullerenes that exhibit analogous mechanical [83-85] and electronic properties [86-87]. They consist of metal layer sandwiched between two inert chalcogenide layers where the metal atom is in trigonal pyramidal or octahedral geometry. The MQ_2 layers are stacked with each other through weak van der waals force of attraction, however within the layer the metal and chalcogen atoms are bonded in covalent fashion. The inertness of the chalcogen layer, that shield metal atom, prohibit further nucleophilic substitution by organic ligand, which makes surface functionalization of LTMC nanostructures a notorious task. This section will provide the research done in surface functionalization of LTMC nanostructures so far.

In 2006, Tremel et al., reported a facile method for the functionalization of LTMC nanostructures that employed nitrilotriacetic acid (NTA) as a robust anchor group to chelate to the outer sulfur layer of LTMC nanostructures [88-91]. Since a direct anchoring of organic ligand onto the sulfur layer is not possible because of its inertness, a chalcophilic transition metal cation (Ni^{+2}) with octahedral coordination is used, whose coordination sphere is completely blocked on one side in umbrella type fashion, and the other half of the coordination sphere is available for docking to the outer sulfur layer of LTMC (Figure 1.7).

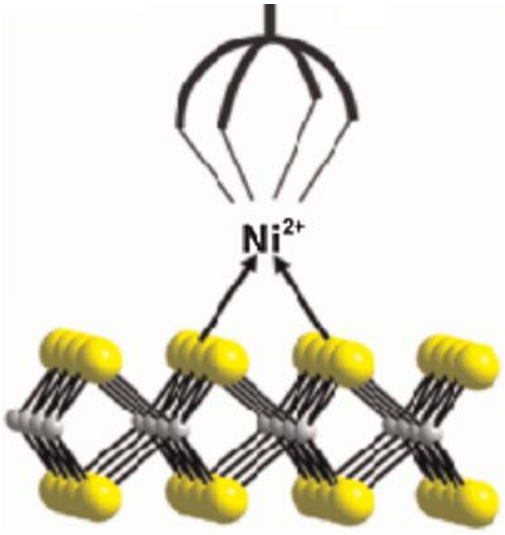

Figure 1.7*. Surface functionalization of LTMC nanostructures where half of the Ni^{+2} coordination is used for docking to sulfur layer because of its chalcophilicity.*

As Nickel wet the outer sulfur layer on one side, the other half of coordination sphere is utilized for binding to robust anchor groups that binds strongly to nickel e.g. NTA [92]. A multifunctional polymeric ligand was devised with different functional moieties in order to achieve the following goals;

1) Improve the solubility of LTMC nanostructures in different polar and nonpolar solvents.
2) To build up novel strategies to attach ligands on its surface which could help in constructing hierarchical assembly of different nanoparticles and synthesize unique nanocomposite.
3) This fabrication strategy also paves the way for self-assembly of metal oxide nanostructures onto the sidewall of metal chalcogenide nanotubes though bio

4) recognition. To achieve all the outstanding goals, a novel polymeric ligand (Figure 1.8) was synthesized which consists of different functional groups e.g.

1) NTA, as anchor group, binds to the outer sulfur layer of LTMC nanoparticles through Ni^{+2}-NTA coordination.
2) 3,4-dihydroxy tyramine hydrochloride (dopamine) as an additional functional group, which can be used for further functionalization of metal oxide nanostructures like TiO_2, ZrO_2, Fe_3O_4, Fe_2O_3 etc. However this functional group can be alkyl chain with thiol as head group which can be used to adhere metal nanoparticles like Au, Ag, and Pt etc.
3) A flourophore e.g. 4-chloro, 7-nitro Benzofurazan (NBD), Texas red or Pyrene, etc that can be used to trace nanoparticles in optical microscopy.

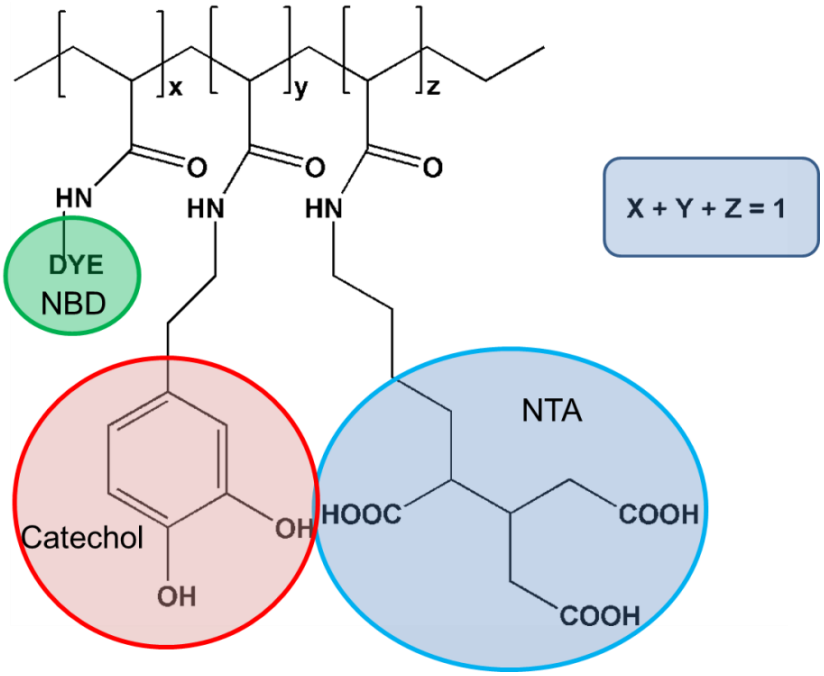

Figure 1.8. *Multifunctional polymeric ligand used for functionalization of LTMC nanostructures.*

1.4.1. Overcoming the insolubility of IF-MoS_2 nanoparticle through a high degree of sidewall functionalization using polymeric chelating ligand.

In 2006, Tahir et al [88], reported a facile method for the surface engineering of IF-MoS_2 nanoparticles that introduces NTA as the robust anchor to immobilize functional molecule on the outer sulfur layer of LTMC. They have reported the similar functionalization strategy that employs a multifunctional polymeric ligand as illustrated in Fig. 1.9. The polymer contains different features i.e. tetra dentate NTA ligand that can be used for binding to Ni^{+2} and the rest two coordination of Ni^{+2} can be exploited to bind to the sulfur layer of IF-MoS_2. The resulting functionalized IF-MoS_2 nanoparticles can be dispersed in water and organic solvents. As we know, LTMC nanostructures are completely insoluble in water because of their hydrophobicity, however they are readily dispersible in organic solvents like chloroform. It has been observed that after functionalization of IF-MoS_2 using polymeric chelating ligand, these nanoparticles could be transferred from apolar chloroform to polar aqueous phase which can be attributed to introduction of polar group (hydroxyl, carbonyl) from polymer on the IF-MoS_2 surface. (Figure 1.9).

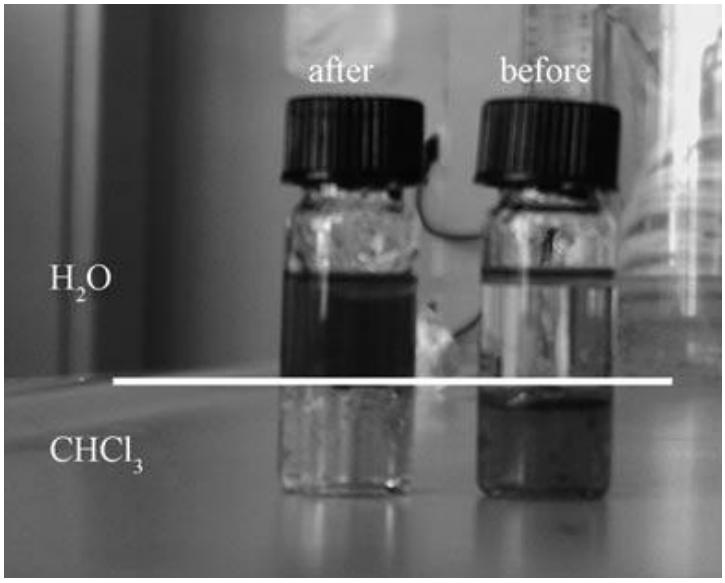

Figure 1.9. *Digital photograph of a solution/dispersion of inorganic fullerene/MoS_2 before (right) and after (left) surface functionalization. Courtesy [88].*

The functionalization was further confirmed by decorating TiO_2 nanorods with IF-MoS_2. The polymeric ligand was modified with catechol groups and NTA functional groups in different ratio. In the first reaction step, the polymeric ligand was immobilized onto IF-MoS_2 and the free catechol groups present in polymer was used for further functionalization with TiO_2 nanorods as catechol group readily binds to metal oxides.

However, it was still unclear whether the Ni^{+2}/NTA units were bound to the close packed sulfur surface layer of IF-MoS_2 or to the surface defects.

1.4.2. Hierarchical assembly of TiO_2 nanoparticles on WS_2 nanotubes achieved through multifunctional polymeric ligands.

In 2007, Tahir et al reported a chemically specific and facile method for the functionalization of NT-WS_2 and subsequent coating of the functionalized WS_2 nanotubes with monocrystalline anatase TiO_2 nanoparticles using the multifunctional polymeric ligand [89]. Similar functionalization strategy has been employed to tailor the surface of NT-WS_2 by exploiting Ni^{+2}/NTA coordination chemistry. As tetra dentate ligand NTA coordinate to the octahedral Ni^{+2}, the rest two vacant coordination sites were used to dock to the outer sulfur layer of NT-WS_2. As the polymeric ligand contains catechol group as an additional functionality, TiO_2 nanoparticles can adhere to the NT-WS_2 surface to form WS2-TiO_2 nanocomposite (Figure 1.10).

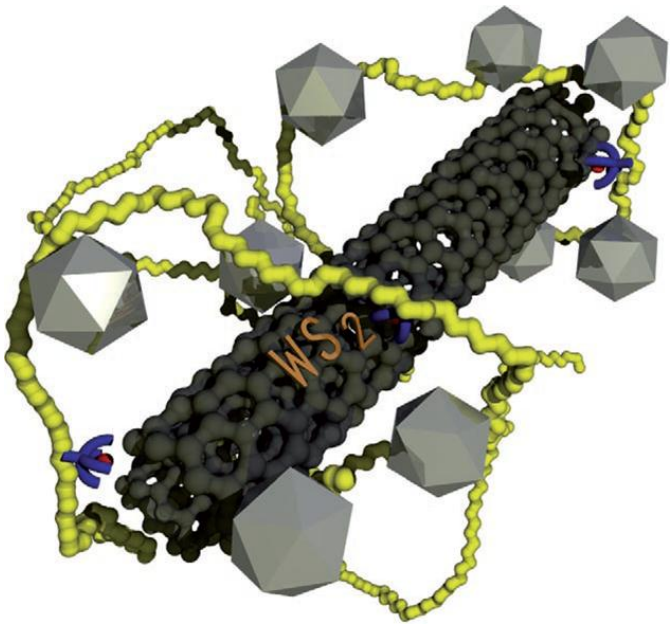

Figure 1.10. *Schematic representation of the NT-WS_2/polymer/TiO_2 nanocomposite. NT-WS_2 (dark grey) is functionalized with the multifunctional polymer (yellow thread) followed by immobilization of TiO_2 nanoparticles.*

Similar functionalization strategy can be generalized for synthesis of LTMC/metal oxide nanocomposites that can be utilized for further applications.

1.4.3. Enzymatic mediated deposition of a TiO_2 coating onto bio functionalized WS_2 chalcogenide nanotubes.

Another chemically specific method for the bio-functionalization of NT-WS_2 was reported by Tahir et al. [90]. The covalent modification strategy is based on the chelating properties of Ni^{+2} that bind to the outer sulfur layer of NT-WS_2 whereas the other coordination sphere binds to tetra dentate ligand (NTA) attached on the backbone of polymeric ligand. NTA also simultaneously acts as an anchor group for the binding of His-tagged proteins to NT-WS_2 through the polymer backbone as demonstrated in Figure 1.11.

Figure 1.11. *Schematic representation of the fabrication of biotitania/NT-WS_2 nanocomposite.*

The formation of biotitania coating is mediated by immobilizing silicatein onto NT-WS_2 surface. The surface bound protein, silicatein, is a biocatalyst used for fabrication of a silica skeleton in marine sponges [93-94]. Silicatein because of its hydrolytic and polycondensating activity is indeed found to be responsible for the formation of outer biotitania layer on NT-WS_2.

1.4.4. IF-ReS_2 with covalently linked porphyrin antennae.

Similar functionalization strategy was employed to bind protoporphyrin onto IF-ReS_2 [91]. This has been achieved by modifying the previously used polymeric ligand. Instead of dopamine functionality, an amine terminated hydrophobic chain is introduced. The amine

functional group was utilized for conjugation of porphyrin, which in turn complexes the Zn^{+2} cation (Figure 1.12).

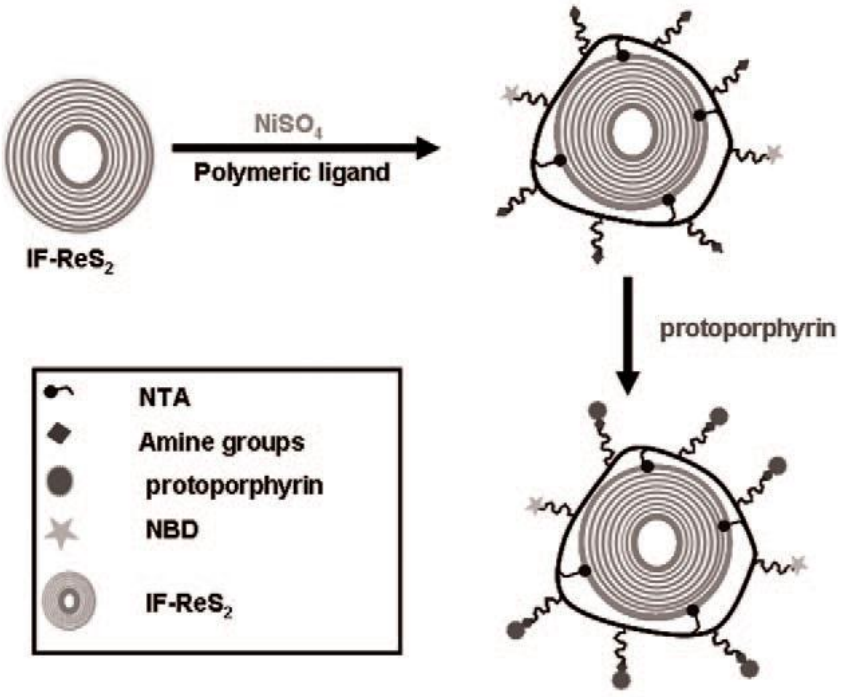

Figure 1.12. *Surface functionalization of IF-ReS_2 and conjugation of protoporphyrins*.

1.4.5. Synthesis of hierarchically grown ZnO@NT-WS_2 nanocomposite.

In 2009, Tahir et al., reported an alternative strategy [95] of surface functionalization of LTMC nanostructures is to grow nanoparticles directly onto the nanotubes by using colloidal nanoparticles [96-98]. This functionalization was achieved without the addition of any organic ligands, polymers or any linkers. The bound nanoparticles thus may have affinity towards the LTMC nanoparticles, depending on their acid base properties, functional group, or Pearson hardness [99-100]. In this communication, ZnO was attached to the sidewalls of NT-WS_2 followed by the growth of ZnO nanorod onto NT-WS_2. (Figure 1.13).

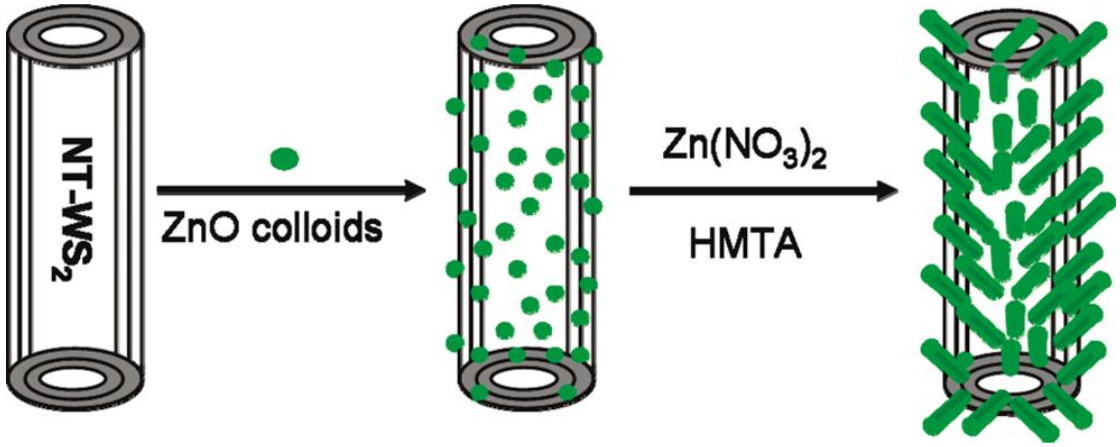

Figure 1.13*. Schematic representation of the fabrication of the ZnO@NT-WS_2 nanocomposite.*

1.4.6. Surface functionalization of IF-WS_2 by alkyl-silane group and subsequent improvement of dispersion of IF-WS_2.

In 2010, Tenne et al., reported surface functionalization of IF-WS_2 nanoparticles with alkyl-silane moieties [101]. It was observed that after functionalization with organosilane (octadecyl trichlorosilane, dodecyl trichlorosilane, hexyltrichlorosilane), there is remarkable improvement of dispersion of IF-WS_2 in oil based suspensions which reduced the agglomeration. They have found out that the stability of IF-WS_2-oil suspension was increased remarkably after surface tailoring of silane group. These results were rationalized by assuming that the silane groups preferentially stick to the defects of IF-WS_2. As in LTMC nanostructures, the coordination between the tungsten and sulfur atoms is not fully satisfied at the edges. Water molecules adsorb [102] to these sites making the IF-WS_2 hydrophilic. These water molecules were further replaced by alkyl silane group making the surface more hydrophobic. This increased hydrophobicity is believed to reduce the surface tension between oil and IF-WS_2, thereby the tendency to agglomerate is reduced. These new coatings of IF-WS_2 improve the stability of the IF-WS_2 solid lubricant oil suspensions, which improves the long term tribological behavior of these nanoparticles.

1.4.7. Gold nanoparticles as surface defect probes for WS_2 nanostructures.

Tenne et al., in 2010, decorated gold nanoparticles onto IF and NT-WS_2 [103]. Here they have demonstrated that the gold nanoparticles served as reactive site probes, mapped by both

scanning and transmission electron microscopy. It has been found out that, gold nanoparticles preferentially adsorb to IF-WS_2 at edges and corners. This can be attributed to the fact that, edges and corners are more reactive in comparison to the bulk, which was further proved by passivating the edges through silane coating followed by immobilization of gold nanoparticles. In this case, the gold nanoparticles don't bind to IF-WS_2.

The nature of interaction of gold nanoparticle and NT-WS_2 was evaluated by AFM pushing experiments and found out that, the interaction was simply not van der waals force. The interaction was estimated to be approximately 2 orders of magnitude stronger than van der Waals interaction, which indicate chemical bonding between NT-WS_2 and gold nanoparticles.

1.5. References

[1] Richard Feynman, "Six Easy Pieces", Addison-Wesley Pub. Co., Menlo Park, CA, 1963.

[2] R. Feynman, *Science* **1991**, *254*, 1300.

[3] S. Zhang, *Biotech. Adv.* **2002**, *20*, 321.

[4] K. Yang, H. Wang, K. Zou, Xiaohong Zhang, *Nanotechnology* **2006**, *17*, S276.

[5] C. Drake, S. Deshpande, D. Bera1, S. Seal, *Int. Mater. Rev.* **2007** *52*, 289.

[6] Y. Wang, G. Du, H. Liu, D. Liu, S. Qin, N. Wang, C. Hu, X. Tao. J. Jiao, J. Wang, Z. L. Wang, *Adv. Funct. Mater.* **2008**, *18*, 1.

[7] G. A. Hughes, *Nanomedicine* **2005**, *1*, 22.

[8] O. C. Farokhzad, R. Langer, *Adv. Drug Delivery Reviews* **2006**, *58*, 1456.

[9] (a) H. B. Na, J. H. Lee, K. An, Y. I. Park, M. Park, I. S. Lee, D. H. Nam, T. S. Kim, S. H. Kim, S. W. Kim, K. H. Lim, K. S. Kim, S. O. Kim, T. Hyeon, *Angew. Chem. Int. Ed.* **2007**, *46*, 5397. (b) L. R. Hirsch, R. J. Stafford, J. A. Bankson, S. R. Sershen, B. Rivera, R. E. Price, J. D. Hazle, N. J. Halas, J. L.West, *Proc. Natl. Acad. Sci. USA* **2003**, *100*, 13549.

[10] (a) O. Rabin, J. Manuel Perez, J. Grimm, G. Wojtkiewicz, R. Weissleder, *Nat. Mater.* **2006**, *5*, 118. (b) D. Kim, S. Park, J. H. Lee, Y. Y. Jeong, S. Jon, *J. Am. Chem. Soc.* **2007**, *129*, 7661.

[11] F. X. Gu, R. Karnik, A. Z. Wang, F. Alexis, E. L. Nissenbaum, S. Hong, R. S. Langer, O. C. Farokhzad. *Nanotoday* **2007**, *2*, 14.

[12] H. W. Kroto, J. R. Heath, S. C. O'Brien, R. F. Curl, R. E. Smalley, *Nature* **1985**, *318*, 162.

[13] S. Iijima, *Nature* **1991**, *354*, 56.

[14] R. Tenne, L. Margulis, M. Genut, G. Hodes, *Nature* **1992**, *360*, 444.

[15] L. Margulis, G. salitra, R. Tenne, M. Talianker, *Nature* **1993**, *365*, 113.

[16] Y. Feldmann, E. Wasserman, D. J. Srolovitz, R. Tenne, *Science* **1995**, *267*, 222.

[17] R. Tenne, C. N. R. Rao, *Phil. Trans. R. Soc. Lond. A* **2004**, *362*, 2099.

[18] M. Remskar, *Adv. Mater.* **2004**, *16*, 1497.

[19] G. R. Patzke, F. Krumeich, R. Nesper, *Angew. Chem. Int. Ed.* **2002**, *41*, 2446.

[20] R. Tenne, *Angew. Chem. Int. Ed.* **2003**, *42*, 5124.

[21] C. N. R. Rao, M. Nath, *Dalton Trans.* **2003**, 1–25.

[22] R. Tenne, *Nat. Nanotech.* **2006**, *1*, 103.

[23] M. N. Tahir, A. Yella, J. K. Sahoo, H. A. Therese, N. Zink, W. Tremel, *Phys. Status Solidi B* **2010**, *247*, 2338.

[24] R. Tenne, M. Redlich, *Chem. Soc. Rev*. **2010**, *39*, 1423.

[25] Y. R. Hachohen, E. Grunbaum, J. Sloan, J. L. Hutchison, R. Tenne, *Nature* **1998**, *395*, 336.

[26] H. A. Therese, F. Rocker, A. Reiber, J. Li, M. Stepputat, G. Glasser, U. Kolb, W. Tremel, *Angew. Chem*. **2005**, *117*, 267; *Angew. Chem. Int. Ed*. **2005**, *44*, 262.

[27] J. Chen, S.-L. Li, Z.-L. Tao, Y.-T. Shen, C.-X. Cui, *J. Am. Chem. Soc.* **2003**, *125*, 5284.

[28] J. A. Hollingsworth, D. M. Poojary, A. Clearfied, W. E. Buhro, *J. Am. Chem. Soc*. **2000**, *122*, 3562.

[29] I. Alexandrou, N. Sano, A. Burrows, R. R. Meyer, H. Wang, A. I. Kirkland, C, J Kiely, G. A. J. Amaratunga, *Nanotechnology* **2003,** *14*, 913.

[30] J. J. Hu, J. E. Bultman, J. S. Zabinski, *Tribol. Lett*. **2004**, *17*, 543.

[31] G. A. Camacho-Bragado, J. L. Elechiguerra, A. Olivas, S. Fuentes, D. Galvan, M. J. Yacaman, *J. Catal*. **2005**, *234*, 182.

[32] W. X. Chen, J. P. Tu, X. C. Ma, Z. D. Xu, R. Tenne, R. Rosentsveig, *Chin. Chem. Lett.* **2003**, *14*, 312.

[33] Y. Feldman, G. L. Frey, M. Homyonfer, V. Lyakhovitskaya, L. Margulis, H. Cohen, G. Hodes, J. L. Hutchison, R. Tenne, *J. Am. Chem. Soc.* **1996**, *118*, 5362.

[34] Y. Feldman, L. Margulis, M. Homyonfer, R. Tenne, *High Temp. Mater. Proc.* **1996**, *15*, 163.

[35] Y. Feldman, A. Zak, R. Popovitz-Biro, R. Tenne, *Solid State Sci*. **2000,** *2*, 663.

[36] A. Zak, Y. Feldman, V. Alperovich, R. Rosentsveig, R. Tenne, *J. Am. Chem. Soc.* **2000**, *122*, 11108.

[37] X. L. Li, Y. D. Li, *Chem. Eur. J*. **2003**, *9*, 2726.

[38] A. Rothschild, R. Tenne, J. Sloan, A. P. E. York, M. L. H. Green, J. Sloan, J. L. Hutchison, *Chem. Commun*. **1999**, *363*.

[39] T. Tsirlina, Y. Feldman, M. Homyonfer, J. Sloan, J. L. Hutchison, R. Tenne, Fullerene *Sci. Technol*. **1998**, *6*, 157.

[40] R. L. D. Whitby, W. K. Hsu, T. H. Lee, C. B. Boothroyd, H. W. Kroto, D. R. M. Walton, *Chem. Phys. Lett*. **2002**, *68*, 359.

[41] K. S. Coleman, J. Sloan, N. A. Hanson, G. Brown, G. P. Clancy, M. Terrones, H. Terrones, M. L. H. Green, *J. Am. Chem. Soc*. **2002**, *124*, 11580.

[42] A. Margolin, R. Popovitz-Biro, A. Albu-Yaron, A. Moshkovich,L. Rapoport, R. Tenne, *Curr. Nanosci*. **2005**, *1*, 253.

[43] C. Schuffenhauer, R. Popovitz-Biro, R. Tenne, *J. Mater. Chem*. **2002**, *12*, 1587.

[44] G. H. Lee, J. W. Jeong, S. H. Huh, S. H. Kim, B. J. Choi, Y. W. Kim, *Int. J. Mod. Phys*. B **2003**, *17*, 1134.

[45] C. M. Zelenski, P. K. Dorhout, *J. Am. Chem. Soc*. **1998**, *120*, 734.

[46] J. Chen, S. L. Li, F. Gao, Z. L. Tao, *Chem. Mater*. **2003**, *15*, 1012.

[47] M. Nath, A. Govindaraj, C. N. R. Rao, *Adv. Mater*. **2001**, *13*, 283.

[48] M. Remskar, A. Mrzel, Z. Skraba, A. Jesih, M. Ceh, J. Demsar, P. Stadelmann, F. Levy, D. Mihailovic, *Science* **2001**, *292*, 479.

[49] M. Remskar, Z. Skraba, M. Regula, C. Ballif, R. Sanjines, F. Levy, *Adv. Mater*. **1998**, *10*, 246.

[50] P. A. Parilla, A. C. Dillon, B. A. Parkinson, K. M. Jones, J. Alleman, G. Riker, D. S. Ginley, M. J. Heben, *J. Phys. Chem. B* **2004**, *108*, 6197.

[51] Y. R. Hacohen, R. Popovitz-Biro, Y. Prior, S. Gemming, G. Seifert, R. Tenne, *Phys. Chem. Chem. Phys.* **2003**, *5*, 1644.

[52] R. Sen, A. Govindaraj, K. Suenaga, S. Suzuki, H. Kataura, S. Iijima, Y. Achiba, *Chem. Phys. Lett*. **2001**, *340*, 242.

[53] C. Schuffenhauer, B. A. Parkinson, N. Y. Jin-Phillipp, L. Joly-Pottuz, J. M. Martin, R. Popovitz-Biro, R. Tenne, *Small* **2005**, *1*, 1100.

[54] D. Vollath, D. V. Szabo, *Mater. Lett*. **1998**, *35*, 236.

[55] D. Vollath, D. V. Szabo, *Acta Mater*. **2000**, *48*, 953.

[56] X. L. Li, J. P. Ge, Y. D. Li, *Chem. Eur. J.* **2004**, *10*, 6163.

[57] S. Bastide, D. Duphil, J. P. Borra, C. Levy-Clement, *Adv. Mater*. **2006**, *18*, 106.

[58] L. Rapoport, Y. Feldman, M. Homyonfer, H. Cohen, J. sloan, J. L. Hutchinson, R. Tenne, *Wear* **1999**, *225*, 975.

[59] (a) L. Joly-Pottuz, F. Dassenoy, M. Belin, B. Vacher, J. M. Martin, N. Fleischer *Tribol.lett.* **2005**, *18*, 477. (b) L. Rapoport, N. Fleischer, R. Tenne, *J. Mater. Chem.* **2005**, *15*, 1782.

[60] J. J. Hu, J. S. Zabinski, *Tribol. Lett.* **2005**, *18*, 173.

[61] W. X. Chen, Z. D. Xu, R. Tenne, R. Rosenstveig, W. L. Chen, H. Y. Gan, J. P. Tu. *Adv. Eng. Mater.* **2002**, *4*, 686.

[62] A. Katz, M. Redlich, L. Rapoport, H. D. Wagner, R. Tenne *Tribol. Lett.* **2006**, *21*, 135.

[63] H. Friedman, O. Eidelman, Y. Feldman, A. Moshkovich, V. Perfiliev, L. Rapoport, H. Cohen, A. Yoffe, R. Tenne, *Nanotechnology* **2007**, *18*, 115703.

[64] (a) F. Dassenoy, L. Joly-Pottuz, J. M. Martin, D. Vrbanic, A. Mrzel, D. Mihailovic, W. Vogel, G. Montagnac, *J. Eur. Ceram. Soc*. **2007**, *27*, 915. (b) A. Katz, M. Redlich, L. Rapoport, H. D. Wagner, R. Tenne, *Tribol. Lett*. **2006**, *21*, 135. (c) M. Redlich, A. Gorodnev, Y. Feldman, I. Kaplan-Ashiri, R. Tenne, N. Fleischer, M. Genut, N. Feuerstein, *J. Mater. Res*. **2008**, *23*, 2909. (d) G. R. Samorodnitzky-Naveh, M. Redlich, L. Rapoport, Y. Feldman, R. Tenne, *Nanomedicine (Lond)* **2009**, *4*, 943.

[65] (a) R. Prins, *Adv. Catal*. **2002**, *46*, 399. (b) C. T. Tye, K. J. Smith, *Top. Catal*. **2006**, *37*, 129. (c) J. V. Lauritsen, M. Nyberg, J. K. Norskov, B. S. Clausen, H. Topsoe, E. Laegsgaard, F. Besenbacher, *J. Catal*. **2004**, *224*, 94. (d) J. V. Lauritsen, M. V. Bollinger, E. Laegsgaard, K. W. Jacobsen, J. K. Norskov, B. S. Clausen, H. Topsoe, F. Besenbacher, *J. Catal*. **2004**, *221*, 510. (e) J. V. Lauritsen, M. Nyberg, R. T. Vang, M. V. Bollinger, B. S. Clausen, H. Topsoe, K. W. Jacobsen, E. Laegsgaard, J. K. Norskov, F. Besenbacher, *Nanotechnology* **2003**, *14*, 385.

[66] (a) N. A. Dhas, K. S. Suslick, *J. Am. Chem. Soc*. 2005, 127, 2368. (b) J. Chen, S. L. Li, Q. Xu, K. Tanaka, *Chem. Commun*. **2002**, 1722. (c) F. Cheng, X. Gou, J. Chen, Q. Xu, *Adv. Mater*. **2006**, *18*, 2561.

[67] I. Kaplan-Ashiri, S. R. Cohen, K. Gartsman, V. Ivanovskaya, T. Heine, G. Seifert, I. Kanevsky, H. D. Wagner, R. Tenne *Proc. Natl. Acad. Sci. USA* **2006,** *103*, 523.

[68] I. Kaplan-Ashiri, S. R. Cohen, K. Gartsman, R. Rosentsveig, G. Seifert, R. Tenne, *J. Mater. Res.* **2004,** *19*, 454.

[69] L. Joly-Pottuz, J. M. Martin, F. Dassenoy, M. Belin, G. Montagnac, B. Reynard, N. Fleischer, *J. Appl. Phys.* **2006**, *99*, 023524.

[70] Y. Q. Zhu, T. Sekine, Y. H. Li, M. W. Fay, Y. M. Zhao, C. H. P. Poa, W. X. Wang, R.Martin, P. D. Brown, N. Fleischer, R. Tenne, *J. Am. Chem. Soc*. **2005**, *127*, 16263.

[71] A. Buchman, H. Dodiuk-Kenig, A. Dotan, R. Tenne, S. Kenig, *J. Adh. Sci. Tech*. **2009**, *23*, 753.

[72] J. V. Barth, G. Costantini, K. Kern, *Nature* **2005**, *437*, 671.

[73] T. D. Schladt, K. Schneider, H. Schild, W. Tremel, *Dalton Transactions* **2011,** *40***,** 6315**.**

[74] V. Wagner, A. Dullaart, A.-K. Bock and A. Zweck, *Nat. Biotechnol.* **2006**, *24*, 1211.

[75] M. E. Davis, Z. Chen andD.M. Shin, *Nat. Rev. Drug Discovery*, **2008**, *7*, 771.

[76] H. Zhang, Z. Li, C. A. Mirkin, *Adv. Mater.* **2002**, *14*, 1472.

[77] H. Zhang, K-B. Li, Z. Li, C. A. Mirkin, *Nanotechnology* **2003**, *14*, 1113.

[78] G-Y. Liu, S. Xu, Y. Qian, *Acc. Chem. Res*. **2000**, *33*, 457.

[79] L. M. Demers, D. S. Ginger, S.-J. Park, Z. Li, S.-W. Chung, C. A. Mirkin, *Science* **2002**, *296*, 1836.

[80] (a) A. Villa, D. Wang, P. Spontoni, R. Arrigo, D. Su, L. Prati, *Catalysis Today* **2010**, *157*, 89. (b) V. Polshettiwar, P. Hesemann, J. J. E. Moreau, *Tetrahedron* **2007**, *63*, 6784.

[81] (a) J. Pan, R. Ganesan, H. Shen, S. Mathur, *J. Phys. Chem. C* **2010,** *114*, 8245.(b) N. Liu, M. L. Tang, M. Hentschel, H. Giessen, A. P. Alivisatos, *Nat. Mater*. **2011**, DOI: 10.1038/NMAT3029.(c) J. L. Johnson, A. Behnam, S. J. Pearton, A. Ural, *Adv. Mater*. 2010, 22, 4877. (d) A. Kolmakov, D. O. Klenov, Y. Lilach, S. Stemmer, M. Moskovits, *Nano Lett*. **2005**, *5*, 667.

[82] (a) O. S-Sobrado , G. Lozano, M. E. Calvo, A. S-Iglesias, L. M. L-Marzán, H. Míguez, *Adv. Mater*. **2011**, *23*, 2108. (b) B. Hatton, L. Mishchenko, S. Davis, K. H. Sandhage, J. Aizenberg, *Proc. Natl. Acd. Sci*. **2010**, *107*, 10354.

[83] Y. R. Hacohen, E. Grunbaum, R. Tenne, J. Sloan, J. L. Hutchison, *Nature* **1998**, *365***,** 336.

[84] A. Q. Zhu, T. Sekine, Y. H. Li, W. X. Wang, M. Y. Fay, H. Edwards, P. D. Brown, N. Fleischer, R. Tenne, *Adv. Mater*. **2005,** *17*, 1500-1503.

[85] I. Kaplan-Ashiri, S. R. Cohen, K. Gartsman, R. Rosentsveig, V. Ivanovskaya, T. Heine, G. Seifert, H. D. Wagner, R. Tenne, *Proc. Natl. Acad. Sci. USA*, **2006**, *103*, 523.

[86] L. Scheffler, R. Rosentzveig, A. Margolin, R. Popovitz-Biro, G. Seifert, S. R. Cohen, R. Tenne, *Phys. Chem. Chem. Phys*. **2002**, *4*, 2095.

[87] M. Nath, S. Kar, A. K. Raychaudhuri, C. N. R. Rao, *Chem. Phys. Lett***. 2003**, *368*, 690.

[88] M. N. Tahir, M. Eberhardt, N. Zink, H. A. Therese, U. Kolb, P. Theato, W. Tremel, *Angew. Chem.* **2006**, *118*, 4927; *Angew. Chem. Int. Ed.* **2006**, *45***,** 4809.

[89] M. N. Tahir, N. Zink, M. Eberhardt, H. A. Therese, U. Kolb, P. Theato, W. Tremel, *Small* **2007**, *3*, 829.

[90] M. N. Tahir, F. Natalio, H. A. Therese, A. Yella, N. Metz, M. R. Shah, E. Mugnaioli, R. Berger, P. Theato, H. C. Schroeder, W. E. G. Müller, W. Tremel, *Adv. Funct. Mater.* **2009**, *19*, 285.

[91] M. N. Tahir, A. Yella, J. K. Sahoo, F. Natalio, U. Kolb, F. Jochum, P. Theato, W. Tremel, *Isr. J. Chem.* **2010**, *50*, 500.

[92] D. Tareste, F. Pincet, M. Brellier, C. Mioskowski, and E. Perez, *J. Am. Chem. Soc*. **2005**, *127*, 3879.

[93] H. C. Schröder, X. Wang, W. Tremel, H. Ushijima, W. E. G. Müller, *Nat. Prod. Rep.* **2008**, *25*, 455.

[94] H. C. Schröder, D. Brandt, U. Schloßmacher, X. Wang, M. N. Tahir, W. Tremel, S. I. Belikov, W. E. G. Müller, *Naturwissenschaften* **2007**, *94*, 339.

[95] M. N. Tahir, A. Yella, H. A. Therese, E. Mugnaioli, M. Panthöfer, H. U. Khan, W. Knoll, U. Kolb, W. Tremel, *Chem. Mater.* **2009**, *21*, 5382.

[96] M. Olek, T. Busgen, M. Hilgendorff, M. Giersig, *J. Phys. Chem. B* **2006**, *110*, 12901.

[97] S. Banerjee, S. S. Wong, *Chem. Commun*. **2004**, 1866.

[98] B. H. Juarez, C. Klinke, A. Kornoski, H. Weller, *Nano Lett*. **2007**, *7*, 3564.

[99] R. G. Pearson, *J. Am. Chem. Soc.* **1963**, *85*, 3533.

[100] A. Alfarra, E. Frackowiak, F. Beguin., *Appl. Surf. Sci*. **2004**, *228*, 84.

[101] C. Shahar, D. Zbaida, L. Rapoport, H. Cohen, T. Bendikov, J. Tannous, F. Dassenoy, R. Tenne, *Langmuir* **2010**, *26*, 4409.

[102] B. Späth, F. Kopnov, H. Cohen, A. Zak, A. Moshkovich, L. Rapoport, W. Jägermann, R. Tenne, *Phys. Status Solidi B* **2008**, *245*, 1779.

[103] C. Shahar, R. Levi, S. R. Cohen, R. Tenne, *J. Phys. Chem. Lett*. **2010**, *1*, 540.

1.6. Objectives of the thesis.

To conclude, surface functionalization is the most important tool to engineer novel materials or devices operating on nanoscale range for various applications to be used in different disciplines. Among these nanomaterials, layered metal chalcogenide nanostructures, because of their extraordinary chemical and physical properties, offer a broad range of applications in different fields such as nanoelectronics, fuel cells, catalysis, ultra filtration membranes etc. Their tensile strength and shock resistivity is very high, which make them excellent candidates for producing bullet-proof vests, helmets, high strength glues and binders.

Until now, major obstacle in applications of such materials has been their inherent inertness to chemical and biological functionalization. Although the surface modification of metal chalcogenide nanostructures has been documented by chelating polymeric ligands through metal co-ordination, where chalcophilic metals like Ni^{+2} 'wet' the outer sulfur surface and the vacant co-ordination sphere of Ni^{+2} is used to bind to tetra-dentate ligand (NTA) present in the polymeric backbone but there is an ever growing demand to achieve new different methods which involves more biocompatible transistion metal cations or directly anchoring the inorganic nanomaterials to explore various optoelectronic properties.

Here in this thesis, we present some novel methodologies for surface engineering of metal chalcogenide nanostructures based on some novel ligands using metal cations like Fe^{+2}, and directly anchoring metal oxides (Fe_2O_3, Fe_3O_4, MnO, ZnO etc.) or metal (Au, Pt) nanoparticles using Pearsons concept. Moreover, these surface functionalization methods are reversible and starting nanomaterials can be recovered and can be recycled. Also customize functionalization of Janus like nanomaterials ($Pt@Fe_3O_4$) onto layered metal chalcogenides nanotubes, with control over binding either Pt or Fe_3O_4 domains to nanotubes surface by camouflaging one of the two domains. In addition, TiO_2 nanowires were functionalized with Janus nanostructures (Au@MnO) where both domains of Janus nanostructure can be selectively tailored with different molecules and in the last; we have explored multicolour photoluminescence of ZrO_2 nanoparticles using surface functionalization.

1.7. Outline

Chapter 2 presents a novel methodology of functionalization of metal oxide nanoparticles (MnO) onto metal chalcogenide nanostructures, manifesting the usage of Pearson Hardness for the first time in nanoscale. It also describes the realization of reversible functionalization in such nanostructures.

Chapter 3 reports a novel procedure of covalent modification of metal chalcogenide nanofullerenes (ReS_2) using terpyridine as an anchor group. It explains the chelation of terpyridine ligand onto the surface of ReS_2 fullerenes using iron co-ordination chemistry. This chapter also compiles the improvement of solubility (both hydrophilic and hydrophobic solvent) of ReS_2 fullerenes by modification of its surface through different terpyridine derivatives.

Chapter 4 describes the functionalization of different metal oxide nanoparticles onto metal chalcogenide nanostructure based on the Pearson hardness of their corresponding metal cation. It also explains the reversibility of such functionalization.

Chapter 5 explains the concentration dependent edge functionalization and customized self-assembly of Pt-Fe_3O_4 Janus nanostructures onto WS_2 nanotube. It describes selective surface binding, e.g. Platinum domain binds to NT-WS_2 because of its softness whereas Fe_3O_4 domain binds to the sidewall of NT-WS_2 by selectively masking the platinum domain with an organic functional ligand.

Chapter 6 describes the rational assembly of Au@MnO nanoflowers onto TiO_2 nanowires by polymeric functionalization. However it has been observed that the individual surfaces of the TiO_2@Au@MnO nanocomposites can further be functionalized. TiO_2 surface can be activated with NBD flourophore whereas the gold surface can be immobilized with Texas red tagged Single Stranded oligonucleotide.

Chapter 7 describes the luminescent behavior of amine functionalized zirconia nanoparticles. ZrO_2 nanoparticles were chlorinated with excess of $SoCl_2$ followed by amination in presence of 1,4-butanediamine. These amine functionalized zirconia nanoparticles develop intrinsic luminescent properties that can be observed in photoluminiscent spectroscopy and confocal laser scanning microscopy. The amine (butadiamine) terminated zirconia retains its morphology and size and is highly biocompartible as proved by dynamic light scattering and shows no toxicity (cytotoxic test).

Chapter 8 Conclusions and outlook.

Chapter 9 Methods and Instrumentations.

Chapter 10 (appendix) describes in detail all the experimental procedures, employed in the work presented in this thesis. Additionally, various characterization techniques and instrumental specifications, supplementary material and a list of figures presented in the thesis are provided.It also contains ^{1}H NMR, FD-MS spectroscopy and XRD data.

2. Rational Reversible Functionalization of Metal Chalcogenide/Metal Oxide Nanostructures Based on Pearson Hardness

Running Title: Reversible Functionalization

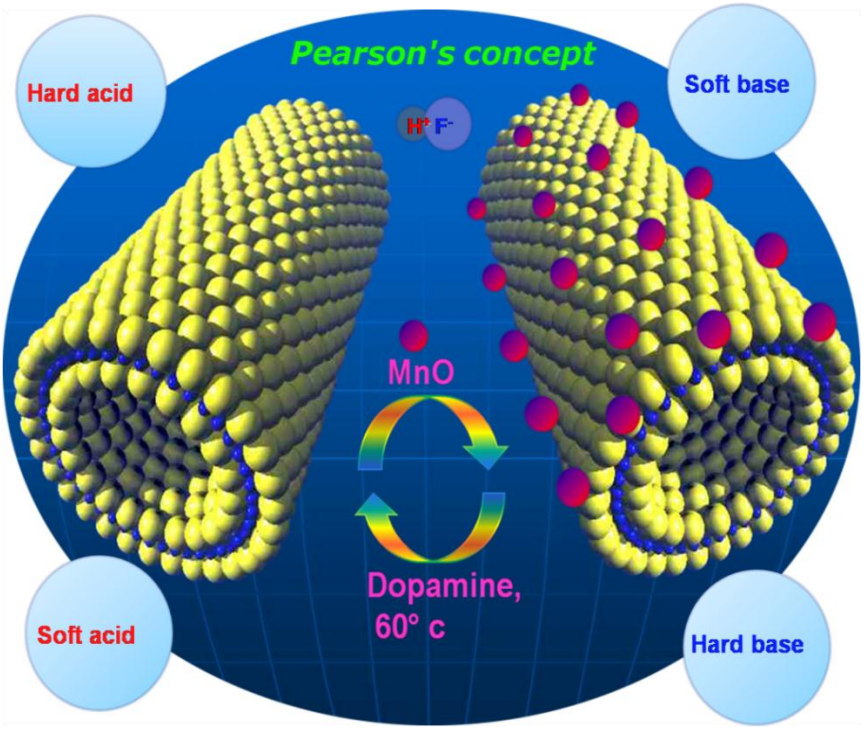

Jugal Kishore Sahoo[a], Muhammad Nawaz Tahir[a], Aswani Yella[a], Thomas D. Schladt[a], Enrico Mugnaioli[b], Ute Kolb[b], Wolfgang Tremel[a].

[a]Institute for Inorganic and Analytical Chemistry

[b]Institute for Physical Chemistry,

Johannes Gutenberg-Universität, Mainz, Germany.

Angew. Chem. 2010, 122, 7741 –7745

Angew. Chem. Int. Ed. 2010, 49, 7578 –7582

2.1. Introduction

Nanotechnology has reached a stage of development where not individual nanoparticles but rather systems of greater complexity are the focus of concern [1]. These complex structures incorporate two or more types of materials, an example of which is the formation of metal-semiconductor hybrids, which effectively combine the properties of both materials [2]. The assembly of multicomponent nanoparticles from constituents with different optical, electrical, magnetic and chemical properties can lead to novel functionalities that are independent of the individual components and may be tailored to fit a specific application. These applications include such far-reaching challenges as solar energy conversion [3], biological sensors [4], mechanical and optical devices [5], and potential methods for drug delivery and medical diagnostics [6].

A specific challenge is to assemble nanoparticles into a hierarchical structure. Nanotubes (NT-MQ_2) [7] and fullerenes (IF-MQ_2) [8], of layered metal chalcogenides are the purely inorganic analogues of carbon fullerenes and nanotubes that exhibit analogous mechanical [9] and electronic properties [10]. They consist of metal atoms sandwiched between two inert chalcogenide layers. Their physical properties [11] are related to their crystal structures, which contain MQ_2 slabs with metal atoms, sandwiched between two inert chalcogen layers. These MQ_2 layers are stacked, with only van der Waals contacts between them. The steric shielding of the metal atoms by the chalcogen surface layers from nucleophilic attack by oxygen or organic ligands makes chalcogenide nanoparticles highly inert and notoriously difficult to functionalize.

Some progress has been made by employing chalcophilic transition metals in combination with multi-dentate surface ligands: The 3d metals “wet” the sulfur surface of the chalcogenide nanoparticles while the multidentate surface ligands partially block one hemisphere of the metal coordination environment. This steric shielding prevents an aggregation of the chalcogenide nanoparticles through inter-particle crosslinking [12].

The assembly of aggregates from different types of nanoparticles typically relies on chemical modifications of the nanoparticle surface in order to achieve a specific linkage. A bifunctional organic linker molecule having specific anchor groups for each type of nanoparticle is bound with one of its anchor groups to the first type of the pre-synthesized nanoparticles. In a subsequent step, the second anchor group is used for the attachment of the second type of nanoparticles [13].

The synthetic goal is to attach a controlled number of target molecules while avoiding aggregation through nonspecific interaction with surfaces and other particles in solution. In order to achieve that goal, the nanoparticles have to be stabilized with a protecting layer containing some chemical anchor points for further modification. This covalent chemical attachment offers high stability in different solvents and ionic environments. Therefore, current strategies for the functionalization of nanoparticles rely (i) either on non-covalent physisorption of linker molecules to the surface of the nanoparticles [14], (ii) electrostatic anchoring of an additional polymeric layer [15], or (iii) the use of short bifunctional cross-linkers. This leads to low yield [16], or surface coverage [17].

An alternative strategy is to grow nanoparticles directly on the nanotubes by using colloidal nanoparticle synthesis methods [18]. Colloidal nanoparticles may have an affinity based on their acid/base properties, functional groups or Pearson hardness [19] for nanotube surfaces that allows their attachment without the aid of linkers.

2.2. Results and Discussions.

In this paper we report a novel synthetic strategy based on Pearson's HSAB principle [19c], that allows the formation of a hierarchical assembly of metal chalcogenide/metal oxide nanostructures. The metal oxide particles can be functionalized in a subsequent reaction step to tailor the chalcogenide surfaces at room temperature or to reversibly detach them from the chalcogenide surfaces with excess surface ligand (Scheme 2.1). The recycled chalcogenide nanoparticles can be used time and again without the use of organic ligands (Scheme 2.2).

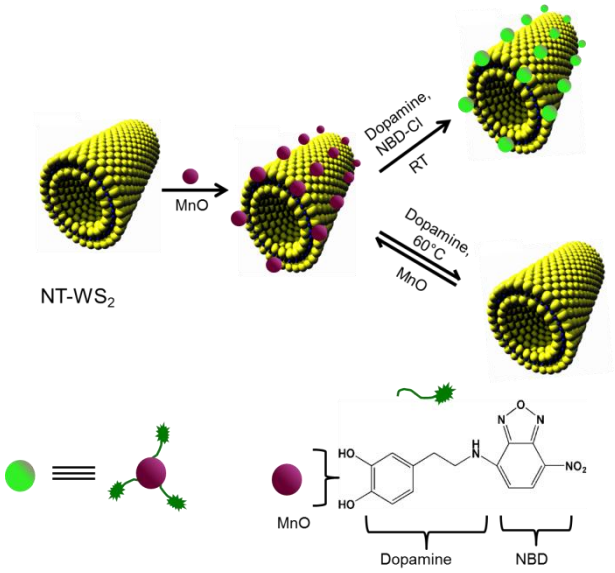

Scheme 2.1. *Schematic representation of reversible immobilization of MnO on NT-WS_2 and surface functionalization through fluorophore labeled dopamine.*

According to Pearson's HSAB (Hard Soft Acid Base) principle, a hard Lewis acid has a tendency to bind with a hard Lewis base and vice versa [19c]. Thus, in the layered metal chalcogenides the soft sulfur surface layer has a tendency to bind with other nanoparticles containing soft transition metal cations. As basic components to build these magnetic nanohybrids, MnO and NT-WS_2 nanoparticles were prepared separately in the first step. Figure 2.1a and b show representative transmission electron microscopy (TEM) images of the building blocks, MnO and NT-WS_2 nanoparticles, produced according to published procedures [20]. As the nanoparticles carry oleic acid molecules surface ligands they are soluble in most organic solvents (cyclohexane, toluene, or THF) [20a]. WS_2 nanotubes (NT-WS_2) were prepared by the sulfidization of WO_3 nanorods obtained via hydrothermal synthesis [20b]. A HRTEM image of one such WS_2 nanotube is shown in Figure 2.1b. The interlayer spacing of 0.65 nm between the tubular walls is consistent with the (002) d-spacing of the 2H-WS_2 lattice.

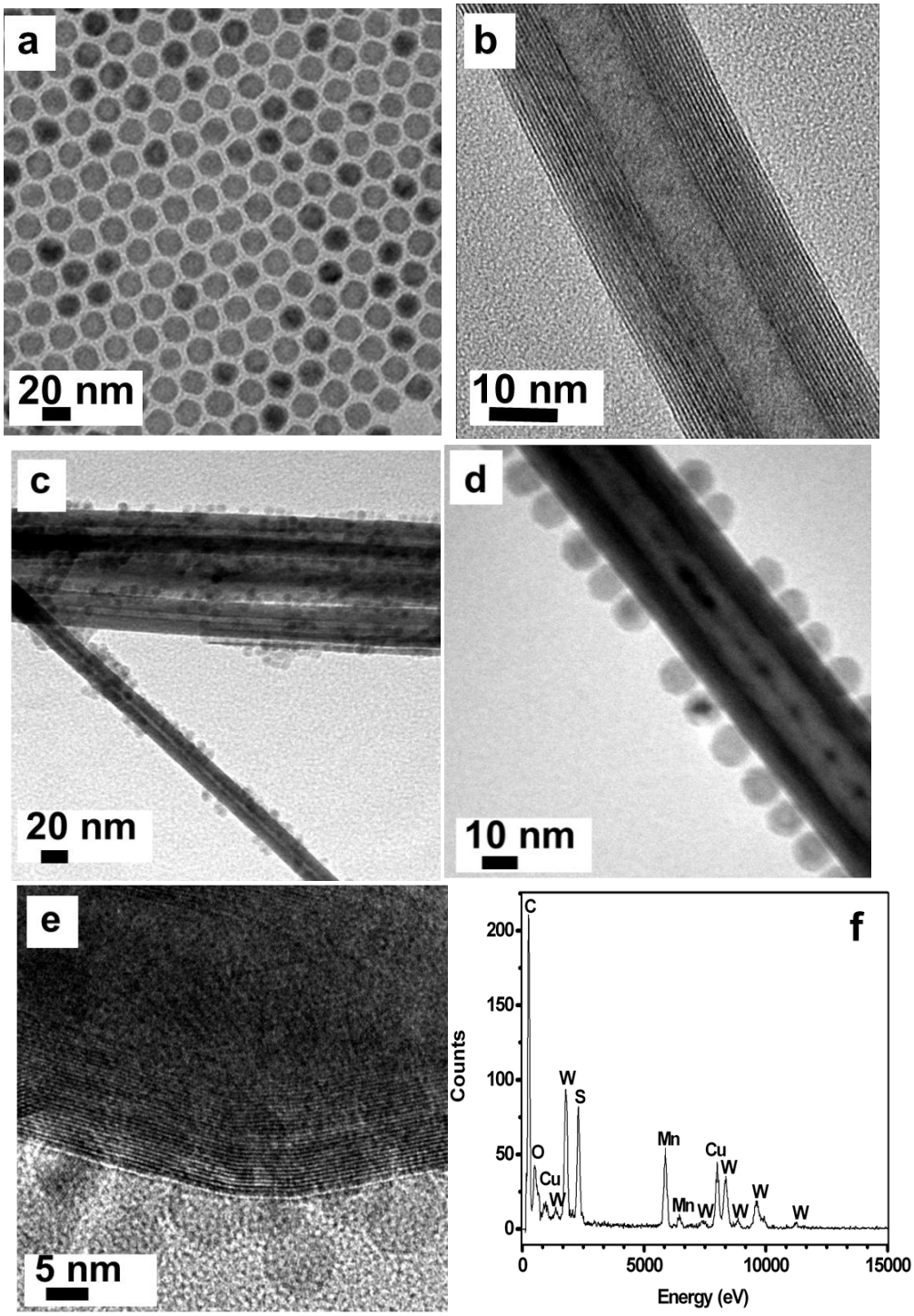
a
20 nm
b
10 nm
c
20 nm
d
10 nm
e
5 nm
f
C
O
Cu
W
W
S
Mn
Mn
Cu
W
W
W
W
W
Counts
Energy (eV)
0
50
100
150
200
0
5000
10000
15000

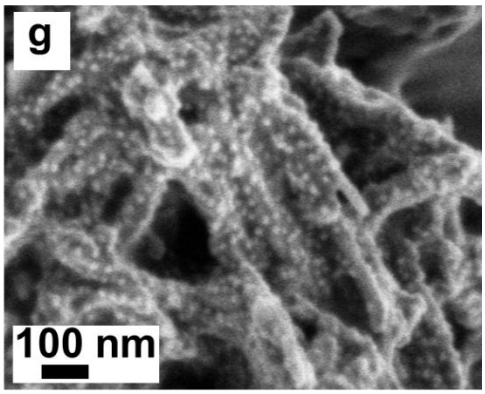

Figure 2.1. *TEM images of the as-synthesized (a) MnO, (b) NT-WS_2 (c-e) TEM images showing the binding of MnO nanoparticles onto NT-WS_2. (c) Overview image, (d and e) HRTEM showing the interface of MnO nanoparticles and sidewalls (d) or the tip (e) of a WS_2 nanotube. (f) EDX spectrum of the MnO@NT-WS_2 composite. (g) SEM image of the MnO@NT-WS_2 composite.*

The assembly of oxide/chalcogenide nanostructures was produced by mixing dispersions of the chalcogenide nanoparticles and metal oxide nanoparticles in toluene under mechanical shaking. During this process, the metal oxide nanoparticles were assembled onto the chalcogenide nanoparticle surface *via* ligand exchange. In this process, the oleic acid capping ligands on the surface of the oxide nanoparticles are substituted by the surface sulfur atoms of the chalcogenide nanoparticles. The binding of MnO nanoparticles to NT-WS_2 and EDX analysis is illustrated in the TEM images in Figure 2.1c-e. The soft basic character of the chalcogenide surface is of prime importance for the surface binding. The chemisorption of ions or molecules involves their acidic or basic properties which have to be opposite to those of the active surface sites. The overview TEM image (Figure 2.1c) shows almost all the nanotubes are covered with MnO nanoparticles and high resolution transmission electron microscopy shows that almost nanoparticles are sitting on the basal plane of nanotubes. The scanning electron microscopy (SEM) (Figure 2.1g) also gives an overview image to confirm the immobilization of MnO nanoparticles on NT-WS_2. Energy-dispersive X-ray analysis (EDX) of the composite nanotubes (Figure 2.1f) indicates the presence of the elements W, S, Mn and O. The analytical data indicate a significant amount of MnO nanoparticles present on the surface of the nanotubes, in accordance with the results of the TEM study.

As described earlier the tailoring of the chalcogenides surfaces is difficult and requires some suitable approaches, whereas the metal oxides surfaces are easy to functionalize. The NT-WS_2

surface bound MnO nanoparticles can be functionalized selectively with catechol-type ligands. In this process, the oleic acid capping ligands are replaced by the free catechol ligand. Figure 2.2a shows the UV-vis spectrum of the NT-WS_2 particles decorated with surface functionalized MnO (full line) nanoparticles with dopamine bound 7-nitrobenzofurazan (NBD) dye. The spectrum shows a characteristic broad absorption band of WS_2 around 660 nm. The absorption band due to NBD appears at 490 nm. The 660 nm absorption band of functionalized NT-WS_2 is weakly visible in the MnO@NT-WS_2 composite. The surface decoration of NT-WS_2 with NBD-functionalized MnO nanoparticles was further proven using confocal laser scanning microscopy as illustrated in Figure 2.2b. A 10 µl droplet of the sample was placed and dispersed carefully on a thin glass slide and the solvent was evaporated. The fluorescence of the NBD dyes was excited at 488 nm and detected from 504 - 514 nm. A 40x (NA 1.25) oil immersion objective was used for the imaging. The overview image of as-functionalized MnO@NT-WS_2 (Figure 2.2b) nanoparticles with NBD ligands shows anisotropic fluorescence images of nearly isolated nanoparticles, while the image of a single isolated nanotube given in the inset. It is reasonable to conclude from the fluorescence images that the nanotubes are fully coated with surface functionalized MnO nanoparticles covalently tethered to the NT-WS_2 surface. It is difficult to comment on the actual size of the functionalized nanotubes because they are below the resolution limits of CLSM. No fluorescence was observed by exciting the unfunctionalized MnO nanoparticles or unfunctionalized NT-WS_2.

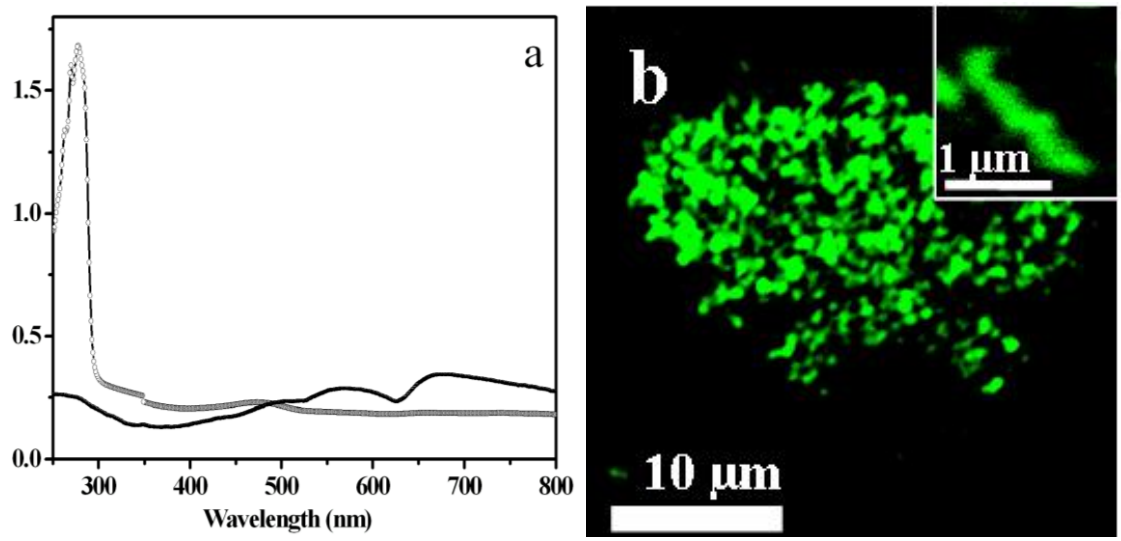

Figure 2.2. *UV-Vis absorption spectrum of a) as synthesized WS_2 nanotubes (red line), b) MnO@NT-WS_2 nanoparticles functionalized with dopamine-NBD b) Confocal laser scanning microscopy images of WS_2 nanotubes coated with dopamine-NBD, the inset shows single nanotube.*

Pearson´s hard-soft acid-base (HSAB) principle states that "hard acids prefer to coordinate with hard bases and soft acids prefer to coordinate with soft bases for both their thermodynamic and kinetic properties". The effect of solvation of ions must be taken into consideration in order to have a proper understanding of the HSAB principle. Due to their chelating properties catechol-type ligands can compete successfully with sulfur for surface metal atoms. Since the solvation increases with increasing the temperature, we used a temperature of 60 °C to remove all surface-bound MnO nanoparticles from the NT-WS_2 surface in the presence of dopamine as chelating ligand for the metal oxide nanoparticles surfaces. However without addition of dopamine, it's not possible to reversibly recover the metal chalcogenides nanotubes.

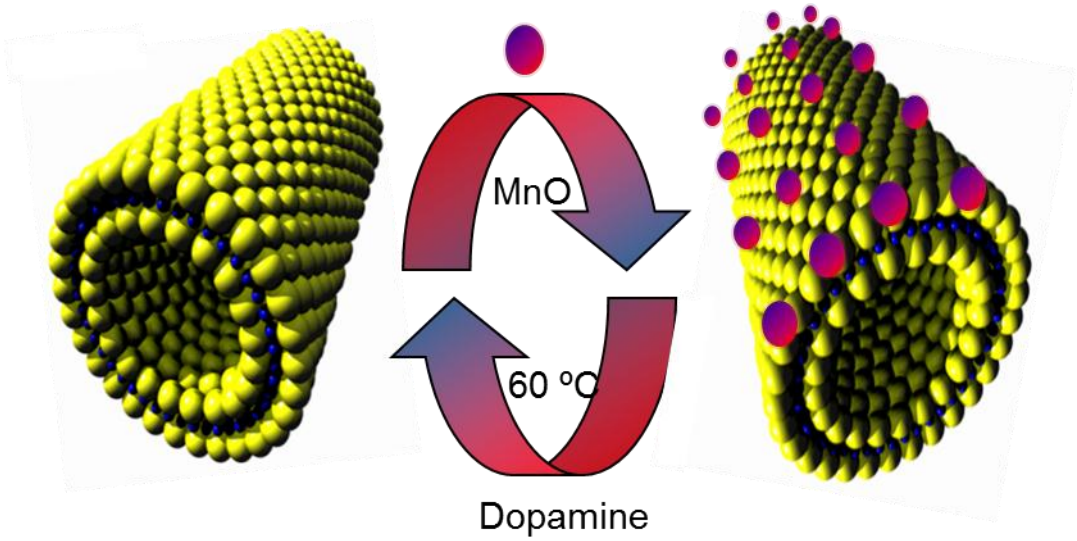

Scheme 2.2. *Illustration of the reversible functionalization of MnO on NT-WS_2.*

Another reason for the stability of the catecholate surface complexes is the valence-taumerism through redox-active ligands and transition metal ions. Catecholate ligands form unstrained and unsaturated five-membered ring chelate systems with surface metal atoms via negatively charged oxygen atoms. Complexes with non-innocent electro-active ligands may exhibit a reversible intramolecular electron transfer between the metal ions and the ligand, leading to stabilization through internal charge redistribution (Scheme 2.3) [21].

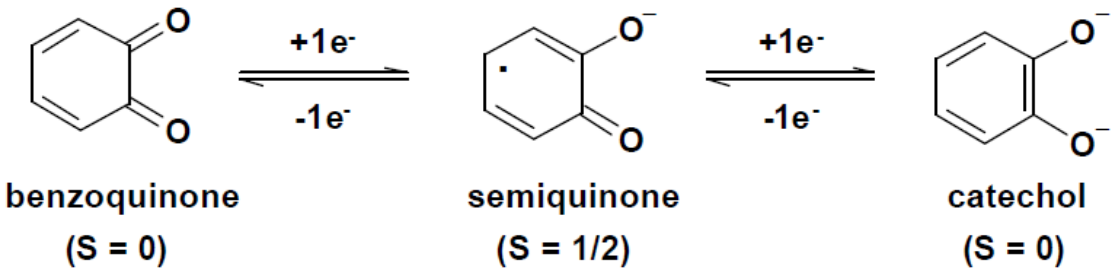

Scheme 2.3. *Valence-taumerism through redox-active chelating ligands and transition metal ions. Complexes with non-innocent electro-active ligands exhibit a reversible intramolecular electron transfer between metal ions and the ligand, leading to internal charge redistribution.*

Scheme 2.2. illustrates the attachment and detachment of MnO nanoparticles to NT-WS_2. Whereas oxides of soft and borderline metals are chemisorbed easily to the sulfur surface atoms, oxides of the hard metals have a much lower tendency for binding. In contrast, the catechol-type ligands bind efficiently to hard or borderline metals (such as Ti^{4+} Fe^{3+}, Al^{3+}, Mn^{2+} etc.). As a result, the binding of chalcogenide nanoparticles and catechol-type ligands to surface metal atoms of borderline metal oxides is a dynamic equilibrium reaction, whose position depends on the reactants and temperature. By increasing the reaction temperature to 60 °C, catechol is a preferred surface ligand for the metal oxide particles. It displaces the surface sulfur atoms of NT-WS_2 leaving unfunctionalized NT-WS_2 nanotubes behind. Adding fresh metal oxide nanoparticles to NT-WS_2 leads to a partial replacement of the oleate surface ligands by the surface sulfur atoms of NT-WS_2 and a concomitant binding of metal oxide nanoparticles to NT-WS_2. This cycle can be repeated several times. The recycled chalcogenide nanoparticles can be re-used (Scheme 2.4.).

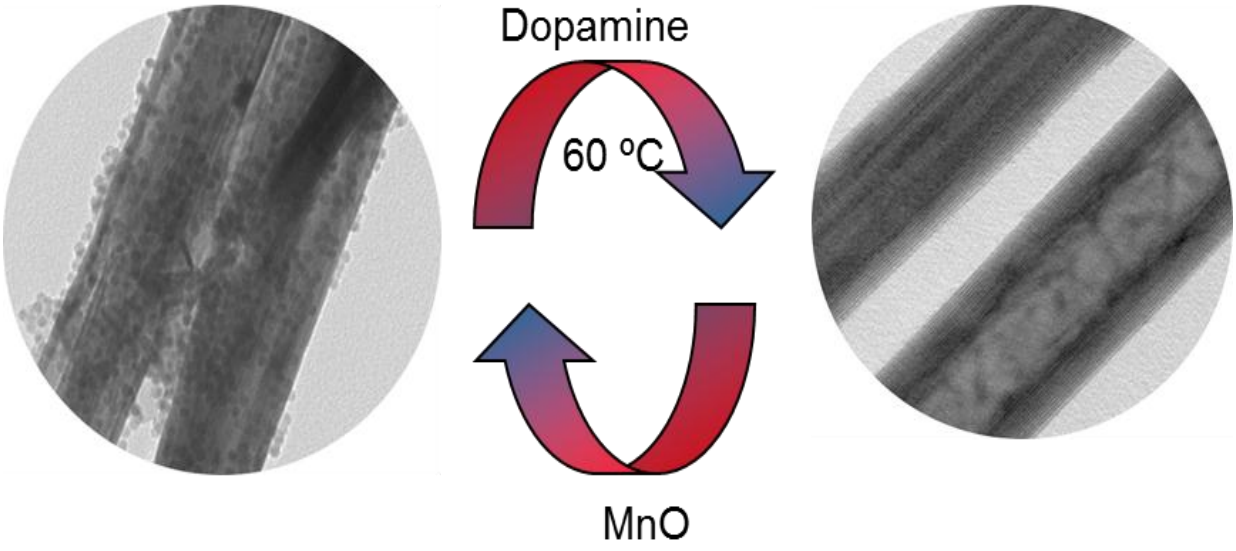

Scheme 2.4*. Schematic representation of reversible immobilization of MnO on NT-WS_2 and surface functionalization through fluorophore labeled dopamine.*

The HSAB model has its basis in arguments related to bonding strength. It is applied for systems where kinetic control, entropy of adduct formation, solvation effects (enthalpic and entropic), ion-pairing effects (enthalpic and entropic), or lattice energy effects (enthalpic and entropic) are large and even dominant. When HSAB considerations are employed, it is

implied that the soft-soft (covalent) or hard-hard (ionic) interactions, dominate the chemistry, i.e. that the reactions are either orbital or charge controlled.

2.3. Summary and Outlook.

In summary, we have used the principles of coordination chemistry to achieve the reversible functionalization of highly inert chalcogenide nanotubes with metal oxide (MnO) nanoparticles. The modification strategy is based on the chalcophilic affinity of Mn^{2+}, as described by the Pearson HSAB concept. The surface-bound nanoparticles are still amenable to functionalization with anchor ligands such dopamine. As the chelating dopamine ligand is a much more potent ligand for surface 3d metals than the sulfur atoms of the chalcogenide nanoparticles, MnO nanoparticles can be detached from the chalcogenide surface at slightly elevated temperature. The remaining chalcogenide particles can be the functionalized again with fresh metal oxide nanoparticles. The "self-assembled" hybrid architecture can incorporate various different selective nanoparticle-substrate interactions based on well-known surface chemistries, and it may be generalized for various layered chalcogenide nanoparticles and transition metal and main group oxides. This assembly technique offers benefits for low-cost and low-waste manufacturing, and such methods are becoming increasingly important in the development of green nanofabrication strategies.

The functionalization of WS_2 nanotubes opens several new fields for this class of materials which have been pursued actively during the past few years for the related carbon nanotubes and various oxide materials: (i) the functionalization of chalcogenide nanotubes for the attachment of electronically active components (metal and semiconductors nanoparticles, light harvesting ligands for solar cell applications) to the sidewalls of the tubes, (ii) dispersion of nanotubes, e.g. for the integration in composites, which is of interest because of their exceptional mechanical properties. (iii) Furthermore, it allows the fabrication of thin films by surface binding of chalcogenide particles to oxide surfaces, which might allow their use as lubricants on seemingly incompatible ceramic materials.

2.4. Experimental Section.

Methods and Materials

3-Hydroxy tyramine hydrochloride, (acros organic), 4-chloro, 7-nitro, benzafurazan (sigma-aldrich) were purchased and used as received without further purification. Solvents such as tetrahydrofurane, chloroform, DMF, were purchased technical grade and used as received.

Synthesis of MnO np's. All reactions were carried out using standard Schlenk conditions. All syntheses were carried out in a home-built metal bath heater equipped with a temperature control and monitoring unit. The heater was made out of brass and equipped with two 180 W heating elements operating at 220 V and a Pt100 temperature sensor. It was filled with 1.2 kg of Wood metal (Roth, T_M = 70 °C).

All syntheses were carried out under Argon and using commercially available reagents: 1-tetradecene (technical grade, 92%, Aldrich), 1-hexadecene (technical grade, 92%, Aldrich), 1-octadecene (technical grade, 90%, ACROS), tri-n-octylamine (98%, Fluka), oleic acid (technical grade, Fisher), methanol, hexane, acetone, ethanol and manganese chloride tetrahydrate ($MnCl_2 \times 4H_2O$, 99%, Aldrich) were used as received.

Synthesis of the manganese oleate precursor. Manganese oleate was prepared according to a reported procedure [20a] with some modifications. 7.94 g (40 mmol) of manganese chloride tetrahydrate and 22.60 g (80 mmol) oleic acid were dissolved in 200 mL of methanol. A solution of 3.2 g (80 mmol) of sodium hydroxide in 200 mL of methanol was added dropwise to the stirred Mn-/oleic acid solution over a period of 1 h. The initially clear colorless mixture turned pink, and a deep red oily substance precipitated. After stirring for another hour the solvent was discarded and the product washed with water, ethanol and acetone. The oily residue was dissolved in hexane and dried over $MgSO_4$. After evaporating the solvent the product was dried *in vacuo* (10^{-2} mbar) at 100-150°C for 2 h to produce a deep red waxy solid.

Synthesis of MnO nanoparticles. In a typical reaction 1.24 g (2 mmol) of the manganese oleate were dissolved in 10 g of 1-octadecene and degassed at 70 °C *in vacuo* (10^{-2} mbar) for 2 h and intermittently backfilled with argon to remove any moisture and oxygen. The reaction mixture was subsequently treated with a definitive temperature program. First of all the solution was rapidly heated to 200 °C with approx. 5 °C/min. For the further course of the reaction the heating rate was fixed to 1.5 °C/min. The as-prepared nanocrystals were easily soluble in non-polar solvents such as hexane or toluene. The nanoparticles were washed three

times according to the following procedure: They were first dissolved in hexane, precipitated with acetone or ethanol and subsequently collected by centrifugation.

Synthesis of NT-WS_2. NT-WS_2 was synthesized using a reported method by Therese et al. [20b].

Binding of MnO nanoparticles onto NT-WS_2. In a typical experiment 4 mg of NT-WS_2 were dispersed in 5 ml of toluene by sonicating the sample for 5-7 minutes. The solution was further degassed under argon for 10-15 minutes. In another centrifuge vial, 8 mg of MnO were dissolved in 5 ml of toluene. Subsequently, the solution was added dropwise to the degassed mixture of WS_2 in toluene over a period of 5-7 minutes. Then the whole reaction mixture was again degassed in argon for 5 minutes and was put in a shaker for 6 hours at room temperature (RT). After the reaction got over, the unbound MnO was washed out by centrifuging the sample thrice at 4000 rpm for 10 minutes. Finally the functionalized NT-WS_2 was characterized morphologically by TEM/HRTEM and EDX and SEM. Samples for TEM were prepared by putting 1-2 drops of dispersed sample on a copper TEM grid followed by drying. Similarly samples for SEM were prepared by putting a drop of dispersed sample.

Reversibility experiment. In a typical experiment, 10 mg of NT-WS_2/MnO nanocomposite was taken in a 50 ml flask and dispersed well with 10 mL of DMF by sonication followed by degassing the mixture in argon. In another flask 40 mg of 3-hydroxy tyramine hydrochloride (dopamine) was taken and dissolved in 10 mL of DMF. Then the dopamine solution was added dropwise to the mixture of NT-WS_2@MnO nanocomposite over a period of 10 min. The whole reaction mixture was heated up to 60 ºC and was stirred overnight. After the reaction got over the reaction mixture was washed by centrifuging the sample thrice at 4000 rpm for 10 minutes. The recycled WS_2, thus obtained, was used for further functionalized with fresh MnO as described above. Similarly the MnO was again fished out of the surface of WS_2 by using dopamine as anchor group in DMF as described above.

Functionalization of MnO @ NT-WS_2 nanocomposite with Dopamine-NBD. In a typical experiment, 4 mg of MnO@NT-WS_2 nanocompositae was taken in a centrifuge vial in 6 ml of DMF and sonicated for 5 minutes followed by degassing in argon for more 5 minutes. This followed by immobilization of 3-hydroxy tyramine for 4 hours and followed by addition of 4-chloro, 7-nitro benzofurazan (NBD) for another 4 hours. The final solution was centrifuged at 4000 rpm for 10 mins and was characterized by UV spectroscopy and CLSM to detect the presence of dopamine and NBD on the nanocomposite.

Nanoparticle characterization. The morphology and composition of the product obtained after functionalization was examined in transmission electron microscope (TEM), high resolution electron microscope (HRTEM, FEI Tecnai F30 ST operated at an extraction voltage of 300 kV, equipped with EDX and Scanning electron microscopy (SEM) was also used to examine the morphology of the product. Also the product was characterized by Ultraviolet-Visible (UV-Vis) spectroscopy, and confocal laser Scanning Microscopy (CLSM).

2.5. References

[1] (a) P. D. Cozzoli, T. Pellegrino, L. Manna, *Chem. Soc. Rev*. **2006**, *35*, 1195. (b) H. Zeng, S. Sun, *Adv. Funct. Mater*. **2008**, *18*, 391. (c) J. A. McGuire, J. Joo, J. M. Pietryga, R. Schaller, V. I. Klimov, *Acc. Chem. Res.* **2008**, *41*, 1810.

[2] (a) V. Subramanian, E. E. Wolf, P. V. Kamat, *J. Phys. Chem. B* **2003**, *107*, 7479. (b) T. Mokari, E. Rothenberg, I. Popov, R. Costi, U. Banin, *Science* **2004**, *304*, 1787. (c) T. Mokari, C. G. Sztrum, A. Salant, E. Rabani, U. Banin, *Nat. Mater*. **2005**, *4*, 855. (d) D. V. Talapin, H. Yu, E. V. Shevchenko, A. Lobo, C. B. Murray, *J. Phys. Chem. C* **2007**, *111*, 14049. (e) J. Yang, H. I. Elim, Q. Zhang, J. Y. Lee, W. Ji, *J. Am. Chem. Soc*. **2006**, *128*, 11921.

[3] A. Rizzo, C. Nobile, M. Mazzeo, M. De Giorgi, A. Fiore, L. Carbone, R. Cingolani, L. Manna, G. Gigli, *ACS Nano* **2009**, *3*, 1506.

[4] (a) K. Sudeep, S. T. S. Joseph, K. G. Thomas, *J. Am. Chem. Soc.* **2005**, *127*, 6516. (b) X. Huang, I. H. El-Sayed, W. Qian, M. A. El-Sayed, *J. Am. Chem. Soc.* **2006**, *128*, 2115.

[5] (a) M. Thomalla, H. Tributsch, *J. Phys. Chem. B* **2006**, *110*, 12167. (b) J.-P. Salvetat, J.-M. Bonard, N. H. Thomson, A. J. Kulik, L. Forrö, W. Benoit, L. Zuppiroli, *Appl. Phys. A* **1999**, *69*, 255.

[6] (a) I. Gorelikov, L. M. Field, E. Kumacheva, *J. Am. Chem. Soc.* **2004**, *126*, 15938. (b) A. K. Salem, P. C. Searson, K. W. Leong, *Nat. Mater*. **2003**, *2*, 668. (c) M. I. Shukoor, F. Natalio, P. Gupta, M. N. Tahir, H. A. Therese, S. Weber, S. Fischer, N. Metz, P. Theato, L. M. Schreiber, H. C. Schröder, W. E. G. Müller, W. Tremel, *Adv. Funct. Mater*. **2009**, *19*, 3717.

[7] (a) L. Margulis, G. Salitra, R. Tenne, M. Talianker, *Nature* **1993**, *365***,** 113. (b) A. Yella, E. Mugnaioli, M. Panthöfer, H. A. Therese, U. Kolb, W. Tremel, *Angew. Chem. Int. Ed.* **2009**, *48*, 6426.

[8] (a) Y. Feldman, E. Wasserman, D. J. Srolovitz, R. Tenne, *Science*, **1995**, *267***,** 222. (b) R. Tenne, M. Homyonfer, Y. Feldman, *Chem. Mater*. **1998**, *10*, 3225. (c) W. Tremel, *Angew. Chem.* **1999**, *111*, 2311; *Angew. Chem. Int. Ed.* **1999**, *38*, 2175.

[9] (a) Y. R. Hacohen, E. Grunbaum, R. Tenne, J. Sloan, J. L. Hutchison, *Nature* **1998**, *365*, 336. (b) A. Q. Zhu, T. Sekine, Y. H. Li, W. X. Wang, M. Y. Fay, H. Edwards, P. D. Brown, N. Fleischer, R. Tenne, *Adv. Mater.* **2005,** *17*, 1500. (c) I. Kaplan-Ashiri, S. R. Cohen, K. Gartsman, R. Rosentsveig, V. Ivanovskaya, T. Heine, G. Seifert, H. D. Wagner, R. Tenne, *Proc. Natl. Acad. Sci. USA* **2006**, *103*, 523.

[10] (a) L. Scheffler, R. Rosentzveig, A. Margolin, R. Popovitz-Biro, G. Seifert, S. R. Cohen, R. Tenne, *Phys. Chem. Chem. Phys.* **2002**, *4*, 2095. (b) M. Nath, S. Kar, A. K. Raychaudhuri, C. N. R. Rao, *Chem. Phys. Lett.* **2003**, *368*, 690.

[11] (a) F. Hulliger, *Structural Chemistry of the Layer-Type Phases, Ed.:* F. Levy, Reidel, 1976. (b) A. Katz, M. Redlich, L. Rapoport, H. D. Wagner, R. Tenne, *Tribol. Lett*. **2006**, *21*, 135.

[12] (a) M. N. Tahir, M. Eberhardt, N. Zink, H. A. Therese, U. Kolb, P. Theato, W. Tremel, *Angew. Chem.* **2006**, *118*, 4927; *Angew. Chem. Int. Ed.* **2006**, *45*, 4809. (b) M. N. Tahir, N. Zink, M. Eberhardt, H. A. Therese, U. Kolb, P. Theato, W. Tremel, *Small* **2007**, *3*, 829. (c) M. N. Tahir, M. Eberhardt, P. Theato, S. Faiß, A. Janshoff, T. Gorelik, U. Kolb, W. Tremel, *Angew. Chem.* **2006**, *118*, 922; *Angew. Chem. Int. Ed*. **2006,** *45*, 908. (d) M. N. Tahir, M. Eberhardt, H. A. Therese, U. Kolb, P. Theato, W. E. G. Mueller, H. C. Schroeder, W. Tremel, *Angew. Chem.* **2006**, *118*, 4921; *Angew. Chem. Int. Ed.* **2006**, *45*, 4803. (e) M. N. Tahir, F. Natalio, H. A. Therese, A. Yella, N. Metz, M. R. Shah, E. Mugnaioli, R. Berger, P. Theato, H. C. Schroeder, W. E. G. Müller, W. Tremel, *Adv. Funct. Mater.* **2009,** *19*, 285. (f) M. N. Tahir, A. Yella, H. A. Therese, E. Mugnaioli, M. Panthöfer, H. U. Khan, W. Knoll, U. Kolb, W. Tremel, *Chem. Mater*. **2009**, *21*, 5382.

[13] (a) I. Robel, B. A. Bunker, P. V. Kamat, *Adv. Mater.* **2005**, *17*, 2458. (b) S. Banerjee, S. S. Wong, *Nano Lett.* **2002**, *2*, 195. (c) L. Sheeney-Haj-Khia, B. Basnar, I. Willner, *Angew. Chem*. **2005**, *117*, 78; *Angew. Chem., Int. Ed.* **2005**, *44*, 78.

[14] D. Spetzler, J. York, D. Daniel, R. Fromme, D. Lowry, W. Frasch, *Biochemistry* **2006**, *45*, 3117.

[15] A. Gole, C. J. Murphy, *Langmuir* **2005**, *21*, 10756.

[16] B. F. Pan, L. M. Ao, F. Gao, H. Y. Tian, R. He, D. X. Cui, *Nanotechnology* **2005**, *16*, 1776.

[17] (a) J. Y. Chang, H. Wu, H. Chen, Y. C. Ling, W. Tan, *Chem. Commun.* **2005**, *8*, 1092. (b) K. K. Caswell, J. N. Wilson, U. H. F. Bunz, C. J. Murphy, *J. Am. Chem. Soc.* **2003**,

125, 13914. (c) A. K. Salem, M. Chen, J. Hayden, K. W. Leong, P. C. Searson, *Nano Lett.* **2004**, *4*, 1163.

[18] (a) M. Olek, T. Busgen, M. Hilgendorff, M. Giersig, *J. Phys. Chem. B* **2006**, *110*, 12901. (b) S. Banerjee, S. S. Wong, *Chem. Commun.* **2004**, 1866. (c) B. H. Juarez, C. Klinke, A. Kornowski, H. Weller, *Nano Lett.* **2007**, *7*, 3564. (d) Y. J. Na, H. S. Kim, J. J. Park, *Phys. Chem. C.* **2008**, *112*, 11218.

[19] (a) R. G. Pearson, *J. Am. Chem. Soc.* **1963**, *85*, 3533. (b) R. G. Pearson, *Chemical Hardness. Applications from Molecules to Solids*, Wiley-VCH, Weinheim 1997. (c) F. Umland, G. Wünsch, Charakteristische Reaktionen Anorganischer Stoffe, 2nd Ed.; Aula Verlag, Wiesbaden, 1991.

[20] (a) T. D. Schladt, T. Graf, W. Tremel, *Chem. Mater.* **2009,** *21*, 3183. (b) H. A. Therese, J. Li, U. Kolb, W. Tremel, *Solid State Sci.* **2005**, *7*, 67. (c) J. Etzkorn, H. A. Therese, F. Rocker, N. Zink, U. Kolb, W. Tremel, *Adv. Mater.* **2005**, *17*, 2372.

[21] (a) The associated valence tautomerism has been studied in depth for molecular compounds. First, they are unique model systems, which provide insight into the basic factors affecting intramolecular electron transfer in coordination complexes. Secondly, from an applied perspective, the large changes in the optical, structural, and magnetic properties that often accompany valence tautomeric interconversion have potential applications in bistable molecular switching materials and devices. (b) C. G. Pierpont, C. W. Lange, *Prog. Inorg. Chem.* **1994**, *41*, 331. (c) P. Gütlich, A. H. Hauser, H. Spiering, *Angew. Chem.* **1994**, *106*, 2109; *Angew. Chem. Int. Ed.* **1994**, *33*, 2024.

3. Soluble IF-ReS_2 Nanoparticles By Surface Functionalization With Terpyridine Ligands

Running Title: ReS_2-TerPy immobilization

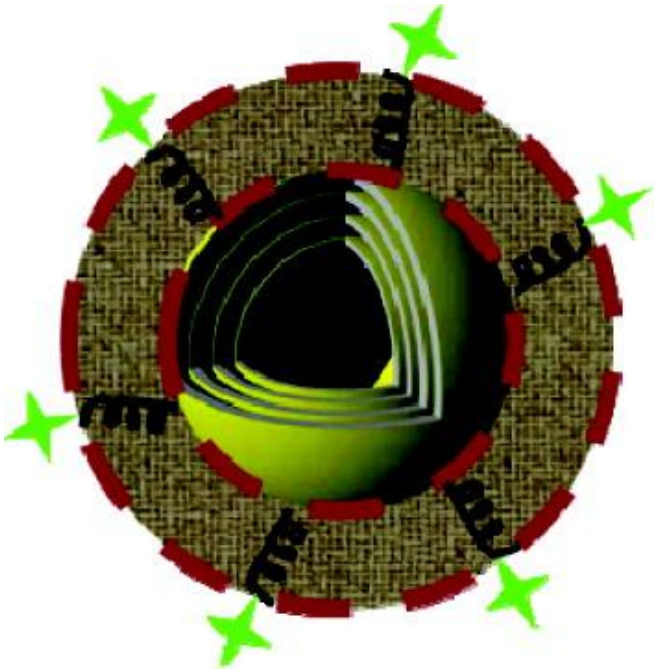

Jugal Kishore Sahoo[a], Muhammad Nawaz Tahir[a], Aswani Yella[a], Robert Branscheid[b], Ute Kolb[b], and Wolfgang Tremel[a].

[a]Institute for Inorganic and Analytical Chemistry

[b]Institute for Physical Chemistry,

Johannes Gutenberg-Universität, Mainz, Germany.

Langmuir 2011, 27 (1), pp 385–391

3.1. Introduction

Carbon nanotubes are an important component in the vastly growing field of nanotechnology. After their discovery by TEM and the invention of numerous large-scale production techniques, nanotubes are on the verge of finding their way into industrial products. Multi-walled carbon nanotubes (MWNTs) are being used for their high thermal conductivity and to add mechanical strength and electrical conductivity to polymer composites. The first real-market applications for carbon nanotubes have already been presented although many properties and fabrication processes are still under intensive research. However, if functional materials want to benefit from the outstanding mechanical and electronic properties of carbon nanotubes, much scientific skill must be devoted to their physical and chemical modification. This includes purification of the starting materials as well as the subsequent chemical surface modification. In general, carbon nanostructures can be functionalized by (i) covalent attachment of chemical groups through bonding to the π-conjugated skeleton of the CNT or (ii) non-covalent adsorption or wrapping of various functional molecules [1-6]. The organic functionalization proceeds via amidation and esterification of the nanotube-bound carboxy groups. Only the solubility of these functionalized carbon nanotubes makes a study of the properties of carbon nanotubes using solution-based techniques possible.

Chalcogenide nanoparticles are the inorganic congeners of carbon nanotubes and nested fullerenes. Inorganic nanotubes (INT) and fullerene-like (IF) nanoparticles are hollow closed structures, which are usually produced from compounds with layered (2D) structures [7], like NbS2 [8], MoS_2 [9], WS_2 [10], ReS_2 [11], or layered oxide/hydroxides such as $Al(OH)_3$ [12], imogulite [13], or TiO_2 [14]. The underlying idea for the synthesis of such hollow nanostructures from layered materials was that in analogy to carbon fullerenes - nanoparticles of layered compounds suffer from inherent chemical instability in their planar form due to their abundant rim atoms. This chemical instability is alleviated by folding and the formation of seamless hollow nanoparticles, which are nevertheless elastically strained. In some favorable cases, the structures and growth mechanism of nested fullerene and nanotube particles were elucidated in some detail [15].

Different from the corresponding carbon nanostructures, the inertness of the (chalcogen) surface makes the targeted surface modification of layered chalcogenide nanostructures a

tedious task. The sulfur atoms sterically shield the metal atoms from nucleophilic attack by organic ligands [16]. Therefore the functionalization of such nanoparticles requires a strategy where the outer "anionic" sulfide layer is attacked by an electrophile, e.g. chalcophilic metal. In order to prevent a cross-linking and subsequent precipitation of the IF-chalcogenide nanoparticles through the remaining vacant coordination sites of the chalcophilic metal, a half-sandwich type of complex must be used where one half of the metal coordination sphere is blocked by a multidentate ligand [17]. This functionalization was realized recently using a nitrilotriacetic acid (NTA) ligand that is typically used in connection with Ni^{2+} and a so-called his-tag for protein purification [18]. Nickel has strong binding affinity to NTA. By conjugating NTA to organic molecules or polymers this functionalization strategy was out on a broader basis (i) to improve the solubility of metal chalcogenides [19], (ii) to produce WS_2/TiO_2 chalcogenide/oxide nanocomposites [20], and (iii) to immobilize proteins onto chalcogenide surfaces [21]. A reversible functionalization of WS_2 chalcogenide nanotubes could be achieved using metal oxide nanoparticles tubes based on Pearson hardness [22].
Here we report a new approach for functionalizing nested chalcogenide nanoparticles using common and commercially available terpyridine (TerPy) ligands that are known to have large complexation constants for metals such as iron or ruthenium [23]. These TerPy ligands cap one half of the coordination sphere of the metal (Fe, Ru) in a half-sandwich-like fashion [24], whereas the second half sphere remains open for docking to the sulfur layer. The central pyridine ring of the TerPy ligand may be functionalized in order to impart various functions (e.g. solubility, fluorescence/optical tracer) to the chalcogenide nanoparticle [25].

3.2. Results and Discussions.

IF-ReS_2 particles were prepared as described previously by a MOCVD method [11]. TerPy – NBD (5) was prepared by reaction of NBD-Cl with 1-amino-5-(2, 2': 6', 2''-terpyrid-4'-yl-oxy) pentane (2) as illustrated in Scheme 3.1 [26, 27]. Details concerning the synthesis of the starting materials, the functionalization and the characterization of the products (Appendix A1-A7) are given in Appendix.

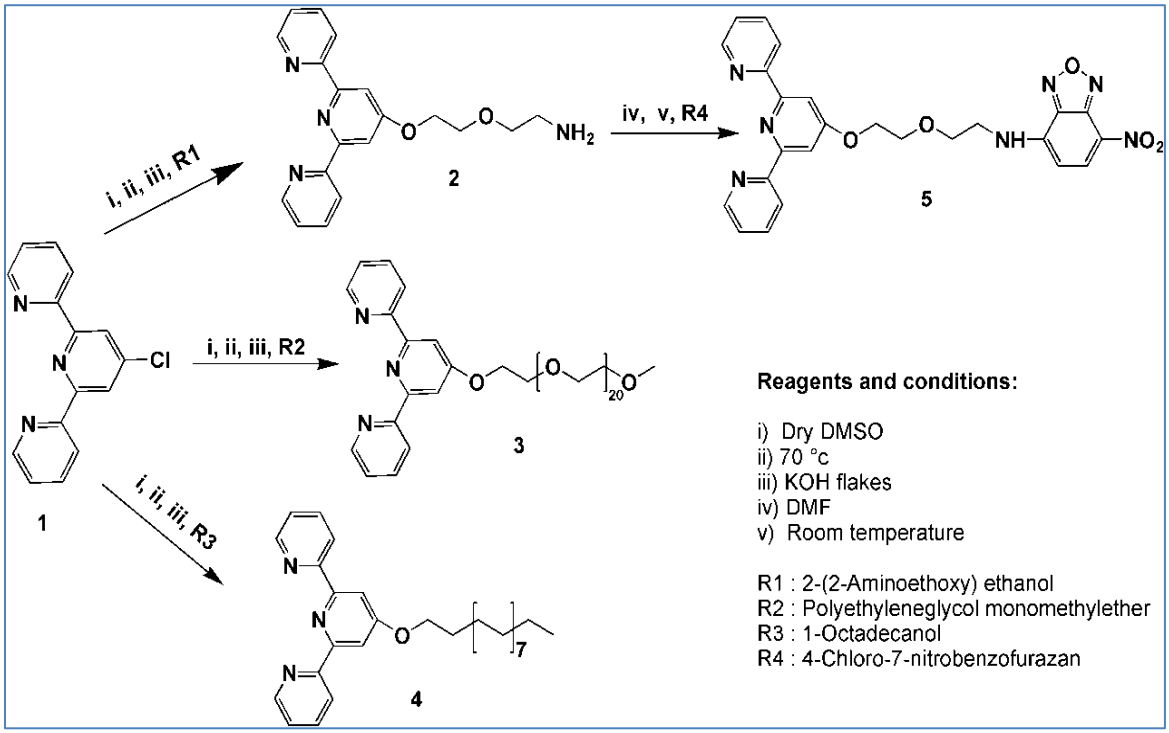

Scheme 3.1. *Synthesis of the TerPy ligands [26,27] for the functionalization of IF-ReS$_2$.*

In a typical functionalization procedure IF-ReS$_2$ was dispersed under sonication in ethanol followed by addition of stoichiometric amounts of Mohr's salt and subsequently TerPy-EG-NBD under argon and heated to reflux. Mohr's salt and TerPy-NBD were taken in a 1:1 stoichiometric ratio to avoid the formation of the fully coordinated iron complex [Fe (TerPy-NBD)$_2$]$^{2+}$. The functionalization of IF-ReS$_2$ is illustrated in Scheme 3.2. The product, TerPy-NBD functionalized IF-ReS$_2$, was characterized by UV-VIS and IR spectroscopy, CLSM, (HR) TEM and EDX.

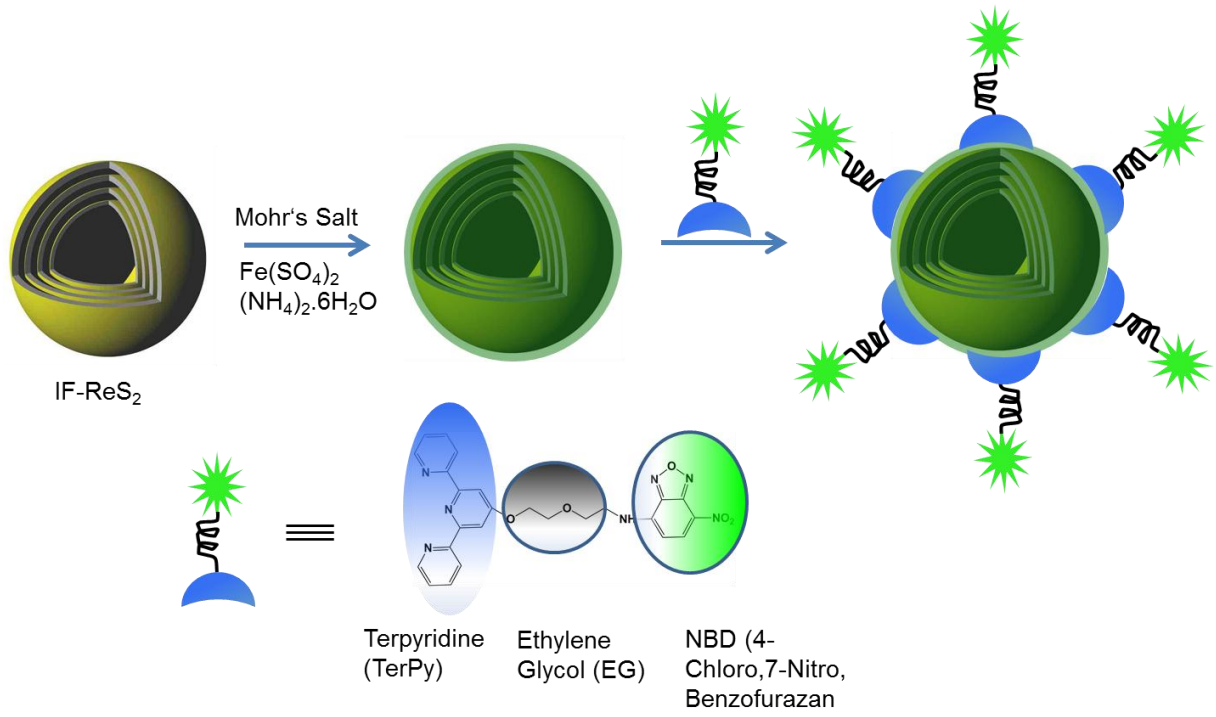

***Scheme 3.2**. Functionalization of IF-ReS$_2$ using a TerPy ligand with an ethylene glycol chain and a NBD fluorophore.*

The functionalized IF-ReS$_2$ could easily be dispersed in various organic solvents like dimethylformamide (DMF), dimethylsulfoxide (DMSO), $CHCl_3$, tetrahydrofurane (THF), ethanol etc. The stable dispersions were characterized by UV-VIS spectroscopy, confocal laser scanning microscopy (CLSM), transmission electron microscopy (TEM), energy dispersive X-ray analysis (EDX) and atomic absorption spectroscopy (AAS).

Figure 3.1a shows a TEM overview image of functionalized IF-ReS$_2$ particles with a diameter of approx. 20 nm. In order to confirm that the binding of the TerPy ligand to the IF-ReS$_2$ nanoparticles was achieved by chelation to IF-ReS$_2$ through iron, AAS (Appendix A12) and EDX analyses were performed. The EDX spectrum of the circled area is marked in Figure 3.1c. Both methods, EDX and AAS, confirm the presence of iron on the functionalized IF-ReS$_2$ thereby validating the surface binding of Fe-TerPy.

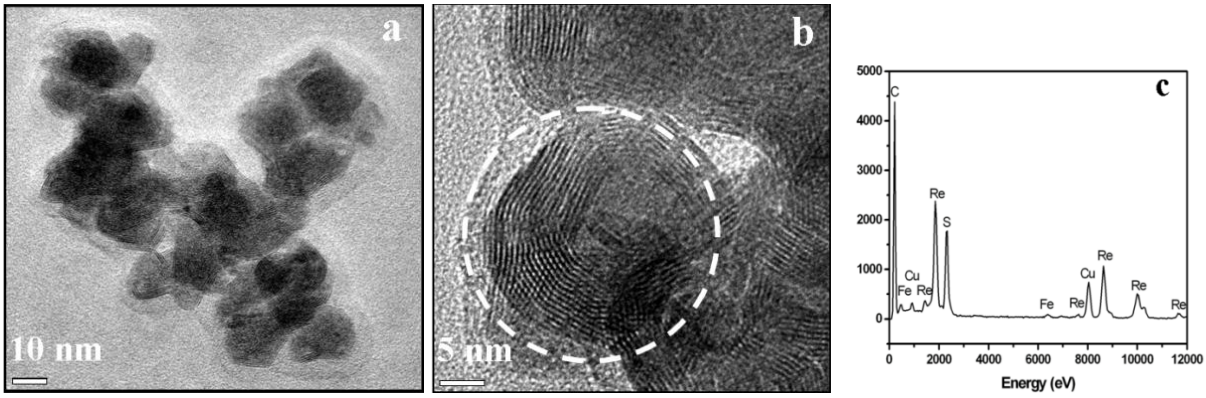

Figure 3.1. *(a)TEM overview and (b) HRTEM images of functionalized IF-ReS$_2$ nanoparticles. (c) EDX spectrum of the area marked by the circle in (b).*

A first visual indication of the successful surface functionalization of IF-ReS$_2$ was based on the solubility of the functionalized IF-ReS$_2$ nanoparticles in water and hexane. Because of its hydrophobicity, IF-ReS$_2$ is completely insoluble in water, whereas it can be dispersed in nonpolar solvents like hexane. After surface functionalization with TerPy-PEG, IF-ReS$_2$ can be transferred from non-polar hexane to the polar aqueous phase. The dark-brown color of the solution arises from the ligand-to-metal charge-transfer interaction of IF-ReS$_2$ and surface bound Fe^{2+} ions. The solubility properties of the functionalized IF-ReS$_2$ nanoparticles are mainly determined by the functional groups of the surface ligand.

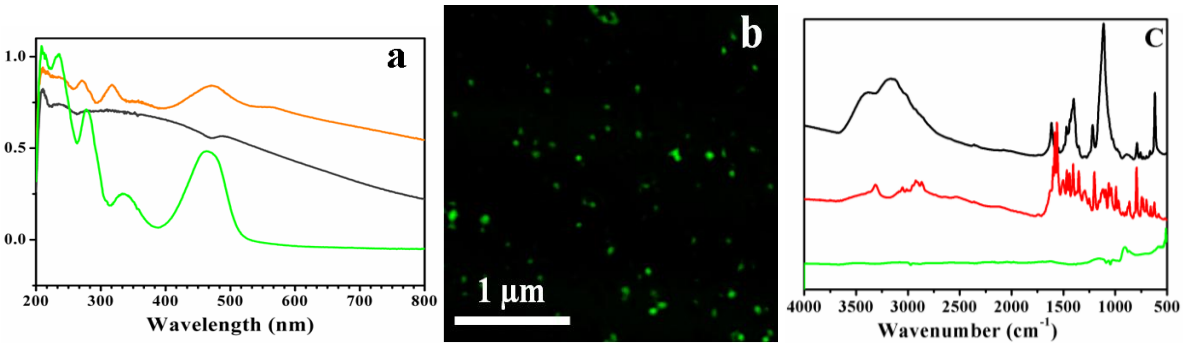

Figure 3.2*. (a)UV-vis spectra of TerPy-NBD functionalized IF-ReS$_2$ (orange line), Unfunctionalized IF-ReS$_2$ (black line), and pure ligand TerPy-NBD (5) (green line). (b) CLSM image of TerPy-NBD functionalized IF-ReS$_2$. (c) FT-IR spectrum of TerPy-amine*

functionalized IF-ReS_2 (black line), the unfunctionalized IF-ReS_2 (green line) and the pure TerPy-amine (red line).

The UV-vis spectra in Figure 3.2a show the characteristic broad absorption band of IF-ReS_2 at about 500 nm (black line), the green line corresponds to the ligand TerPy-NBD. The orange line corresponds to the TerPy-NBD functionalized IF-ReS_2. The weak visible absorption of TerPy-NBD functionalized IF-ReS_2 is an overlay of the allowed metal-to-ligand charge-transfer (MLCT) transitions (roughly between 290 and 330 nm) involving d-π Fe orbitals as the donor orbitals and π* terpyridine orbitals as acceptor orbitals. Such an assignment is based on the absence of visible bands in the absorption spectra of the free TerPy ligand (green line) at 260 nm, 240 nm, and 229 nm as described by Nakamoto [28]. The absorption band at 460 nm is assigned to the TerPy bound NBD fluorphor.

Final evidence for the surface modification of IF-ReS_2 was obtained from confocal laser scanning microscopy (CLSM) where the green NBD fluorophore tagged to IF-ReS_2 could be observed. Figure 3.2b shows the CLSM image of IF-ReS_2 after surface functionalization with TerPy-NBD which exhibits strong fluorescence when bound to primary amine groups. A 10 µL droplet of the sample was placed and dispersed carefully on a thin glass slide and the solvent was evaporated. The fluorescence of the NBD dye was excited at 514 nm and detected from 520 - 540 nm. A 40x (NA 1.25) oil immersion objective was used for the imaging [29]. It is reasonable from the fluorescence image that the IF-ReS_2 nanoparticles are fully coated with TerPy-NBD complex (**5**) via the Fe^{2+} connector ion. It is, however, difficult to comment on the actual size of the functionalized nanoparticles because they are beyond the resolution limits of CLSM. A control measurement was done with no TerPy-NBD bound to IF-ReS_2 (Appendix A13), where no fluorescence was observed.

Further evidence of the surface functionalization of IF-ReS_2 was obtained by IR spectroscopy (Figure 3.2c). The most prominent bands in the 3500-3300 cm^{-1} region arise from NH_2 stretching vibrations of the TerPy ligand, the bands at 2926 and 2855 cm^{-1} can be assigned to the stretching vibrations of the CH_2 groups, the bands in the region 1750–1250 cm^{-1} correspond to bending vibrations of amine as well as C-O, CH_2 of the terpyridine end group. A shift of the C=C and C=N stretch vibrations for the metal complexes compared to the free ligand (region between 1650 and 1550 cm^{-1}) is compatible with a complete complex formation.

In order to estimate the amount of ligand attached to the IF-ReS$_2$ surface, we performed a thermogravimetric analysis (DTA/TG) as shown in Appendix A14 (Supplementary Information). The IF-ReS$_2$/Fe^{+2}/TerPy composite exhibits two thermal responses. The thermal decomposition of the ligand begins at 220 °C and is finished around 490°C. It is also consistent with the reported data that iron coordinated TerPy amine starts decomposing above 200 °C [30]. The final signal around 670 °C may be related to an ordering of the IF-ReS$_2$ nanoparticles. The associated weight loss indicates that the amount of the ligand is comparable to the amount of IF-ReS$_2$ which means the TerPy ligand covers the surface of the fullerenes almost completely.

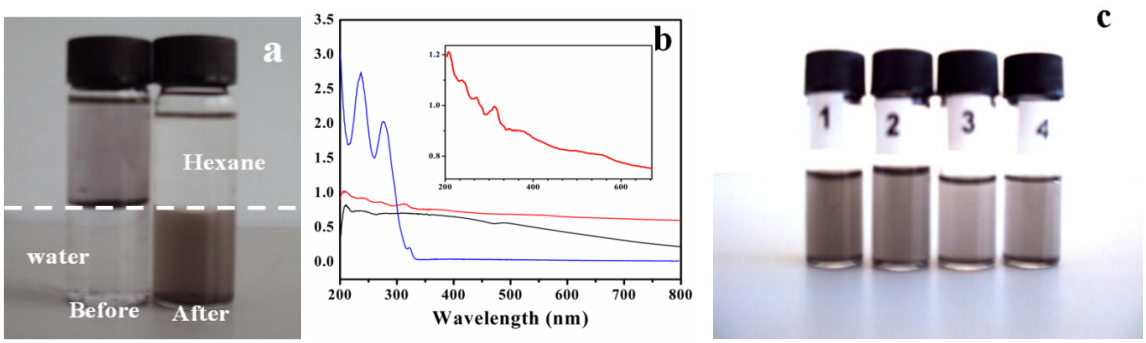

Figure 3.3. *(a) Distribution of IF-ReS$_2$ in water-hexane before and after PEGylation. (b) UV-VIS spectra of TerPy-PEG (3) functionalized IF-ReS$_2$ (red line), unfunctionalized IF-ReS$_2$ (black line), and pure ligand (TerPy-PEG). (c) Stable dispersions of IF-ReS$_2$ in DMSO (1), DMF (2), THF (3) and CHCl$_3$ (4, from left to right). The solubility corresponds to the polarity of the solvents.*

An IF-ReS$_2$ particle, which has an average diameter of 20 nm and approx. 10 layers, has a mass of about 23 x 10^{-6} g/particle, which is approximately 7 x 10^4 times the molar mass of a ligand molecule (336 g/mol). Therefore, each IF-ReS$_2$ particle is covered by about 7 x 10^4 ligand molecules. We can assume that most of the TerPy anchor groups are attached to the surface. With an approximate surface area of 3000 nm^2 of an IF-ReS$_2$ particle we derive a surface area of approx. 0.04 nm^2 for a ligand molecule, if full surface coverage is assumed. However, as the monomer is not likely to be attached homogeneously around the nanoparticle surface, a somewhat lower coverage may by possible. The small surface area value obtained for a single monomer unit indicates an almost full surface coverage by the surface ligands.

A similar functionalization procedure was pursued to endow IF-ReS$_2$ with water solubility by PEGylation and to improve its stability in different polar organic solvents such as DMSO,

DMF, THF (or $CHCl_3$ for comparison, see Figure 3.3a and c). For this purpose, polyethylene glycol monomethyl ether proved to be a useful starting material. The different functional groups at the chain ends allow a facile functionalization with two different functionalities, in the present case terpyridine and the benzofurazene derivative NBD. In the first step, the hydroxy group of polyethylene glycol monomethyl ether was functionalized with a terpyridine moiety through a nucleophilic aromatic substitution on 4´-chloro, 2, 2'; 6', 2''-terpyridine in DMSO in the presence of KOH for 7 h at 70 °C (see Scheme 3.1). The resulting terpyridine-functionalized compound **3**, which contains a methoxy group for further functionalization, was obtained in 80% yield after extraction with CH_2Cl_2, followed by precipitation in diethyl ether. The polymeric product **3** was characterized by ^{1}H NMR, FT-IR, and UV/vis spectroscopy. The functionalization of IF-ReS_2 was performed by sonication in ethanol for 15 min, followed by degassing under argon for another 15 min. Mohr's salt in water was added dropwise in 10 min. Subsequently, the system was allowed to reflux under argon before adding TerPy-PEG ligand. The reaction was allowed to reflux for 4 h followed by centrifuging in ethanol. The PEGylated IF-ReS_2 was characterized by UV-vis spectroscopy (Figure 3.3b), where the terpyridine bands are now clearly visible. The functionalization was confirmed based on the distribution of PEGylated IF-ReS_2 in water and hexane (Figure 3.3a). The stability and dispersibility of the PEGylated IF-ReS_2 was examined in different polar organic solvents such as DMSO, DMF, THF and $CHCl_3$ (Figure 3.3c). The solubility in these solvents corresponded to their polarity. All dispersions remained stable for at least one week.

A similar modification strategy was emplyed to improve the solubility of IF-ReS_2 in hydrophobic solvents such as hexane, cyclohexane, 1, 4-dioxane and toluene. A tailor-made surface ligand was synthesized by taking 1-octadecanol as starting precursor. The hydroxyl group of 1-octadecanol was further exploited for nucleophilic substitution by 4-chloro, 2, 2': 6', 2''-terpyridine (1) to form 18-(2, 2': 6', 2''-terpyrid-4'-yl-oxy) octadecane (**4**) (Scheme 3.1). This hydrophobic chain with 18 CH_2 units introduces hydrophobicity to the metal chalcogenide nanostructures. Typically 5 mg of IF-ReS_2 was dispersed in ethanol by sonication for 15 min. followed by degassing under argon for another 15 min. Before addition of Mohr's salt the surface ligand (4) was added dropwise to the reaction mixture under reflux. A detailed description of the individual steps is provided in the experimental section. After functionalization the dispersibility and stability of the modified IF-ReS_2 was studied in various non-polar solvents such as hexane, cyclohexane, 1,4-dioxane and toluene (Figure 3.4). The stable dispersion in these hydrophobic solvents is inverse to their polarity.

Figure 3.4. *Stable dispersions of IF-ReS$_2$ in hexane (**1**), cyclohexane (**2**),1,4-dioxane (**3**) and toluene (**4**) (from left to right).*

3.3. Summary and Outlook.

The functionalization protocol using the Fe^{2+}-TerPy unit described in this work can be generalized for all layered chalcogenide nanoparticles. In addition, the TerPy "anchor group" might be replaced by a range of related ligands like bispyridine (bipy) or 1, 10-phenanthroline (phen), which brings the surface functionalization of layered chalcogenide nanoparticles into the realm of inorganic coordination chemistry. The functionalization of fullerene-type chalcogenide nanoparticles opens new fields of application for this class of materials e.g. in electronically active components (metal and semiconductors nanoparticles, light harvesting ligands for solar cell applications), dispersion of nanoparticles, e.g. for an integration in composites which is of interest because of their exceptional tribological and mechanical properties [31-34]. Furthermore, it allows the fabrication of thin films by surface binding of chalcogenide particles to oxide surfaces, which might allow their use as lubricants on seemingly incompatible ceramic materials.

3.4. Experimental Section

Methods and Materials

4-Chloro-2, 2': 6', 2''-terpyridine (Sigma-Aldrich, 99 %), 2-(2-Aminoethoxy) ethanol, (Acros Organic, 98%), Polyethylene glycol monomethyl ether (Sigma-aldrich), 1-octadecanol, (Sigma-aldrich) dimethylsulfoxide (DMSO, Anhydros, Acros Organics), 4-chloro, 7-nitro, benzafurazan (Sigma-Aldrich) were purchased and used as received without further purification. Solvents such as ethanol, chloroform, DMF, dichloromethane, methanol, diethyl ether were purchased technical grade and used as received.

Synthesis of 1-amino-5-(2, 2': 6', 2''-terpyrid-4'-yl-oxy) pentane (2).

The synthesis of this compound was carried out following literature [26b]. In a typical experiment 1.6 mg (in excess) of ground KOH flakes were weighed and added to a 3 neck round bottom flask and dispersed in anhydrous DMSO at 60°C for 15 min followed by addition of 2-(2-aminoethoxyethanol) (1 mM) onto the reaction chamber. The reaction was allowed for 30 min., before adding 4'-chloro, 2, 2': 6', 2''- terpyridine (1 mM) into the reaction chamber. The reaction was carried out at 70°C for 6h. After the reaction got over, the flask was allowed to cool down to room temperature before addition of 120 ml of milipore water. The reaction was mixture was extracted in dichloromethane (3 x 30 ml). The organic fraction was collected and dried in anhydrous sodium sulphate followed by evaporating the solvent in a rotary evaporator. The crude product was purified by column chromatography (DCM: methanol, 9:1). The purified compound was further characterized by ^{1}H NMR, FD-MS, IR, and UV-vis spectroscopy.

^{1}H NMR (400 MHz, DMSO-d_6): 2.7 (t, 2H, CH_2, H_d),3.2 (s, broad, NH_2), 3.5 (t, 2H, CH2, H_c), 3.82 (t, 2H, CH2, H_b), 4.35 (t, 2H, CH_2, H_a), 7.5 (ddd, 2H, CH_{terpy}, $H_{5,5''}$), 7.98 (s, 2H, CH_{terpy}, $H_{3',5'}$), 8.00 (m, 2H, CH_{terpy}, $H_{4,4''}$), 8.62 (d, 2H, CH_{terpy}, $H_{3,3''}$), 8.72 (dd, 2H, CH_{terpy}, $H_{6,6''}$). (Appendix A1)

FD-MS: [M+H] = 337 g/mol (Appendix A5)

Synthesis of 1-(2, 2': 6', 2''-terpyrid-4'-yl-oxy)polyethylene glycol 1000 monomethyl ether (3). The synthesis was carried out following reported procedure [27]. In a typical synthesis procedure 1.6 mg (in excess) of ground KOH flakes were weighed into the 100 ml round bottom flask and dispersed at 60°C for 15 min in anhydrous DMSO. After 15 min polyethylene glycol 1000 monomethyl ether (1 mM) was added into the reaction chamber,

and the solution was stirred for 30 min before adding 4'-chloro- 2, 2': 6',2''-terpyridine (1 mM). The reaction was stirred at 70°C for 6 h. After the reaction was complete, the flask was allowed to cool down to room temperature before adding 120 ml of millipore water. The crude product was extracted in dichloromethane (3 x 30 ml) in a separating funnel. The solution was dried in anhydrous sodium sulphate followed by evaporating the solvent in rotary evaporator. The crude product was purified by precipitating the compound in diethyl ether and followed by filteration. The purified compound was characterized by ^{1}H NMR, UV-visible spectroscopy.

^{1}H NMR (400 MHz, D_2O): 3.32 (s, 3H, OCH_3, H_e),3.4-3.8 (m, PEG units), 7.5 (ddd, 2H, CH_{terpy}, $H_{5\ ,5''}$), 7.98 (s, 2H, CH_{terpy}, $H_{3',\ 5'}$), 8.00 (m, 2H, CH_{terpy}, $H_{4,4''}$), 8.62 (d, 2H, CH_{terpy}, $H_{3,\ 3''}$), 8.72 (dd, 2H, CH_{terpy}, $H_{6,\ 6''}$). (Appendix A2)

Synthesis of the 1-(2, 2': 6', 2''-terpyrid-4'-yl-oxy) Octadecane. (4) In a typical experiment 1.6 mg (in excess) of ground KOH flakes were weighed and added to a 3 neck round bottom flask and dispersed in anhydrous DMSO at 60°C for 15 min followed by addition of 1-Octadecanol (1 mM) onto the reaction chamber. The reaction was allowed to stir for 30 min., before adding 4'-chloro, 2, 2': 6', 2''- terpyridine (1mM) into the reaction chamber. The reaction carried out at 70°C for 6h. After the reaction got over, the flask was allowed to cool down to room temperature before addition of 120 ml of milipore water. The reaction was mixture was extracted in dichloromethane (3 x 30 ml). The organic fraction was collected and dried in anhydrous sodium sulphate followed by evaporating the solvent in a rotary evaporator to get the desired product.

^{1}H NMR (400 MHz, $CDCl_3$): 0.86 (t, 3H, CH_3, H_f),1.22 (m, 28H, CH2, Hc,d), 1.24 (m, 2H, CH_2, H_e), 1.8 (m, 2H, CH_2, H_b), 4.22 (t, 2H, OCH2, H_a), 7.5 (ddd, 2H, CH_{terpy}, $H_{5\ ,5''}$), 7.88 (m, 2H, CH_{terpy}, $H_{4,\ 4''}$), 8.00 (m, 2H, CH_{terpy}, $H_{3',5''}$), 8.62 (d, 2H, CH_{terpy}, $H_{3,\ 3''}$), 8.66 (dd, 2H, CH_{terpy}, $H_{6,\ 6''}$). (Appendix A3)

FD-MS: [M+H] = 501 g/mol (Appendix A6)

Synthesis of the terpyridine-NBD complex. (5)The synthesis was carried out following standard procedure [19]. In a typical experiment 1-amino-5-(2, 2': 6', 2''-terpyrid-4'-yl-oxy) pentane was dissolved in DMF and was cooled to 0 °C. 4'-Chloro-7-nitro-benzafurazan was added to the reaction dropwise over a period of 15 min. Subsequently the reaction mixture was allow to heat up to room temperature and stirred overnight. The solvent was evaporated by rotary evaporation, and the crude product was purified by precipitating in diethyl ether.

The obtained compound was characterized by ^{1}H NMR, FD-MS, IR, and UV-visible spectroscopy.

^{1}H NMR (400 MHz, DMSO-d_6): 3.10 (m, 2H, CH_2, H_d), 3.4 (t, 2H, CH_2, Hc), 3.85 (m, 2H, CH_2, H_b), 4.4 (m, 2H, CH_2, H_a), 6.42 (d, 1H, CH, H_e), 7.5 (ddd, 2H, CH_{terpy}, $H_{5\,,5''}$), 7.88 (s, 2H, CH_{terpy}, $H_{3',5'}$), 8.00 (m, 2H, CH_{terpy}, $H_{4,4''}$), 8.4 (d,1H, CH, H_f), 8.58 (d, 2H, CH_{terpy}, $H_{3,\,3''}$), 8.66 (m, 2H, CH_{terpy}, $H_{6,\,6''}$). (Appendix A4)

FD-MS: [M+H] = 499 g/mol (Appendix A7)

Synthesis of IF-ReS_2. IF- ReS_2 was synthesized following reported synthetic procedure [11]. Firstly, a MOCVD synthesis (e.g. at 750°C, reaction time 2h) was carried out and the resulting material – collected from the inner walls of the small glass cylinder – was subjected to thermal annealing (e.g. at 800°C for 1h under Ar) in a conventional tube furnace.

In a typical MOCVD run 0.150g of $Re_2(CO)_{10}$ (Aldrich, 99%) and 0.256 g of S (Alfa Aesar, 99,5%+, -100 mesh, sublimed) were weighed in and inserted into the setup under constant Ar flow. Prior to the synthesis the setup was flushed with Ar for at least 30 min. Subsequently, the graphite receptor was heated to the desired reaction temperature (temperature at the graphite receptor (T_{ind}) = 550, 650, 750, and 850°C respectively) by induction. Once the appropriate reaction temperature was reached, the precursors were heated. The heating rates were chosen in such a way that both reactants reached their final temperature in about the same time in order to provide a homogeneous reaction mixture for the whole duration of the experiment. The possibility of fast heating/cooling of the reaction zone makes this induction heated setup advantageous as compared to a slow tube furnace because "quenching" of the reaction is possible at any time. This allowed us to monitor the structure of the reaction products as a function of the reaction time by taking samples after given time intervals.

Annealing of the samples was performed by taking the sample from the MOCVD setup in a corundum boat and placing it in the middle of the horizontal tube furnace at the specified temperature with a heating rate of 5°C per minute under constant Argon gas flow of 100 sccm for 1h.

Functionalization of IF-ReS_2 using the NBD-terpyridine ligand (5).

In a typical experimental procedure, 10 mg of IF-ReS_2 were taken in a Schlenk flask and dispersed in ethanol under sonication for 15 min followed by degassing the mixture under argon for another 10 min. The reaction flask was connected to reflux condenser under flowing argon. The dispersed IF-ReS_2 was allowed to stir for 5 min under argon followed by addition

of Mohr' s salt (32 mg in 2 ml of millipore water) under flowing argon. The reaction chamber was allowed to reflux. After 1 h refluxing 30 mg of the terpyridine-NBD complex in 10 ml of ethanol were added dropwise to the reaction mixture followed by refluxing for another 4 h. After the reaction was complete, the flask was allowed to cool to room temperature, and the product was separated and purified by three dispersion/centrifugation cycles (washing with ethanol followed by centrifugation at 4000 rpm ethanol).

Functionalization of IF-ReS_2 using the the terpyridine-PEG ligand (3).

In a typical experimental procedure, 10 mg of IF-ReS_2 was taken in a Schlenk flask and dispersed in ethanol under sonication for 15 min followed by degassing the mixture under argon for another 10 min. The reaction flask was connected to reflux condenser under flowing argon. The dispersed IF-ReS_2 was allowed to stir for 5 min under argon followed by addition of Mohr' s salt (32 mg in 2 ml of millipore water) under flowing argon. The solution was refluxed for 1 h; subsequently 30 mg of the terpyridine-PEG complex in 10 ml of ethanol were added dropwise to the reaction mixture, followed by refluxing for another 4 h. After the reaction was complete, the solution was allowed to cool to room temperature, and the product was separated and purified by three dispersion/centrifugation cycles (washing with ethanol followed by centrifugation at 4000 rpm ethanol).

Functionalization of IF-ReS_2 using 1-(2, 2': 6', 2''-terpyrid-4'-yl-oxy) Octadecane (4).

In a typical experimental procedure, 10 mg of IF-ReS_2 was taken in a Schlenk flask and dispersed in ethanol under sonication for 15 min followed by degassing the mixture under argon for another 10 min. The reaction flask was connected to reflux condenser under flowing argon. The dispersed IF-ReS_2 was allowed to stir for 5 min under argon followed by addition of Mohr' s salt (32 mg (0.08 mM) in 2 ml of millipore water) under flowing argon. The solution was refluxed for 1 h; subsequently 40 mg (0.08 mM) of the terpyridine-PEG complex in 10 ml of ethanol were added dropwise to the reaction mixture, followed by refluxing for another 4 h. After the reaction was complete, the solution was allowed to cool to room temperature, and the product was separated and purified by three dispersion/centrifugation cycles (washing with ethanol followed by centrifugation at 4000 rpm ethanol).

Nanoparticle Characterization. The morphology and composition of the product obtained after the functionalization were examined using transmission electron microscopy (TEM) and high resolution electron microscopy (HRTEM, FEI Tecnai F30 ST operated at an extraction voltage of 300 kV, equipped with EDX and scanning electron microscopy (SEM). In addition,

the products were characterized spectroscopically by UV-Vis, IR, and atomic absorption spectroscopy (AAS) and microscopically by confocal laser scanning microscopy (CLSM), transmission electron microscopy (TEM), and high resolution transmission electron microscopy (HRTEM).

3.5. References

[1] (a) A. Hirsch, *Angew. Chem. Int. Ed.*, **2002**, *41*, 1853. (b) Y. Liu, Z. Yao, A. Adronov, *Macromolecules* **2005**, *38*, 1172.

[2] (a) A. Hirsch, O. Vostrowsky, *Top. Curr. Chem*. **2005**, *245*, 193. (b) Y. Sun, K. Fu, Y. Lin, W. Huang, *Acc. Chem. Res*. **2002**, *35*, 1096.

[3] (a) D. Tasis, N. Tagmatarchis, A. Bianco, M. Prato, *Chem. Rev.* **2006**, *106*, 1105. (b) H. Wu, X. Chang, L. Liu, F. Zhaoa, Y. Zhao, *J. Mater. Chem*. **2010**, *20*, 1036. (c) K. M. Lee, L. Li, L. Dai, *J. Am. Chem. Soc*. **2005**, *127*, 4122.

[4] (a) M. Prato, K. Kostarelos, A. Bianco, *Acc. Chem. Res.* **2008**, *41*, 60. (b) S. Ciraci, S. Dag, T. Yildirim, O. Gülseren, R. T. Senger, *J. Phys. Condens. Matter*. **2004**, *16*, R901.

[5] K. L. Klein, A. V. Melechko, T. E. McKnight, S. T. Retterer, P. D. Rack, J. D. Fowlkes, D. C. Joy, M. L. Simpson, *J. Appl. Phys.* **2008**, *103*, 061301.

[6] D. Eder, *Chem. Rev.* **2010**, *110*, 1348.

[7] W. Tremel, *Angew. Chem.* **1999,** *111*, 2311; *Angew. Chem. Int. Ed*. **1999**, *38*, 175.

[8] C. Schuffenhauer, R. Popovitz-Biro, R. Tenne, *J. Mater. Chem*. **2002**, *12*, 1587.

[9] L. Margulis, G. Salitra, R. Tenne, M. Talianker, *Nature* **1993**, *365*, 113. (b) H. A. Therese, N. Zink, U. Kolb, W. Tremel, *Solid. State Sci*. **2006**, *8*, 1133. (c) I. Wiesel, H. Arbel, A. Albu-Yaron, R. Popovitz-Biro, J. M. Gordon, D. Feuermann, R. Tenne, *Nano Res.* **2009**, *2*, 416. (d) X. Lin Li, Y. Dong Li, *Chem. Eur. J.* **2003**, *9*, 2726.

[10] H. A. Therese, J. Li, U. Kolb, W. Tremel, *Solid. State Sci*. **2005**, *7*, 67. (b) J. Chen, S. Li, F. Gao, Z. Tao, *Chem. Mater.* **2003**, *15*, 1012. (c) M. Remskar, M. Virsek, A. Jesih, *Nano. Lett.* **2008**, *8*, 76. (d) R. Tenne, L. Margulis, M. Genut, G. Hodes, *Nature* **1992**, *360*, 444.

[11] A. Yella, H. A. Therese, N. Zink, M. Panthöfer, W. Tremel, *Chem. Mater*. **2008,** *20*, 3587.

[12] B. Alinejad, K. Mahmoodi, K. Ahmadi, *Mater. Chem. Phys.* **2009**, *118*, 473.

[13] A. Kuc, T. Heine, *Adv. Mater.* **2009**, *21*, 4353.

[14] G. Armstrong, R. A. Armstrong, J. Canales, P. G. Bruce, *Chem. Commun.* **2005**, 2454.

[15] (a) A. Zak, Y. Feldman, V. Alperovich, R. Rosentsveig, and R. Tenne, *J. Am. Chem. Soc.* **2000**, *122*, 11108. (b) A. Rothschild, J. Sloan, R. Tenne, *J. Am. Chem. Soc.* **2000**,

122, 5169. (c) Y. Feldman, E. Wasserman, D. J. Srolovitz, R. Tenne, *Science* **1995**, *267*, 222.

[16] B.A. Rozenberg, R. Tenne. *Prog. Polym. Sci*. **2008**, *33*, 40.

[17] M. N. Tahir, M. Eberhardt, N. Zink, H. A. Therese, U. Kolb, P. Theato, W. E. G. Müller, H. C. Schröder, W. Tremel, *Angew. Chem.* **2006**, *118*, 4921; *Angew. Chem. Int. Ed.* **2006**, *45*, 4803.

[18] (a) P. Hengen, *Trends Biochem Sci*. **1995**, *20*, 285. (b) M. N. Tahir, P. Theato, W. E. G. Müller, H. C. Schröder, A. Janshoff, J. Zhang, J. Huth, W. Tremel, *Chem. Commun.* **2004**, 2848. (c) M. N. Tahir, P. Theato, W. E. G. Müller, H. C. Schröder, A. Borejko, S. Faiß, A. Janshoff, J. Huth, W. Tremel, *Chem. Commun*. **2005**, 5533.

[19] M. N. Tahir, M. Eberhardt, N. Zink, H. A. Therese, U. Kolb, P. Theato, W. Tremel, *Angew. Chem.* **2006**, *118*, 4927; *Angew. Chem. Int. Ed.* **2006**, *45*, 4809.

[20] M. N. Tahir, N. Zink, M. Eberhardt, H. A. Therese, U. Kolb, P. Theato, W. Tremel, *Small* **2007**, *3*, 829.

[21] M. N. Tahir, F. Natalio, H. A. Therese, A. Yella, M. R. Shah, R. Berger, H.-J. Butt, N. Metz, P. Theato, H. C. Schröder, W. E. G. Müller, W. Tremel, *Adv. Funct. Mater*. **2009**, *19*, 285.

[22] J. K. Sahoo, M. N. Tahir, A. Yella, T. D. Schladt, E. Mugnaioli, U. Kolb, W. Tremel, *Angew. Chem.* **2010**, *122*, 7741, *Angew. Chem. Int. Ed*. **2010**, *49*, 7578.

[23] R. H. Holyer, C. D. Hubbard, S. F. A. Kettle, R. G. Wilkins, *Inorg. Chem*. **1966**, *5*, 622.

[24] (a) S. Trofimenko, *Chem. Rev.*, **1993**, *93*, 943. (b) S. Trofimenko, Imperial College Press, London, 1999.

[25] U. S. Schubert, H. Hofmeier, G. R. Newkome, Wiley-VCH, Weinheim 2006.

[26] (a) B. G. Lohmeijer, U. S. Schubert, *Macromol. Chem. Phys*. **2003**, *204*, 1072. (b) U. S. Schubert, C. Eschbaumer, O. Hien, P. R. Andreas, *Tetrahedron Lett*. **2001**, *42*, 4705.

[27] H. Hofmeier, J. Pahnke, C. H. Weidl, U. S. Schubert, *Biomacromolecules*, **2004**, *5*, 2055.

[28] K. Nakamoto, *J. Phys. Chem*. **1960**, *64*, 1420.

[29] M. N. Tahir, P. Theato, P. Oberle, G. Melnyk, S. Faiss, U. Kolb, A. Janshoff, M. Stepputat, W. Tremel, *Langmuir* **2006**, *22*, 5209.

[30] G. A. Koohmareh, M. Sharifi, *J. App. Poly. Sci.* **2010**, *116*, 179.

[31] L. Rapoport, Y. Bilik, Y. Feldman, M. Homyonfer, S. R. Cohen, R. Tenne, *Nature* **1997**, *387*, 791.

[32] L. Rapoport, M. Lvovsky, I. Lapsker, V. Leshchinsky, Y. Volovik, Y. Feldman, A. Margolin, R. Rosentsveig, R. Tenne, *Nano Lett.* **2001**, *1*, 137.

[33] I. Kaplan-Ashiri, S. R. Cohen, K. Gartsman, V. Ivanovskaya, T. Heine, G. Seifert, I. Wiesel, H. D. Wagner, R. Tenne, *Proc. Natl. Acad. Sci. USA* **2006**, *103*, 523.

[34] J. Tannous, F. Dassenoy, I. Lahouij, T. L. Mogne, B. Vacher, A. Bruhacs, W. Tremel, *Tribol. Lett.* **2011**, *41*, 55.

4. Self-Assembly Of Metal Chalcogenide/Metal Oxide Nanostructures Based On The Degree Of Pearson Hardness.

Running Title: Degree of functionalization

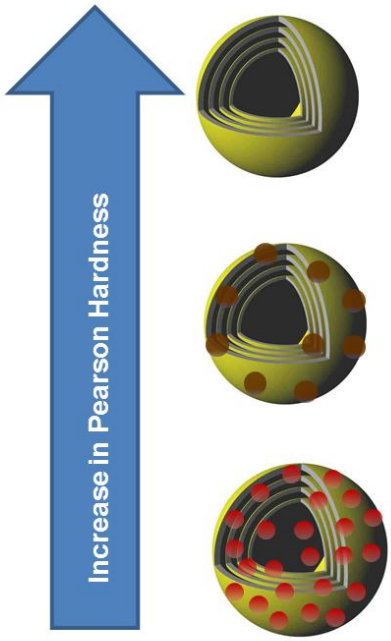

Jugal Kishore Sahoo[a], Muhammad Nawaz Tahir[a], Aswani Yella[a], Thomas D Schladt[a], Steffen Pfeifer[a], Bahar Nakhjavan[a], Enrico Mugnaioli[b], Ute Kolb[b], and Wolfgang Tremel[a].

[a]Institute for Inorganic and Analytical Chemistry

[b]Institute for Physical Chemistry,

Johannes Gutenberg-Universität, Mainz, Germany.

Chem. Mater. 2011. (Accepted)

4.1. Introduction.

Current efforts and success of nanoscale science and technology are related to the fabrication of functional materials and devices in which the individual units and their spatial arrangement are engineered down to the nanometer level [1]. One promising way of achieving this goal is to assemble different nanomaterials to form hybrid nanocomposites which effectively combine the properties of the different materials involved. Furthermore, the assembly of multicomponent nanomaterials from constituents with different optical, electrical, magnetic and chemical properties can lead to novel functionalities that even surpass those of the individual components and may be tailored for specific applications. The generation of such hybrid nanocomposites could represent a new approach to nanoscale building blocks.

Surface functionalization is a one of the requirements for controlling the assembly of nanoparticles to aggregates with hierarchical structure [2]. Surface chemistry is "coordination chemistry in two dimensions", i.e. most nanoparticles (e.g. metals, metal sulfides or metal oxides) can be surface-treated in a straightforward fashion using the concepts of coordination chemistry [3]. In general, a surface ligand contains an anchor group that strongly attaches onto the surface of the regarding nanomaterial and a (long) hydrocarbon or polyether chain that confers solubility in apolar or polar solvents. A terminal group (e.g. an amino group) provides connectivity to additional functional ligands. Typical anchor groups include phosphines [4], amines [5], thiols [6], carboxylates [7], phosphates [8], or catecholates [9]. As a result, a dense ligand shell is formed around each nanoparticle, preventing particle aggregation and providing chemical protection against oxidation plus long-term solvent stability.

In contrast to most nanoparticles, inorganic nanotubes (NT-MQ_2) [10] and fullerenes (IF-MQ_2) [11] of layered metal chalcogenides consist of metal atoms sandwiched between two inert chalcogenide layers. These MQ_2 layers are stacked with only van der Waals contacts between them. The steric shielding of the metal atoms by the chalcogen surface layers from nucleophilic attack by oxygen or organic ligands makes chalcogenide nanoparticles highly inert and notoriously difficult to functionalize. While a covalent surface chemistry of their carbon congeners (fullerenes and nanotubes) has been established through acid-induced oxidation of the carbon nanotube surface defects [12], the covalent surface functionalization of layered chalcogenides is *anion coordination chemistry*: metals with a high sulfur affinity

whose coordination sphere is partially blocked by chelating groups must serve as a "glue" for anchoring organic ligands to the sulfur surface.

Some progress has been made by employing chalcophilic transition metals in combination with multi-dentate surface ligands: The 3d metals "wet" the sulfur surface of the chalcogenide nanoparticles while the multidentate surface ligands partially block one hemisphere of the metal coordination environment. This steric shielding prevents an aggregation of the chalcogenide nanoparticles through inter-particle crosslinking [13]. This covalent attachment offers high stability in different solvents and ionic environments. An alternative strategy is to attach nanoparticles directly onto the chalcogenide nanoparticles [14]. In this case the sulfur atoms of the chalcogenide particles outcompete the protecting ligand of the nanoparticle surface, i.e. their affinity is based on their acid/base properties or Pearson hardness [15], which allows their attachment without the aid of linkers.

In this paper we report a general synthetic strategy based on Pearson's HSAB principle16 that allows the formation of a hierarchical assembly of metal chalcogenide/metal oxide nanostructures. The binding capabilities of the 3d metals are dictated by their Pearson hardness. Whereas Pearson hard cations such as Ti^{4+} (TiO_2) or Fe^{3+} (Fe_2O_3) do not bind to the chalcogenide surfaces, borderline metals such as Fe^{2+} (Fe_3O_4) or Zn^{2+} (ZnO) bind reversibly und can be detached reversibly from the chalcogenide surfaces with excess surface ligand. Pearson-soft metals like gold bind irreversibly.

4.2. Results and Discussion

Immobilization of Metal Oxide Nanoparticles on IF-MoS_2 Surfaces

The constituent IF-MoS_2 nanoparticles were prepared following a MOCVD approach [11c]. MnO [19], Fe_2O_3 [18], and Fe_3O_4 [17] as well as TiO_2 [20] and Au [21] nanoparticles were synthesized by wet-chemical methods. These constituent nanoparticles were characterized by TEM as shown in Figure 4.1. The X-ray diffractograms of MnO, Fe_2O_3 and Fe_3O_4 are provided in Figure S2 (Supporting Information). The functionalization scheme of the IF-MoS_2 nanoparticles is illustrated in Scheme 4.1. In a typical experiment, IF-MoS_2 was dispersed under sonication in toluene followed by addition of the metal oxide nanoparticles to the dispersion of the chalcogenide nanoparticles. The products, metal oxide functionalized IF-MoS_2 was characterized by TEM and EDX.

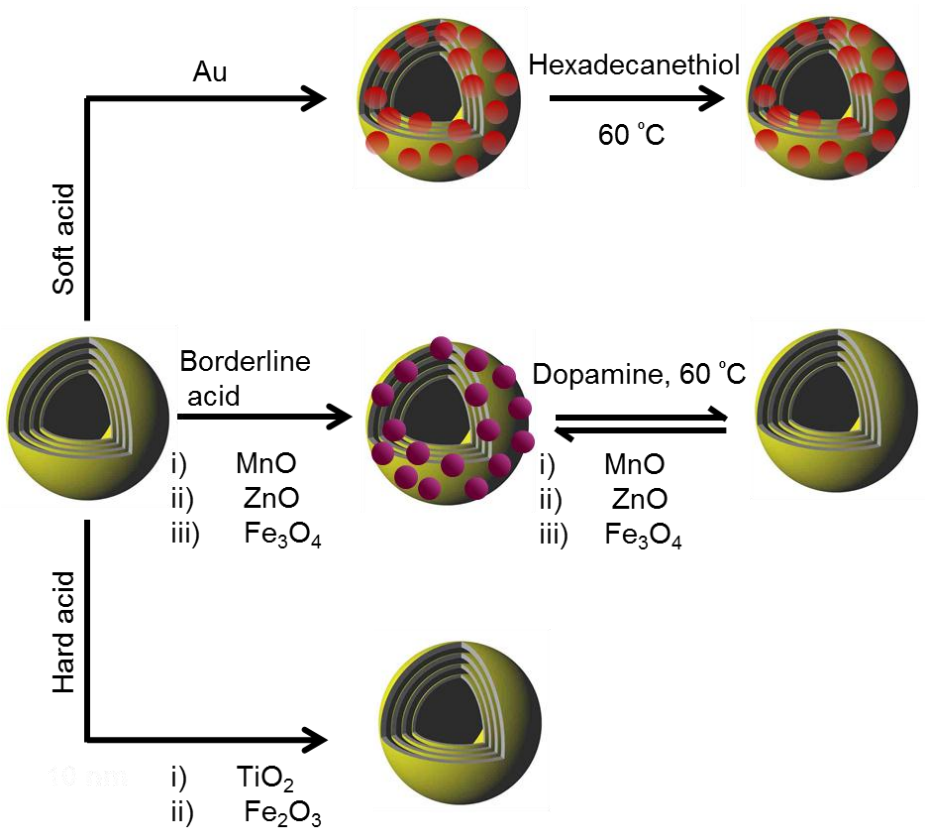

Scheme 4.1. *Schematic representation of the reversible immobilization of metal oxide and irreversible binding of Au nanoparticles onto IF-MoS_2.*

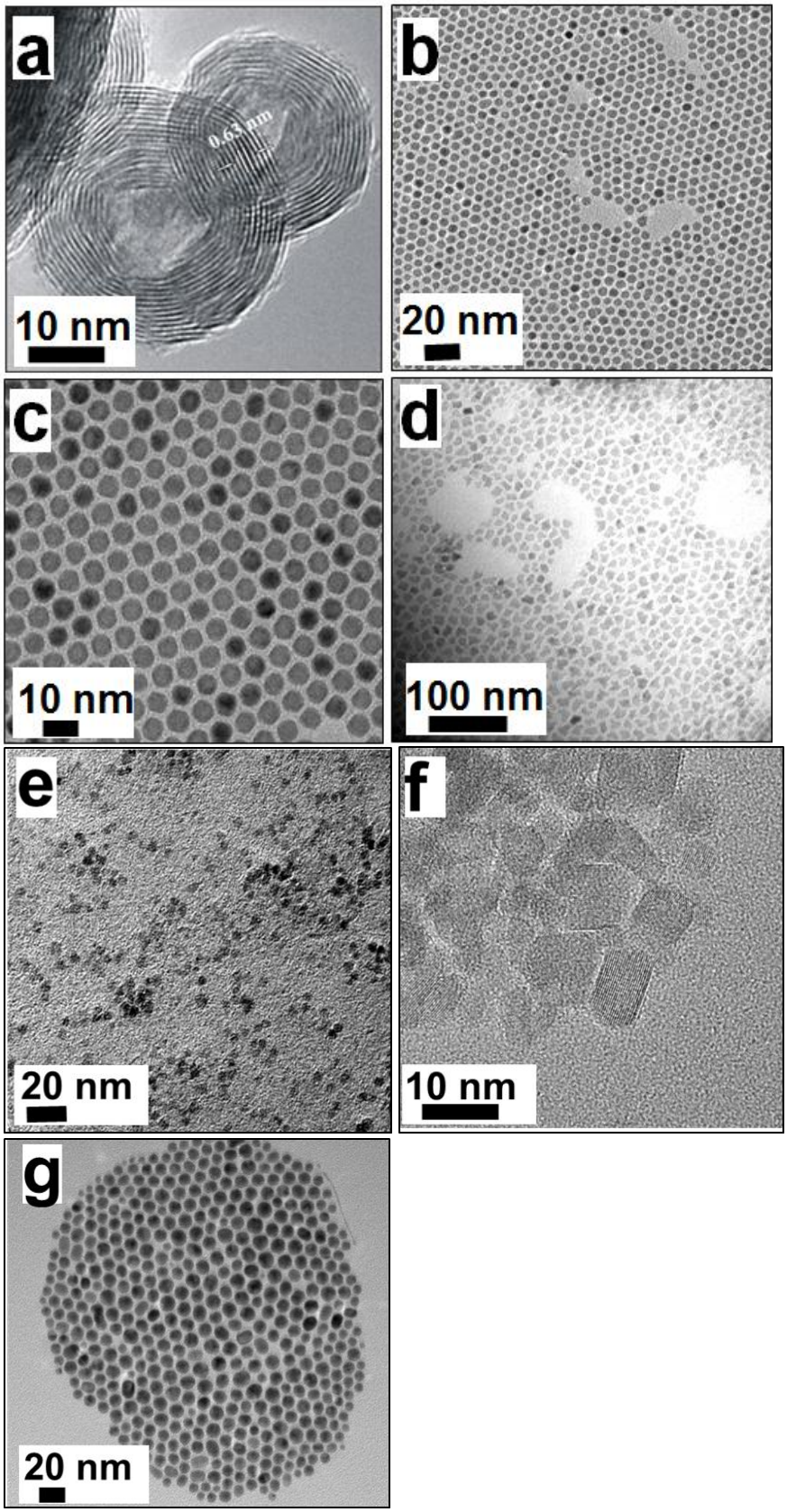
a
0.63 nm
10 nm
b
20 nm
c
10 nm
d
100 nm
e
20 nm
f
10 nm
g
20 nm

***Figure 4.1**. Electron microscopy images of as synthesized nanoparticles. (a) IF-MoS_2, (b) Fe_2O_3, (c) MnO, (d) Fe_3O_4. (e) ZnO. (f) TiO_2. (g) Au.*

Figure 4.2a shows a TEM overview image of MnO nanoparticles surface-bound to IF-MoS_2. The layered structure of IF-MoS_2 with an interlayer separation of 0.63 nm is apparent from the HRTEM micrograph in Figure 2b. The affinity of MnO (with the Pearson borderline metal Mn^{2+}) to IF-MoS_2 (with Pearson soft sulfide anions) is large enough ensure the formation of a full MnO monolayer (with a number of defects) on the chalcogenide surface. The surface of the MnO particles is blocked by the oleic acid capping ligands from the particle synthesis which prevents a self-aggregation of the MnO particles. The surface binding of the MnO particles is assumed to proceed by a "nucleophilic" substitution of the oleic acid capping ligands by the chalcogenide sulfur atoms. The functionalization was confirmed from EDX spectrum which shows the presence of Mo, S, Mn, and O in the nanocomposites. The Cu signals are from the Cu TEM grids.

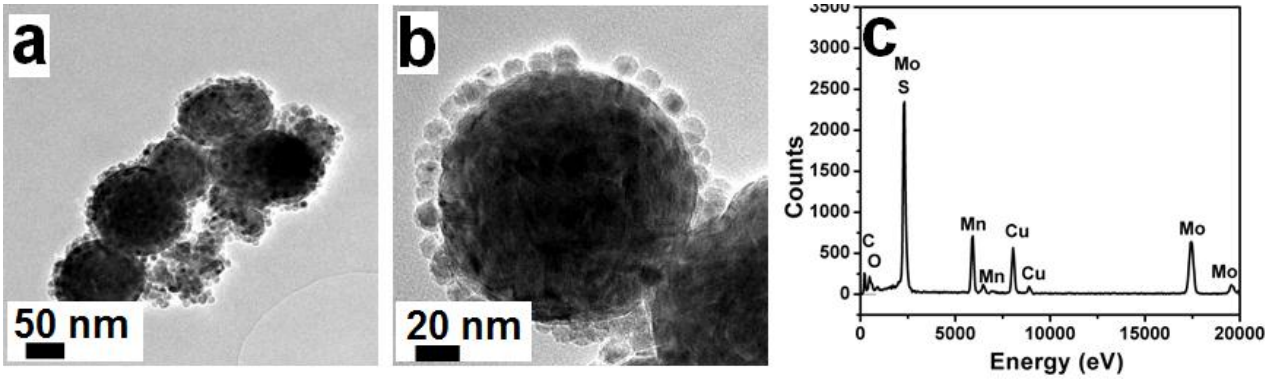

***Figure 4.2.** (a) TEM overview and (b) HRTEM image of MnO coated IF-MoS_2 nanoparticles. (c) EDX spectrum showing the presence of Mo and S as well as Mn and O. The Cu signal is due to the Cu TEM grid.*

Figure 4.3a shows a TEM overview micrograph of Fe_3O_4 functionalized IF-MoS_2. The corresponding HRTEM image is provided in Figure 4.3b showing the interlayer separation of the IF-MoS_2 particles and the lattice fringes of the "satellite" Fe_3O_4 nanoparticles. The EDX spectrum in Figure 4.3c shows signals of Mo, S, Fe and O together with the Cu signals of the Cu grid. According to the Pearson hardness scale in Table 4.1 magnetite containing Fe^{3+} and Fe^{2+} at the octahedral sites and Fe^{3+} at the tetrahedral sites of the spinel lattice should have a lower affinity to the surface sulfur atoms of IF-MoS_2. Although this trend could not be substantiated by a competitive detachment experiment with Fe_3O_4 and MnO, it is supported

by a comparison of the surface binding of maghemite (Fe_2O_3) and anatase (TiO_2). The Pearson hardness [15,16] of the constituent metals Fe^{3+} (13.1 eV) and Ti^{4+} (> $\eta(Sc^{3+})$ 24.6 eV) prevent a binding of maghemite and anatase to the IF-MoS_2 surface, i.e. the harder capping ligands of the surfaces of the Fe_2O_3 and TiO_2 particle outcompete the soft sulfur atoms, i.e. no substitution of these ligands by sulfur is possible. Figure 4.4b. shows the absence of binding of TiO_2 to the chalcogenide particle. The binding of TiO_2 nanoparticles to the incompatible chalcogenide surface could, however, be achieved with the aid of specially designed surface ligands containing tailor-made anchor groups for the chalcogenide and oxide surfaces [22].

Cations	**Pearson hardness η (eV)**
Fe^{3+}	13.1
Zn^{2+}	10.8
Mn^{2+}	9.3
Fe^{2+}	7.2
Au	3.5

Table 4.1. *Pearson hardness* [15,16] *of transition metal species used for the assembly of metal oxide or metal particles on chalcogenide nanoparticles.*

A comparison of the binding tendencies of the iron oxides is given in Figure 4.5, showing surface-bound Fe_3O_4 (IF-MoS_2@Fe_3O_4) and unbound Fe_2O_3 and IF-MoS_2 nanoparticles. The magnetic Fe_3O_4 and Fe_2O_3 nanoparticles are attracted by the permanent magnet. Whereas the sample containing the surface-bound magnetite nanoparticles (left) becomes transparent by attraction of the composite IF-MoS_2@Fe_3O_4 to the magnet, the IF-MoS_2 particles remain unbound and well dispersed, thereby leaving a turbid sample (right).

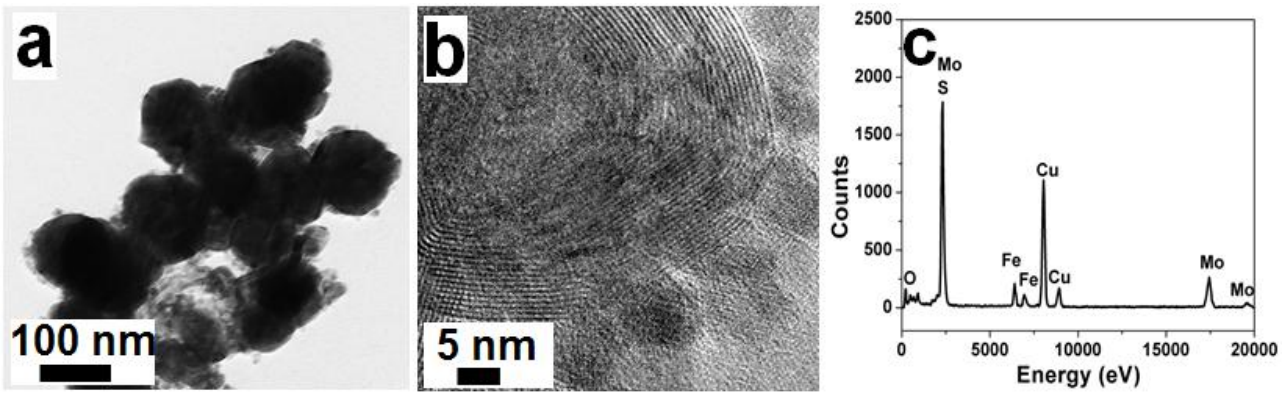

***Figure 4.3**. (a) TEM overview and (b) HRTEM images of Fe_3O_4 nanoparticles bound onto IF MoS_2 particles. (c) EDX spectrum showing the presence of Mo and S as well as Mn and O. The Cu signal is due to the Cu TEM grid.*

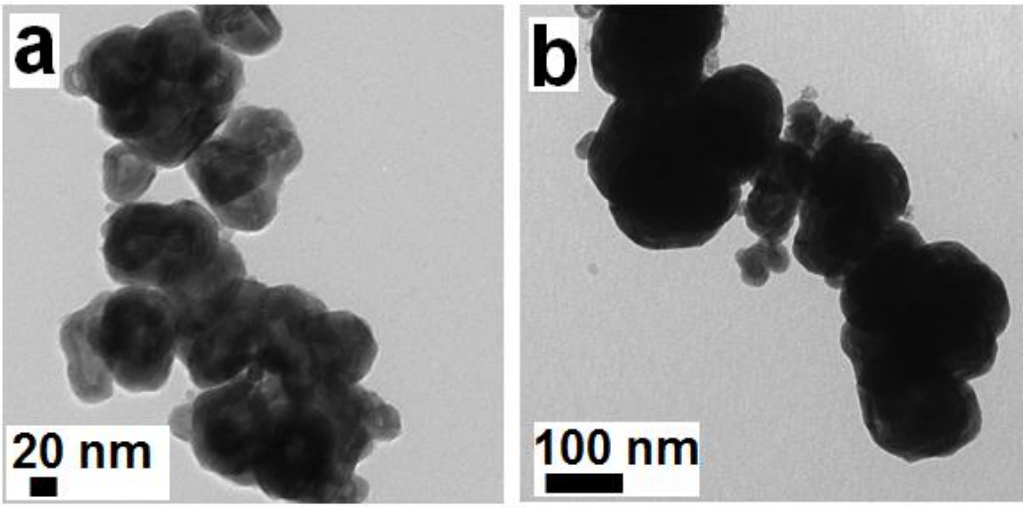

***Figure 4.4.** TEM image of IF-MoS_2 after mixing with (a) Fe_2O_3 nanoparticles, (b) TiO_2 nanoparticles confirming that hard cations like Fe (III) and Ti (IV) do not bind to layered metal chalcogenide surfaces.*

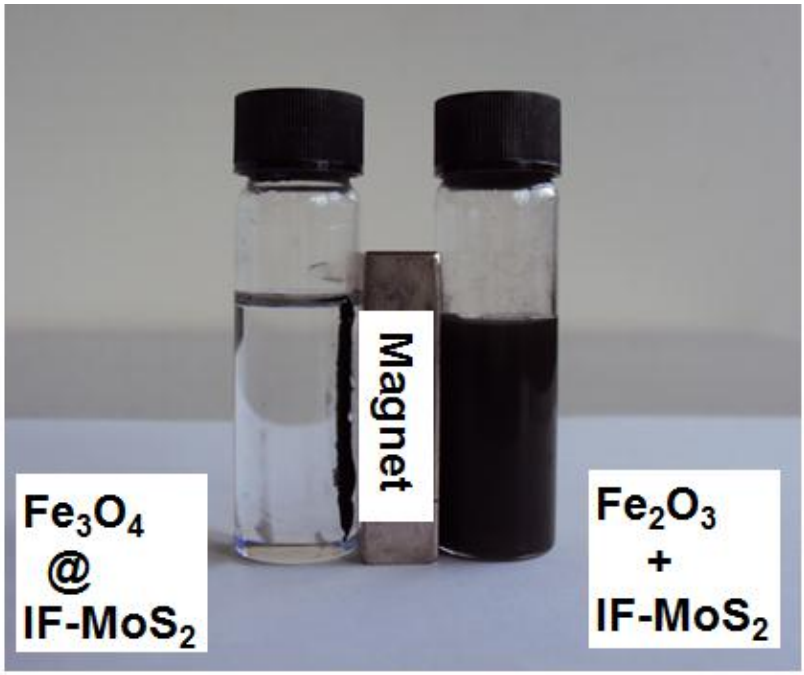

***Figure 4.5.** Digital image of surface bound Fe_3O_4 (IF-MoS_2@Fe_3O_4) and unbound Fe_2O_3 nanoparticles. The magnetic nanoparticles are attracted by the permanent magnet. Whereas*

the sample containing the surface-bound magnetite nanoparticles (left) becomes transparent through the attraction by the magnet, the unbound IF-MoS_2 particles remain dispersed leaving a turbid sample (right).

Similar experiments were carried out to study the binding affinity of other metal oxide particles such as ZnO to IF-MoS_2. ZnO nanoparticles bind strongly to the surface of IF-MoS_2 or WS_2 nanotubes [23]. Figure 4.6a shows the monolayer coverage of ZnO colloidal particles on the surface of IF-MoS_2 nanoparticles. The binding of Zn^{2+} cations to sulfide surfaces is not unexpected because it is well-known that Zn^{2+} in aqueous solutions readily forms ZnS precipitates in the presence of sulfide (or H_2S). Likewise, solid ZnO can be sulfidized easily with H_2S. Au as one of the softest metals (Pearson hardness 3.5 eV) is known to be highly chalcophilic; this property of gold and the coinage metals is the basis of the established SAMs [24] and a very rich chalcogenide chemistry [26]. As a consequence, Au nanoparticles strongly bind to IF-MoS_2 as illustrated in Figure 4.7.

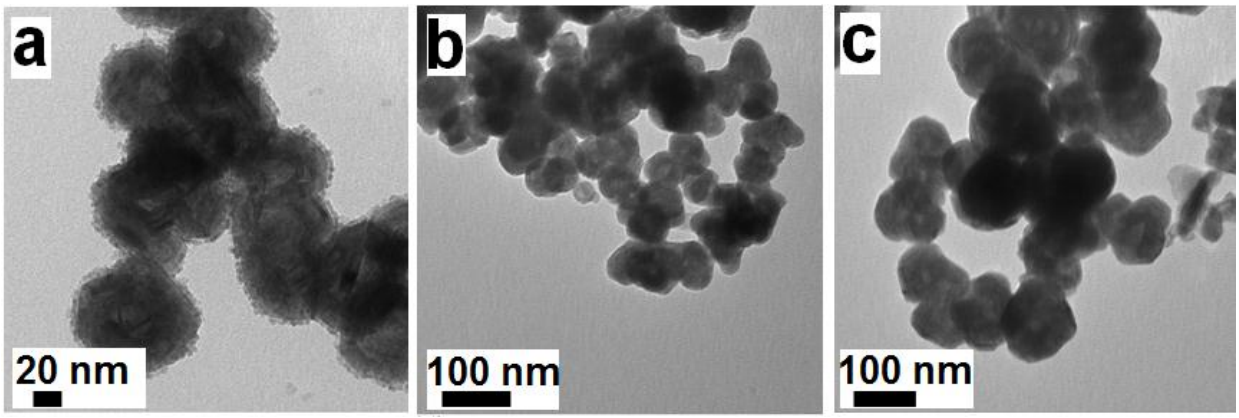

Figure 4.6*. (a) TEM micrograph of IF-MoS_2 nanoparticles with a monolayer of surface-bound ZnO particles. (b) IF-MoS_2 nanoparticles after detachment of the ZnO particles or (c) Fe_3O_4 particles with catecholate ligands.*

Reversible detachment of metal Oxide (MnO, Fe_3O_4, ZnO) nanoparticles from IF-MoS_2 surfaces.

The IF-MoS_2 surface bound metal oxide nanoparticles can be functionalized selectively with various surface ligands. In this process, either the original (e.g. oleic acid) capping ligands or the chalcogenide surface ligands are replaced by competing ligands which can have a higher affinity for the metal ions Mn^{2+}, Fe^{2+} and Zn^{2+}. However, surface ligands can be replaced by competing ligands with a lower binding affinity under equilibrium reactions, as long as there is a sufficiently large excess of the competing ligand.

Each of the metal ions Mn^{2+}, $Fe^{2+/3+}$ and Zn^{2+} bound to the IF-MoS_2 surface can be functionalized highly efficiently and selectively with "non-innocent" redox-active ligands such as catechol [9]. Unlike most ligands used in inorganic chemistry, such as amines or phosphines, redox-active, or "noninnocent," ligands [26] have more energetically accessible levels that allow redox reactions to change their charge state. As a result, many coordination compounds with non-innocent ligands are very stable, which makes them useful in analytical chemistry [27]. Catecholates or diimines have a distinctive ability to form non-innocent surface species which makes them powerful anchor groups for nanoparticle functionalization [28]. In this process, the oleic acid capping ligands are replaced by the free catechol ligand. Due to its chelating properties catechol can compete highly successfully with sulfur for surface metal atoms. In particular hard acids such as Fe^{3+} (or Al^{3+} and Ti^{4+}) prefer coordination to donor groups such as hydroxamate, phenolate, and catecholate [29]. The catecholate ligands form unstrained and unsaturated five-membered ring chelate systems with surface metal atoms via negatively charged oxygen (or nitrogen) atoms. Thus ligands with oxygen donors form stable surface complexes with trivalent or tetravalent metals, whereas those with softer donor atoms such as nitrogen (intermediate) or sulfur (soft) also favor soft metals such as Zn^{2+} [30].

Due to their chelating properties, catechol type ligands can compete successfully with sulfur atom of fullerene surface for the surface metal atom. Solvation is an important factor that determines the surface binding of the oxide nanoparticles. As the solvation increases with increasing the temperature, we used a slightly elevated temperature of 60 °C to remove the surface-bound oxide nanoparticles from the chalcogenide surface in the presence of dopamine as chelating ligand for the metal oxide nanoparticles. Using thus strategy, MnO, Fe_3O_4 and ZnO particles could be detached completely from the chalcogenide particles. However, without addition of the competing ligand, a recovery of the chalcogenide nanoparticles was not possible.

For attempts to detach gold nanoparticles from IF-MoS_2 monodentate thiols (e.g. hexadecanethiol) were used as the competing ligands. However, Au nanoparticles could not be detached from the IF-MoS_2 particle surfaces. Figure 4.7.

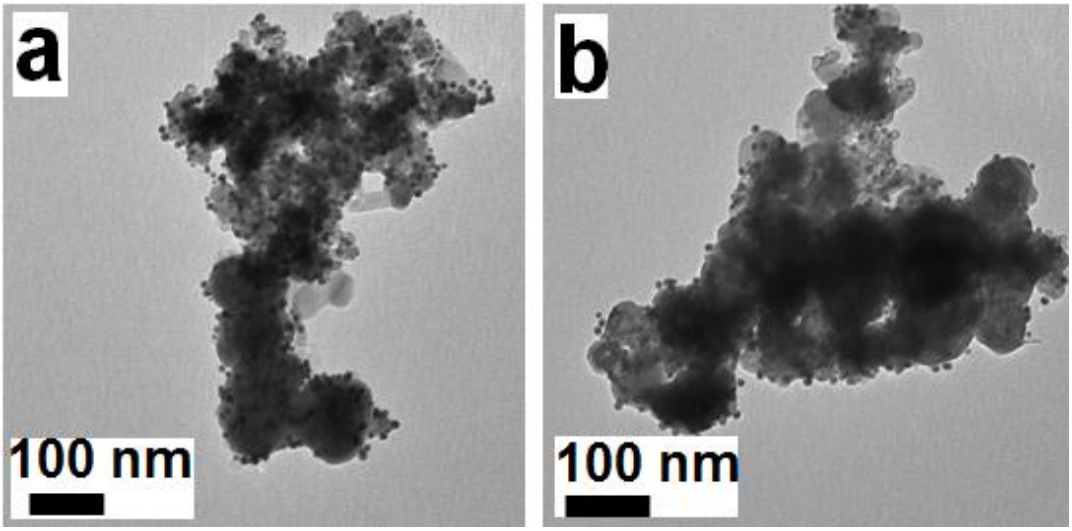

Figure. 4.7. *TEM images of (a) Au nanoparticles functionalized IF-MoS_2 (b) after addition of 1-hexadecanethiol to Au@IF-MoS_2, which confirms the irreversible binding of gold nanoparticles onto IF-MoS_2.*

Our results are summarized in Scheme 4.1. Whereas oxides of soft and borderline metals are chemisorbed easily to the surface sulfur atoms, oxides of the hard metals have a much lower tendency for binding. The catechol-type ligands bind efficiently to hard or borderline metals (such as Ti^{4+} Fe^{3+}, Al^{3+}, Mn^{2+} etc.). As a result, the binding of chalcogenide nanoparticles and catechol-type ligands to surface metal atoms of borderline metal oxides is a dynamic equilibrium reaction, whose position depends on the reactants and temperature. By increasing the reaction temperature to 60°C, catechol is a preferred surface ligand for the metal oxide particles. It displaces the surface sulfur atoms of IF-MoS_2 from the oxide particles leaving unfunctionalized and separated IF-MoS_2 particles. The addition of new metal oxide nanoparticles to IF-MoS_2 leads to a partial replacement of the oleate surface ligands by the surface sulfur atoms of IF-MoS_2 and a concomitant binding of metal oxide nanoparticles to the chalcogenide surface. This cycle can be repeated several times. The recycled chalcogenide nanoparticles can be re-used.

The HSAB model has its basis in arguments related to bonding strength. It is applied for systems where kinetic control, entropy of adduct formation, solvation effects (enthalpic and entropic), ion-pairing effects (enthalpic and entropic), or lattice energy effects (enthalpic and entropic) are large and even dominant. When HSAB considerations are employed, it is

implied that the soft-soft (covalent) or hard-hard (ionic) interactions, dominate the chemistry, i.e. that the reactions are either orbital or charge controlled.

Thus, the reversible binding of MnO, Fe_3O_4 and ZnO nanoparticles to the chalcogenide surface can be attributed to the relative hardness of the metal cations of the respective metal oxide nanoparticles. The hardness of Au(0) is 3.5 eV, whereas the corresponding values for Mn^{+2}, Fe^{2+}, Fe^{3+} and Zn^{+2} are 9.3, 7.2, 13.1 and 10.8 eV, respectively [15,16]. Therefore, the binding of the divalent metals is reversible, and the trivalent metal does not bind to the chalcogenide surface. The binding of chalcophilic Au is irreversible [31].

4.3. Conclusions and Outlook.

In summary, we have demonstrated a generalized strategy for the functionalization of chalcogenide particles using metal oxide and metal nanoparticles. In their pristine form chalcogenide nanoparticles are highly inert and difficult to functionalize. The Pearson hardness of the different metal cations was used as a basis for the binding of the metal oxides to the chalcogenide surface. The "self-assembled" hybrid architecture can incorporate various different selective nanoparticle-substrate interactions based on well-known surfaces chemistry, and it may be generalized for various layered chalcogenide nanoparticles and transition metal and main group oxides. This assembly technique offers benefits for low-cost and low-waste manufacturing, and such methods are becoming increasingly important in the development of green nanofabrication strategies.

The functionalization of the chalcogenide nanoparticles opens new fields for this class of materials which have been pursued actively during the past few years for the related carbon nanotubes and oxide materials: (i) dispersion of nanoparticles, e.g. for the integration in composites, which is of interest because of the exceptional mechanical properties of chalcogenide nanoparticles. (ii) It allows the fabrication of thin films by surface binding of chalcogenide particles to oxide surfaces, which might allow their use as lubricants on seemingly incompatible ceramic materials. (iii) Finally, it enables the functionalization of chalcogenide nanoparticles for the attachment of electronically active components (e.g. metal and semiconductors nanoparticles, light harvesting ligands for solar cell applications).

4.4. Experimental Section

Methods and Materials

3-Hydroxy tyramine hydrochloride, (Acros organic), 1-hexadecanethiol (Sigma-Aldrich) were purchased and used as received without further purification. Solvents such as, toluene, chloroform, DMF, were purchased technical grade and used as received.

Synthesis of Fe_3O_4 nanoparticles. Fe_3O_4 nanoparticles were synthesized using a reported procedure [17]. Typically iron(III) acetylacetonate ($Fe(acac)_3$, 150 mg) was mixed in dioctylether (10 mL) with 1,2-hexadecanediol (250 mg), oleic acid (0.06 mL), and oleylamine (0.06 mL) in a glove box under argon. Under mechanical stirring, the reaction mixture was heated to 280 °C for 30 min. Ethanol (20 mL) was added after the reaction mixture was cooled to room temperature. A dark-brown precipitate (magnetite seeds) was acquired after centrifugation. The magnetite seeds (25 mg) were dissolved in 10 mL of dioctylether and mixed with $Fe(acac)_3$ (150 mg), 1,2-hexadecanediol (250 mg), oleic acid (0.06 mL), and oleylamine (0.06 mL). The mixture was heated to 280 °C for 30 min under mechanical stirring. After the mixture was cooled to room temperature it was treated with ethanol and a dark-brown material was precipitated from the solution. The product was dissolved in hexane and reprecipitated with ethanol to yield uniform Fe_3O_4 nanoparticles.

Synthesis of ZnO colloids. A batch of ZnO colloids were synthesized by dissolving 110 mg (0.5 mmol) of $Zn(CH_3COO)_2\ 2H_2O$ in 25 mL of ethanol with sonication for 15 min at 0 C. To the above solution was added 21 mg (0.5mmol) of $Li(OH)_x3H_2O$ and sonication was continued for another 15 min at the same temperature. A stable and optically transparent dispersion of ZnO nanoparticles was obtained.

Synthesis of Fe_2O_3 nanoparticles. Fe_2O_3 nanoparticles were prepared following ref [18]. Typically $Fe(CO)_5$ (0.2 mL, 1.52 mmol) was injected under vigorous stirring into a solution containing 0.91 g of lauric acid (4.56 mmol), 7 mL of octyl ether, and 0.57 g of $(CH_3)_3NO$ (7.60 mmol) at 100 °C in an argon atmosphere. As soon as $Fe(CO)_5$ was injected into the mixture, the temperature rose to 120 °C and the solution became dark-red, which indicated the successful oxidation of $Fe(CO)_5$. The reaction mixture was stirred for 1 h at 120 °C, and the solution was slowly heated to reflux. The color of the solution gradually turned black, indicating that nanoparticles were formed. After refluxing for 1 h, the solution was cooled to

room temperature, and a black precipitate was obtained upon adding excess ethanol and centrifuging. The precipitate can be easily redispersed in toluene.

Synthesis of IF-MoS_2. IF-MoS_2 was synthesized as described in ref. [11c].

Synthesis of MnO, TiO_2, Au nanoparticles. MnO [19], TiO_2 [20], and Au [23] nanoparticles were synthesized using reported procedures.

Binding of metal oxide (MnO, Fe_3O_4, Fe_2O_3) nanoparticles onto IF-MoS_2. In a typical experiment 4 mg of IF-MoS_2 were dispersed in 5 ml of toluene by sonicating the sample for 5-7 min. The solution was further degassed under argon for 10-15 min. In another centrifuge vial, 8 mg of metal oxide, NP's were dissolved in 5 ml of toluene. Subsequently, the solution was added dropwise to the degassed mixture of IF-MoS_2 in toluene over a period of 5-7 min. Subsequently, the reaction mixture was degassed again under argon for 5 min and put in a shaker for 6 h at room temperature (RT). After the reaction was complete, the unbound metal oxide nanoparticles were washed out by centrifuging the sample thrice at 4000 rpm for 10 min. Finally, the functionalized IF-MoS_2 was characterized by TEM/HRTEM combined with EDX. Samples for TEM were prepared by putting 1-2 drops of dispersed sample on a copper TEM grid followed by drying.

Binding of ZnO and TiO_2 and Au colloids onto IF-MoS_2. In a typical experiment 4 mg of IF-MoS_2 were dispersed in 5 ml of ethanol by sonicating the sample for 5-7 min. The solution was further degassed under argon for 10-15 min. In another centrifuge vial, 8 mg of ZnO or TiO_2 nanoparticles were taken in 5 mL of ethanol. Subsequently, the nanoparticles solution was added dropwise to the degassed mixture of IF-MoS_2 in toluene over a period of 5-7 min. Finally, the reaction mixture was degassed again in argon for 5 min and in a shaker for 6 h at room temperature. After the reaction was complete, the unbound ZnO (TiO_2) colloids were washed out by centrifuging the sample thrice at 4000 rpm for 10 minutes. Finally the functionalized IF-MoS_2 was characterized by TEM/HRTEM combined with EDX. Samples for TEM were prepared by putting 1-2 drops of dispersed sample on a copper TEM grid followed by drying. A similar experimental method was used for the Au nanoparticles (with H_2O as solvent).

Reversibility experiments. In a typical experiment, 10 mg of the IF-MoS_2/metal oxide nanocomposite was taken in a 50 mL flask and dispersed with 5 mL of DMF by sonication followed by degassing the mixture in argon. In another flask 40 mg of 3-hydroxytyramine hydrochloride (dopamine) was taken and dissolved in 10 mL of DMF. The dopamine solution was added dropwise to the mixture of the IF-MoS_2@metal oxide nanocomposite over a period

of 10 min. The reaction mixture was heated up to 60º c and stirred overnight. After the reaction was complete the reaction mixture was washed by centrifuging the sample thrice at 4000 rpm for 10 minutes. The recycled IF-MoS_2 can be used for further functionalization with fresh metal oxide nanoparticles. Similarly, the metal oxide was removed from the surface of MoS_2 by using dopamine in DMF as a competing ligand as described above. The reaction was monitored by transmission electron microscopy. A similar procedure was used for the reversibility experiment of other metal oxide nanoparticles and IF-MoS_2. For the reversibility experiment with IF-MoS_2/Au nanocomposites, hexadecanethiol instead of dopamine was used as competing ligand

Characterization

TEM analysis and characterization of the products. Transmission electron microscopy (TEM) was carried out on a Philips EM420 instrument with a twin lens and a Philips CM12 with a twin lens at an acceleration voltage of 120 kV. High resolution images were taken with a Philips FEI TECNAI F30 ST electron microscope (field-emission gun, 300 kV extraction voltage) equipped with an Oxford EDX (energy-dispersive X-ray) spectrometer with a Si/Li detector and an ultrathin window for elemental analysis. Samples for TEM measurements were prepared from ethanolic suspensions of the samples. Three drops of the ultrasonicated suspension were administered on a Cu grid coated with FORMVAR polymer and an amorphous carbon layer.

4.5. References

[1] (a) P. D. Cozzoli, T. Pellegrino, L. Manna, *Chem. Soc. Rev*. **2006**, *35*, 1195. (b) H. Zeng, S. Sun, *Adv. Funct. Mater*. **2008**, *18*, 391. (c) J. A. McGuire, J. Joo, J. M. Pietryga, R. Schaller, V. I. Klimov, *Acc. Chem. Res.* **2008**, *41*, 1810.

[2] (a) M. P. Pileni, Nanocrystals Forming Mesoscopic Structures; Pileni, M.-P., Ed.; Wiley VCH: Weinheim, Germany, 2005. (b)A. C. Balazs, T. Emrick, T. P. Russell, *Science* **2006**, *314*, 1107. (c) H. Kang, F. A. Detcheverry, A. N. Mangham, M. P. Stoykovich, K. C. Daoulas, R. J. Hamers, M. Müller, J. J. de Pablo, P. F. Nealey, *Phys. Rev. Lett*. **2008**, *100*, 148303. (d) D. V. Talapin, J. S. Lee, M. V. Kovalenko, E. V. Shevchenko, *Chem. Rev*. **2010**, *110*, 389.

[3] J. Ribas Gispert, *Coordination Chemistry*, 1st ed.; Wiley-VCH: Weinheim, 2008.

[4] (a) E. Ramirez, S. Jansat, K. Philippot, P. Lecante, M. Gomez, A. M. Masdeu-Bulto, B. J. Chaudret, *Organomet. Chem*. **2004**, *689*, 4601. (b) G. H. Woehrle, J. E. Hutchison, *Inorg. Chem*. **2005**, *44*, 6149.

[5] M. G. Warner, J. E. Hutchison, in: Baraton, M. I. (ed.) Synthesis, Functionalization and Surface Treatment of Nanoparticles. Stevenson Ranch 2003, 67.

[6] (a) M. Brust, M. Walker, D. Bethell, D. J. Schiffrin, R. J. Whyman, *Chem. Soc. Chem. Commun.* **1994**, 801. (b) M. Bartz, J. Küther, G. Nelles, N. Weber, R. Seshadri, W. Tremel, *J. Mater. Chem.* **1999**, *9*, 1121.

[7] (a) B. O'Regan, M. Grätzel, *Nature* **1991**, *353*, 737. (b) M. Brust, J. Fink, D. Bethell, D. J. Schiffrin, C. Kiely, *J. Chem. Soc. Chem. Commun*. **1995**, 1655. (c) R. C. Doty, T. R. Tshikhudo, M. Brust, D. G. Fernig, *Chem. Mater*. **2005**, *17*, 4630. (d) H. Jiang, K-S. Moon, Y. Li, C. P. Wong, *Chem Mater*. **2006**, *18*, 2969.

[8] (a) A. Subbiah, D. Pyle, A. Rowland, J. Huang, R. A. Narayanan, P. Thiyagarajan, J. Zon, A. Clearfield, *J. Am. Chem. Soc*. **2005**, *127*, 10826. (b) N. Adden, L. J. Gamble, D. G. Castner, A. Hoffmann, G. Gross, H. Menzel, *Langmuir* **2006**, *22*, 8197. (c) C. Viornery, Y. Chevolot, D. Leonard, B. O. Aronsson, P. Pechy, H. J. Mathieu, P. Descouts, M. Graetzel, *Langmuir* **2002**, *18*, 2582. (d) E. Hoque, J. A. DeRose, G. Kulik, P. Hoffmann, H. J. Mathieu, B. Bhushan, *J. Phys. Chem. B* **2006**, *110*, 10855. (e) M. A. White, J. A. Johnson, J. T. Koberstein, N. J. Turro, *J. Am. Chem. Soc.* **2006**, *128*, 11356.

[9] (a) J. H. Waite, M. L. Tanzer, *Science* **1981**, *212*, 1038. (b) C. Xu, K. Xu, H. Gu, R. Zheng, H. Liu, X. Zhang, Z. Guo, B. Xu, *J. Am. Chem. Soc.* **2004**, *126*, 9938. (c) M. N. Tahir, M. Eberhardt, P. Theato, S. Faiß, A. Janshoff, T. Gorelik, U. Kolb, W. Tremel, *Angew. Chem*. **2006**, *118*, 922; *Angew. Chem. Int. Ed.* **2006**, *45*, 908.

[10] (a) L. Margulis, G. Salitra, R. Tenne, M. Talianker, *Nature* **1993**, *365*, 113. (b) H. A. Therese, J. Li, U. Kolb, W. Tremel, *Solid State Sci.* **2005**, *7*, 67.

[11] (a) Y. Feldman, E. Wasserman, D. J. Srolovitz, R. Tenne, *Science* **1995**, *267*, 222. (b) R. Tenne, M. Homyonfer, Y. Feldman, *Chem. Mater*. **1998**, *10*, 3225. (c) J. Etzkorn, H. A. Therese, F. Rocker, N. Berntsen, U. Kolb, W. Tremel, *Adv. Mater*. **2005**, *17*, 2372. (d) N. Zink, J. Pansiot, J. Kieffer, H. A. Therese, M. Panthöfer, F. Rocker, U. Kolb, W. Tremel, *Chem. Mater.* **2007**, *19*, 6391.

[12] A. Hirsch, O. Vostrowsky, *Top. Curr. Chem*. **2005**, *245*, 193.

[13] (a) M. N. Tahir, M. Eberhardt, N. Zink, H. A. Therese, U. Kolb, P. Theato, W. Tremel, *Angew. Chem*. **2006**, *118*, 4927; *Angew. Chem. Int. Ed.* **2006**, *45*, 4809. (b) J. K. Sahoo, M. N. Tahir, A. Yella, R. Branscheid, U. Kolb, W. Tremel, *Langmuir* **2011**, *27*, 385.

[14] J. K. Sahoo, M. N. Tahir, A. Yella, T. D. Schladt, E. Mugnaioli, U. Kolb, W. Tremel, *Angew. Chem.* **2010**, *120*, 7741; *Angew. Chem. Int. Ed*. **2010**, *49*, 7578.

[15] (a) R. G. Parr, R. G. Pearson, *J. Am. Chem. Soc.* **1983**, *105*, 7512. (b) R. G. Pearson, *Chemical Hardness. Applications from Molecules to Solids*, Wiley-VCH, Weinheim 1997.

[16] (a) R. G. Pearson, *J. Am. Chem. Soc.* **1963**, *85*, 3533. (b) R. G. Pearson, *J. Chem. Educ.* **1968**, *45*, 581. (c) R. G. Pearson, *J. Chem. Educ.* **1968**, *45*, 643.

[17] R. Zheng, H. Gu, B. Xu, K. K. Fung, X. Zhang, S. P. Ringer, *Adv. Mater*. **2006**, *18*, 2418.

[18] T. Hyeon, S. S. Lee, J. Park, Y. Chung, H. B. Na, *J. Am. Chem. Soc*. **2001**, *123*, 12798.

[19] T. D. Schladt, T. Graf, W. Tremel, *Chem. Mater.* **2009**, *21*, 3183.

[20] M. N. Tahir, P. Theato, P. Oberle, G. Melnyk, U. Kolb, M. Stepputat, W. Tremel, *Langmuir* **2006**, *22*, 5209.

[21] J. Küther, R. Seshadri, G. Nelles, H. J. Butt, W. Knoll, W. Tremel, *Adv. Mater.* **1998**, *10*, 401.

[22] (a) M. N. Tahir, M. Eberhardt, H. A. Therese, U. Kolb, P. Theato, W. E. G. Mueller, H. C. Schroeder, W. Tremel, *Angew. Chem.* **2006**, *118*, 4921; *Angew. Chem. Int. Ed.* **2006**,

45, 4803. (b) M. N. Tahir, N. Zink, M. Eberhardt, H. A. Therese, U. Kolb, P. Theato, W. Tremel, *Small* **2007**, *3*, 829. (c) M. N. Tahir, F. Natalio, H. A. Therese, A. Yella, N. Metz, M. R. Shah, E. Mugnaioli, R. Berger, P. Theato, H. C. Schroeder, W. E. G. Müller, W. Tremel, *Adv. Funct. Mater.* **2009**, *19***,** 285.

[23] M. N. Tahir, A. Yella, H. A. Therese, E. Mugnaioli, M. Panthöfer, H. U. Khan, W. Knoll, U. Kolb, W. Tremel, *Chem. Mater*. **2009**, *21*, 5382.

[24] A. Ulman, *Chem. Rev*. **1996**, *96*, 1533. (b) J. C. Love, L. A. Estroff, J. K. Kriebel, R. G. Nuzzo, G. M. Whitesides, *Chem. Rev.* **2005**, *105*, 1103.

[25] B. Krebs, G. Henkel, *Angew. Chem.* **1991**, *103*, 785; *Angew. Chem. Int. Ed.* **1991**, *30*, 769.

[26] C. K. Jørgensen, *Coord. Chem. Rev.* **1966**, *1*, 164.

[27] F. Umland, Wünsch, G. Charakteristische Reaktionen Anorganischer Stoffe, 2nd Ed.; Aula Verlag, Wiesbaden, 1991.

[28] (a) C. G. Pierpont, C. W. Lange, *Prog. Inorg. Chem.* **1994**, *41*, 331. (b) P. Chaudhuri, C. N. Verani, E. Bill, E. Bothe, T. Weyhermüller, K. Wieghardt, *J. Am. Chem. Soc.* **2001**, *123*, 2213. (c) C. G. Pierpont, *Coord. Chem. Rev.* **2001**, *216-217*, 99. (d) C. G. Pierpont, *Coord. Chem. Rev.* **2001**, *219-221*, 415.

[29] W. Kaim, B. Schwederski, *Coord. Chem. Rev*. **2010**, *254*, 1580.

[30] R. D. Hancock, A. E. Martell, *Chem. Rev*. **1989**, *89*, 1875.

[31] W. Tremel, A. Yella, M. N. Tahir, M. Panthöfer, S. Meuer, R. Zentel, *Mater. Res. Soc. Symp. Proc*. **2009**, *1140*, PP07-01. (b) C. Shahar, R. Levi, S. R. Cohen, R. Tenne, *J. Phys. Chem. Lett.* **2010**, *1*, 540.

5. Molecular Camouflage: Making use of Protection Group Chemistry to Control the Self-Assembly of Inorganic Janus Particles on Metal Chalcogenide Nanotubes by Pearson Hardness

Running Title: Molecular camouflage

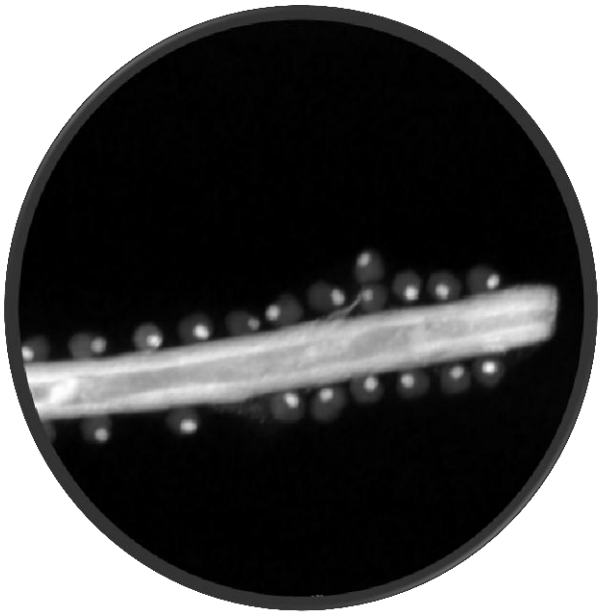

Jugal Kishore Sahoo[a], Muhammad Nawaz Tahir[a], Faegheh Hoshyargar[a], Bahar Nakhjavan[a], Robert Branscheid [b], Ute Kolb [b] and Wolfgang Tremel[a]

[a]Institute for Inorganic and Analytical Chemistry

[b]Institute for Physical Chemistry,

Johannes Gutenberg-Universität, Mainz, Germany

Angew. Chem. Int. Ed. 2011 (submitted)

5.1. Introduction

One of the goals in current nanoscience is to develop strategies for assembling nanoscale components into larger-scale, organized structures with desired properties and/or functionalities [1]. Unlike in molecular chemistry, however, where bond specificity and directionality are inherent to atoms of different types, nanoparticles mostly interact through symmetric interaction potentials (e.g., electrostatic, [2] van der Waals [3] or dipole–dipole [4]) and typically assemble into bulk, three-dimensional aggregates [4,5] or crystals [2, 4, 5]. The available methods of directional bonding/assembly at the nanoscale are limited so far to either the use of already directional organic templates (e.g. DNA, [6] proteins, [7] small molecules [8]) or the formation of topological defects at the "poles" of metal nanoparticles[8b] or nanorods [9] which then assemble into short, linear oligomers. Here, we show that the toolbox of "nanosynthesis" can be greatly enhanced by extending the all-important chemical concepts of protection groups and steric hindrance to the nanoscale.

Surface functionalization is a stringent requirement for controlling the assembly of nanoparticles to aggregates with hierarchical structure. Using "coordination chemistry in flatland" most nanoparticles (metals, metal sulfides or oxides) can be surface-treated in a straightforward fashion using established concepts of coordination chemistry. In general, surface ligands contain an anchor group (phosphines,[10] thiols,[11] carboxylates,[12] phosphates[13] or catecholates[14]) that strongly attaches to the surface of the respective nanomaterial and a (long) hydrocarbon or polyether chain that confers solubility in apolar or polar solvents.[15] A terminal group (e.g. an amino group) provides connectivity to additional functional ligands.[14d] As a result, a dense ligand shell is formed around each nanoparticle, preventing particle aggregation and providing chemical protection against oxidation and long-term solvent stability.

Inorganic nanotubes [16] (NT-MQ_2) and inorganic fullerenes (IF-MQ_2)[17] of layered metal chalcogenides are the inorganic congeners of carbon fullerenes and nanotubes that exhibit analogous mechanical[18] and electronic properties.[19] Their excellent lubrication properties[20] are related to their crystal structures. Different from other inorganic nanoparticles, layered chalcogenide nanotubes (NT-MQ_2 with M= W, Mo, Nb and Q=S, Se) and inorganic fullerenes (IF-MQ_2) have long resisted functionalization using standard surface chemistry. The inert chalcogenide layers sandwiching the metal atoms provide efficient steric

shielding from nucleophilic attack by organic ligands and makes chalcogenide nanoparticles inert and notoriously difficult to functionalize. While a covalent surface chemistry of their carbon congeners (fullerenes and nanotubes) is achieved through acid-induced oxidation of the carbon nanotube surface defects, [21] In contrast, covalent surface functionalization of layered chalcogenides needs anion coordination chemistry: metals with a high sulfur affinity, whose coordination sphere is partially blocked by chelating groups, must serve as a "glue" for anchoring organic ligands to the sulfur surface.

This has been demonstrated by employing chalcophilic transition metals in combination with multi-dentate surface ligands: The 3d metals "wet" the sulfur surface of the chalcogenide nanoparticles while the multidentate surface ligands partially block one hemisphere of the metal coordination environment. This steric shielding prevents an aggregation of the chalcogenide nanoparticles through inter-particle crosslinking. [22]

An alternative strategy is to attach nanoparticles directly to the chalcogenide nanoparticles.[23] In this case the sulfur atoms of the chalcogenide particles outcompete the protecting ligand of the nanoparticle surface, i.e. their affinity is based on their acid/base properties or Pearson hardness,[24] which allows their attachment without the aid of linkers or ligands. It has also been observed that the density of binding of different nanoparticles is related to the degree of Pearson hardness of their respective metal cations [24e]. An interesting group of asymmetric nanoparticles composed of two different building blocks with different Pearson hardness are inorganic Janus particles (JPs) because they might allow comparing reaction behavior based on Pearson hardness for a single particle. In addition, the perception that anisotropic shape and interactions through chemical "patchiness" are powerful tools for engineering the assembly of particular targeted structures has fuelled the discovery of new chemical, physical and biosynthetic methods for the synthesis of anisotropic nanoparticle and colloidal building blocks. In this contribution we report a synthetic strategy that allows the customized binding of inorganic Pt@Fe_3O_4 Janus particles onto WS_2 nanotubes (NT-WS_2) either via their Pt or Fe_3O_4 domains.

According to Pearson's HSAB (Hard Soft Acid Base) principle, a hard Lewis acid has the tendency to bind to a hard Lewis base and vice versa thus, in case of the metal chalcogenides the soft sulfur surface layer will have tendency to bind to other nanoparticles containing soft acid cations. The customized binding was achieved by making use of the Pearson hardness of the JPs: the soft Pt block (3.5 eV) has a higher sulfur affinity than the magnetite face (Fe^{+2}) 7.2 eV). This binding preference can be reversed by masking the Pt face with an organic

ligand. In the absence of a masking ligand the binding of the $Pt@Fe_3O_4$ JPs proceeds preferentially via the Pt face (Scheme 5.1).

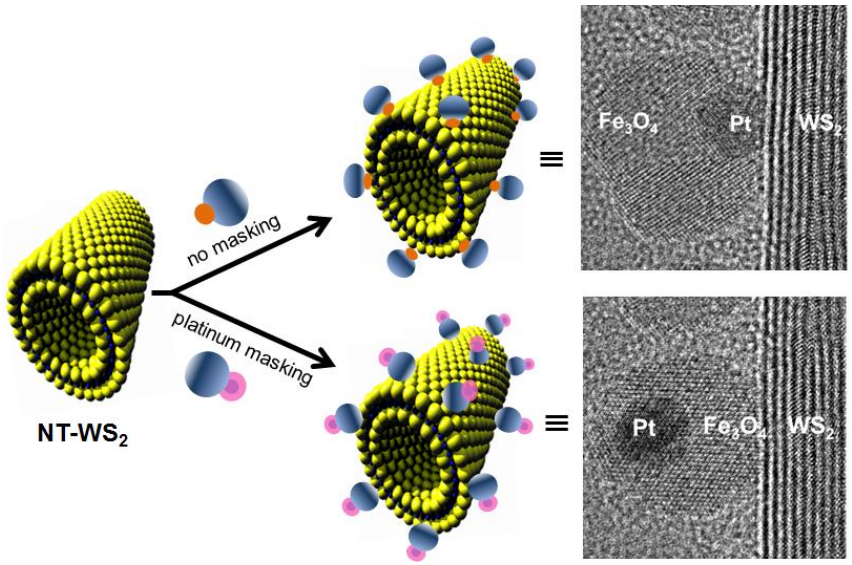

Scheme 5.1. *Customized binding of $Pt@Fe_3O_4$ JPs on NT-WS_2 via their Pt and Fe_3O_4 faces.*

5.2. Results and Discussions

NT-WS_2 nanotubes were prepared by sulfidization of tungsten oxide nanorods with H_2S [25]. $Pt@Fe_3O_4$ JPs were synthesized by a modified one-step method [26]. Figure 5.1 shows representative transmission electron microscopy (TEM) images of NT-WS_2 (Figure 5.1a) and $Pt@Fe_3O_4$ JPs (Figure 5.2b). The HRTEM image in the inset of Figure 5.1b reveals the distinct Pt (dark contrast) and Fe_3O_4 (light contrast) nano-domains. The oleic acid capping agents makes the $Pt@Fe_3O_4$ JPs soluble in most non-polar solvents (hexane, toluene etc). The XRD patterns of NT-WS_2 and $Pt@Fe_3O_4$ are provided in Appendix A8 and A11 respectively.

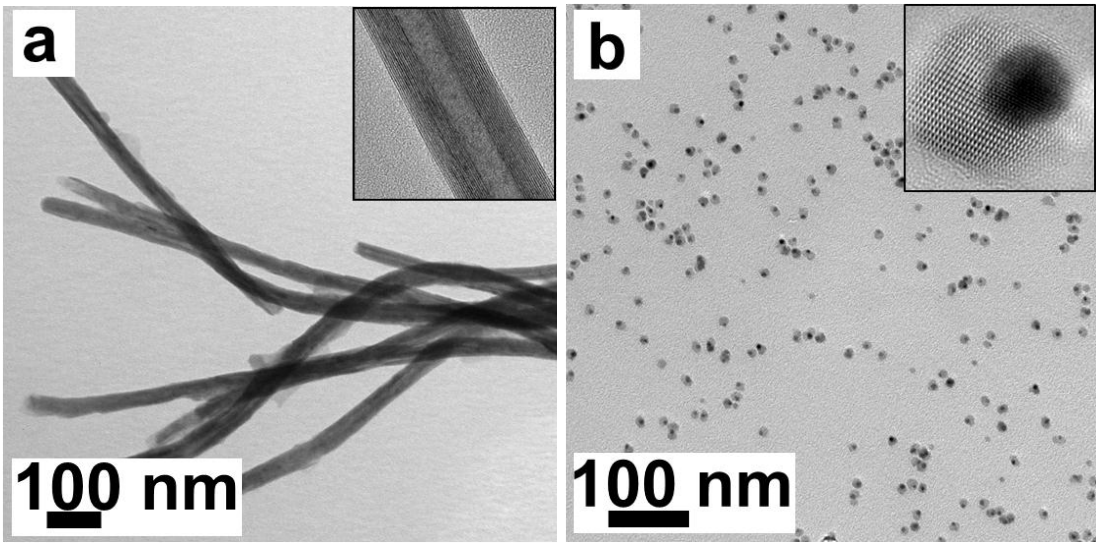

Figure 5.1. *TEM images of (a) NT-WS_2 and (b) Pt@Fe_3O_4 JPs. The HRTEM image in (b) shows the Pt and Fe_3O_4 of a single Pt@Fe_3O_4 JP.*

Functionalized NT-WS_2 was produced by mixing the NT-WS_2 and Pt@Fe_3O_4 nanoparticle solutions in chloroform under strong mechanical shaking. During this process, the Pt@Fe_3O_4 JPs assembled on the NT-WS_2 surface *via* ligand exchange. In this process, the oleic acid capping ligands on the surface of the Pt faces are substituted by the surface sulfur atoms of the chalcogenide nanotubes. The binding of the Pt@Fe_3O_4 JPs is illustrated in the TEM images in Figure 5.2. The TEM image reveal that the nanoparticles tend to adhere onto NT-WS_2 rather than stay in $CHCl_3$ and it has been observed that on an average 70 percent of the Janus particles attach to the sidewall of the nanotube through platinum domain. Figure 5.2a shows the low resolution TEM image of the nanocomposite whereas Figure 5.2b corresponds to high resolution TEM image which clearly indicates that it is the platinum domain that orients towards the outer layer of the NT-WS_2. The STEM mode image of Pt-Fe_3O_4@NT-WS_2 (Figure 5.2c) gives a better 2D view to conclude that Pt domain which appears bright spot in the corresponding image are mostly oriented towards the outer wall of the chalcogenide nanotubes. The inset in Figure 5.2c shows the corresponding histogram plotted by quantitatively calculating the orientation of different Janus domain towards surface of NT-WS_2. It has been observed that more than 75 percent of the Janus particles prefer to bind via platinum domain whereas the rest bind through magnetite domain. The binding through magnetite domain can be attributed to its size. The size of the magnetite domain is two times bigger than the platinum domain which makes it easier for binding. However, even though

both the Janus domains are susceptible to bind to the sidewall of NT-WS_2, the relative tendency of binding of platinum is more than that of magnetite domain because of its softness. Inorganic JPs in general have two chemically distinct surfaces which can be exploited selectively for the formation of hierarchical assemblies. In the case of Pt@Fe_3O_4 JPs, the platinum domain may be considered synonymous with other soft coinage metals like Au, Ag or Cu, whose surface can be tailored with thiol ligands, whereas the magnetite domain offers a surface chemistry comparable with that of other metal oxide nanoparticles like MnO, TiO_2 or ZrO_2 and can be tailored with ligands containing suitable (e.g. catechol) anchor groups [27]. As Pt is one of the softest metals (Pearson hardness 3.5 eV, the Pt domain will have in the absence of any masking ligands a higher tendency to bind to the soft sulfur layer of the metal chalcogenide rather than the magnetite domain containing either hard Fe^{3+} (Pearson hardness of Fe^{+3}: 13.1) or intermediate Fe^{2+} (Pearson hardness of Fe^{+2}: 7.2 eV) [24d].

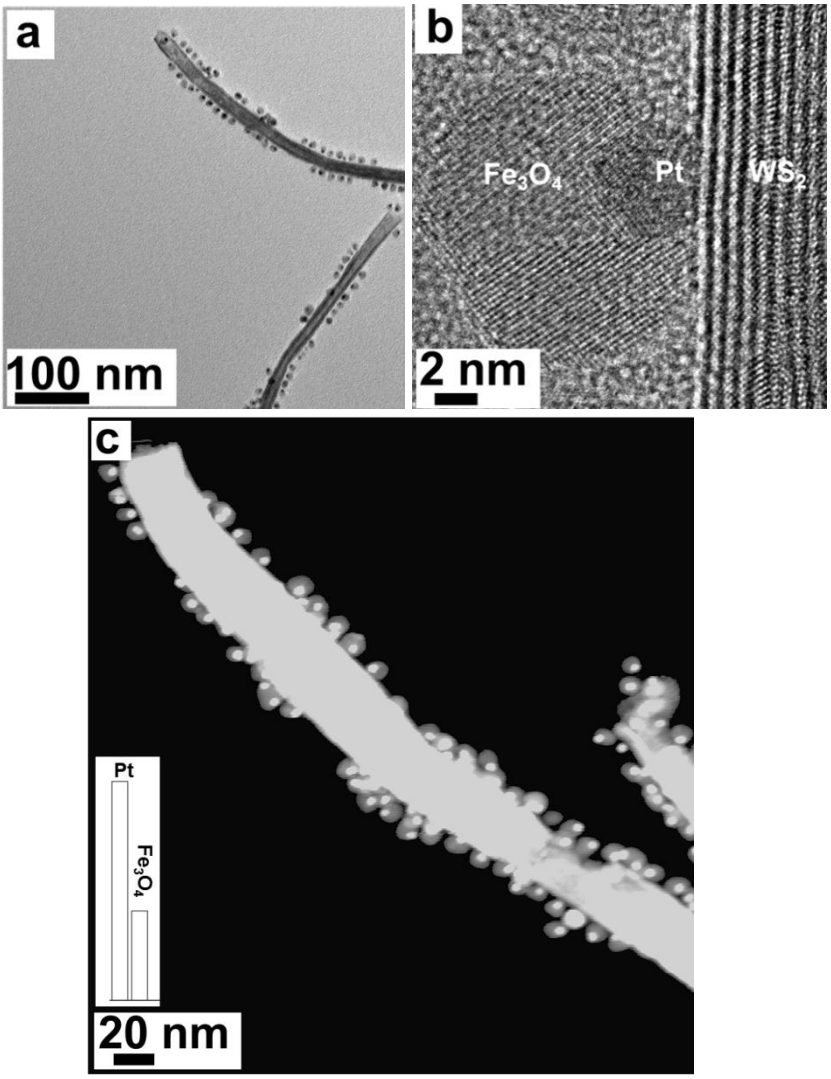

Figure 5.2. *(a) TEM, (b) HRTEM and (c) STEM images of $Pt@Fe_3O_4$ JPs chemisorbed on NT-WS_2. (a) Overview TEM image of a WS_2 nanotube having a monolayer with nearly full coverage of $Pt@Fe_3O_4$ JPs. (b) HRTEM image showing the binding of the Pt face of a single $Pt@Fe_3O_4$ JP to the surface of NT-WS_2. (c) STEM image showing the quantitative binding of the Pt Janus faces onto NT-WS_2. The histogram in the inset shows the binding ratio of Pt and Fe_3O_4 domains (70:30), average from 63 individual particles.*

Owing to the chemical distinctiveness of the JP surfaces it is possible to selectively camouflage each Janus face by an organic ligand that facilitates the binding of the other domain to the chalcogenide surface. However, masking the Pt face (or similarly Au, Ag, Cu etc.) by O-[2-(3-mercaptopropionylamino)ethyl]-O′-methyl polyethylene glycol - 5,000 (SH-PEG-OCH_3) with a soft thiol anchor group (i.e. replacing the oleic acid originally present on the Pt face) inverts the binding pattern of the JP: it binds almost now exclusively through the Fe_3O_4 face [28]. The PEG moiety confers stability to the particle in polar solvents, and – together with the terminal methoxy group camouflages the Pt domain and facilitates the binding of the JP via its unmasked Fe_3O_4 domain as illustrated in Scheme 5.1.

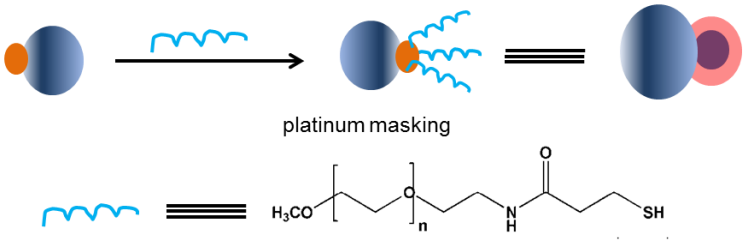

Scheme 5.2. *Selective masking of the Pt domain of the $Pt@Fe_3O_4$ JP by the SH-PEG-OCH_3 ligand*

Figure 5.3a shows a representative TEM image of the $Pt@Fe_3O_4$/NT-WS_2 nanocomposite, the HRTEM image in Figure 5.3b demonstrates the attachment of the $Pt@Fe_3O_4$ through their magnetite domains. The interlayer distance in NT-WS_2 is 0.63 nm as reported for other WS_2 nanotubes. The STEM image in Figure 5.3c shows the preferential orientation of magnetite domain towards the outer NT-WS_2 sulfur layer, and the inset in Figure 5.3c summarizes the orientation of different Janus domains with respect to the outer NT-WS_2 layers. Now more than 90 % of the JPs (average over 65 nanoparticles) stick to the NT-WS_2 sidewalls through

their magnetite domains. This unprecedented result can be explained by the masking of the Pt domains which enforces binding through the Fe_3O_4 domains. The corresponding EDX spectrum in Figure 5.4 confirms the composition of the nanocomosites (W, S, Pt, Fe and O). The presence of carbon (C), and copper (Cu) can be attributed to the carbon coated copper grids used for electron microscopy.

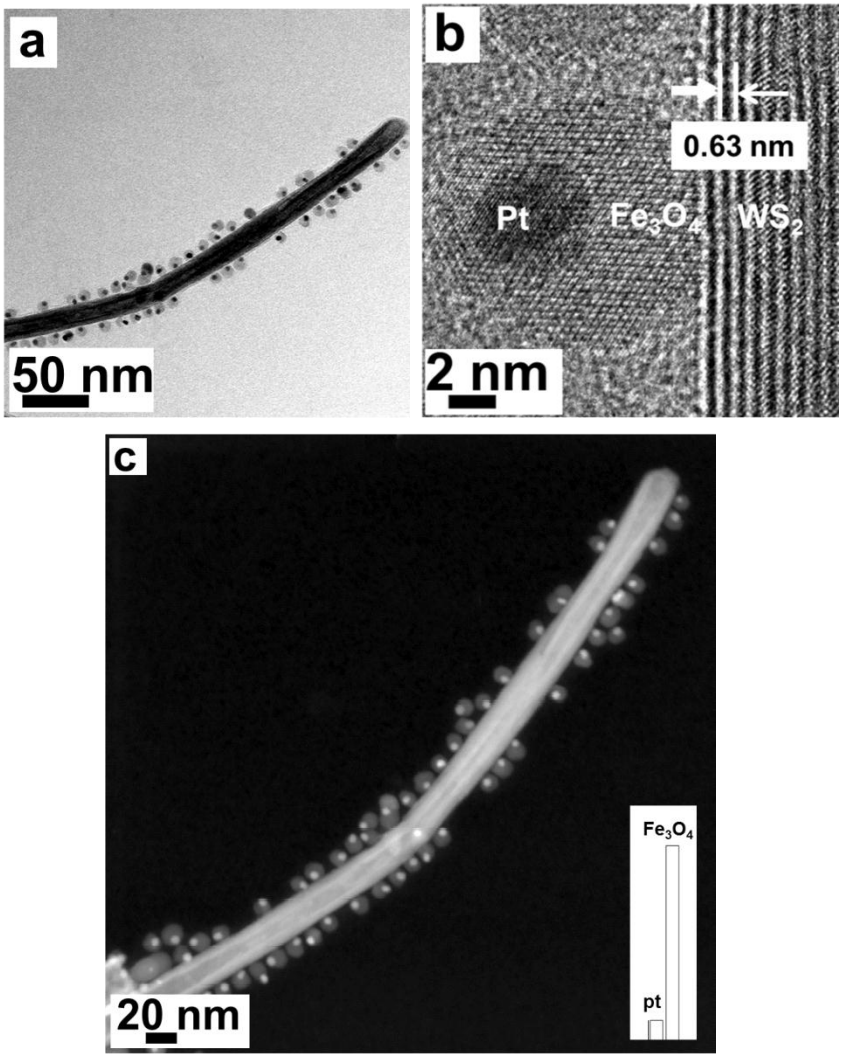

Figure 5.3. *(a) TEM image of Pt@Fe_3O_4 JP whose Pt domain was masked with an organic ligand of immobilized on NT-WS_2 (b) HRTEM image showing binding of the Fe_3O_4 magnetite face of the JP to NT-WS_2. (c) STEM image showing the preferred binding of the Fe_3O_4 faces to NT-WS_2. The histogram in the inset shows the binding ratio of Pt and Fe_3O_4 domains* (90:10), *average from 65 individual particles).*

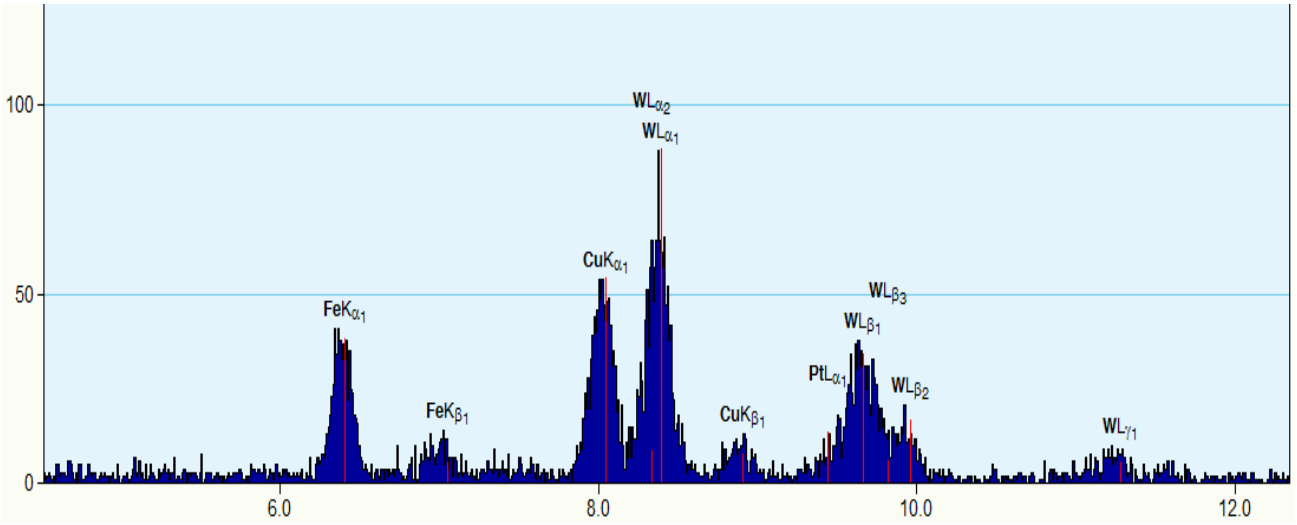

Figure 5.4. *EDX spectrum showing the presence of tungsten (W), sulfur(S), platinum (Pt), iron (Fe). The presence of Copper (Cu) and carbon(C) can be assigned to the carbon coated copper grid used for electron microscope.*

5.3. Summary and Conclusions

In summary, we have demonstrated that the hierarchical assembly Pt@Fe_3O_4 Janus particles onto WS_2 nanotubes is dictated by the principles of Pearson´s HSAB concept, i.e. Pt compared to Fe_3O_4 is the preferred binding partner because of its Pearson hardness. This binding preference can be inverted by camouflaging the Pt domain with an organic ligand. The assembly of the Pt@Fe_3O_4 particles onto WS_2 nanotubes in $CHCl_3$ solution can be quantitatively controlled in terms of their stoichiometric ratio below a critical particle concentration.

The Pt@Fe_3O_4/NT-WS_2 aggregates reported here may be viewed molecular analogs of metal oxide gated layered chalcogenide transistors. Traditional metal–oxide–semiconductor (MOS) structures are obtained by growing a layer of metal oxide on top of a semiconductor substrate and depositing a layer of metal (or silicon). Recently, Kis and coworkers used a HfO_2 gate dielectric to demonstrate a room-temperature single-layer MoS_2 mobility, similar to that of graphene nanoribbons, and to demonstrate transistors with room-temperature on/off current and ultralow standby power dissipation [29]. Chalcogenide nanotubes or graphene layers “gated” by metal oxide (such as Fe_3O_4, Fe_2O_3 or Al_2O_3) particles epitaxially connected to

conductive metals (such as Pt or Au) might therefore exhibit interesting properties that require thin transparent semiconductors, such as optoelectronics and energy harvesting.

5.4. Experimental Section.

Methods and Materials.

Platinum acetylacetonate ($Pt(acac)_2$), oleic acid, oleylamine, octadecane, $Fe(CO)_5$, O-[2-(3-Mercaptopropionylamino)ethyl]-O′-methylpolyethylene glycol-5,000 were purchased and used as received without further purification. Solvents such as tetrahydrofuran, chloroform, DMF, were purchased technical grade and used as received.

Apparatus. The morphology and composition of the product obtained after functionalization was examined in transmission electron microscope (TEM), high resolution transmission electron microscope (HRTEM, FEI Tecnai F30 ST operated at an extraction voltage of 300 kV, equipped with EDX and by selected area electron diffraction techniques (SAED).

Synthesis of Pt-Fe_3O_4 Janus Nanoparticles.

Under a constant flow of argon (Ar), 1 mmol platinum acetylacetonate $Pt(acac)_2$, 3 mmol oleic acid, 3 mmol oleylamine and 10 ml octadecane were mixed. The solution was heated to 120 ºC with a constant rate of 3 ºC/min. After reaching to this temperature, 4 mmol $Fe(CO)_5$ was added and the temperature was raised to 280ºC and kept at this temperature for 20 minutes. The product was precipitated by addition of excess of ethanol and collected by centrifugation (9000 rpm, 10 min, RT). The nanoparticles were repeatedly washed by dissolving them in hexane, precipitating them with ethanol and centrifugation (9000 rpm, 10 min, RT). Finally, the product was dissolved in toluene, flushed with argon (Ar) and stored at +4 ºC.

Synthesis of NT-WS_2. NT-WS_2 was synthesized using a reported method by Therese et al [25].

SH-PEG-OCH_3 Immobilization onto Pt-Fe_3O_4 (Platinum masking).

The Platinum face of the Janus nanoparticles was masked by immobilizing O-[2-(3-Mercaptopropionylamino)ethyl]-O′-methyl polyethylene glycol - 5,000 (SH-PEG-OCH_3) onto the janus nanoparticles. Typically, 10 mg of Pt-Fe_3O_4 was weighed into the reaction chamber in 10 ml of chloroform followed by addition of 20 mg of PEGylated thiol in 5 ml of chloroform. The reaction was allowed to stir at room temperature (RT) for 6 hours under

argon. After the reaction got over, the nanoparticles were precipitated in hexane and centrifuged (6000 rpm, 10 min, 2 times) and redissolved in chloroform before further use.

Immobilization Of Thiolated Pt-Fe_3O_4 onto NT-WS_2

Typically, 1 mg of NT-WS_2 was dispersed in 5 ml of chloroform in a ultra sonication bath fo 5-10 mins, followed by degassing under argon, for 5 mins, 20 µl (from a standard solution of 1mg/ml) of thiolated Pt-Fe_3O_4 was added drop wise to the NT-WS_2 solution under sonication. The reaction mixture was allowed to degas for 5 min. more before allowing it to react in a shaker for 4 hrs at RT. After the reaction got over, the unbound Janus nanoparticles were washed away by centrifugation (4000 rpm, 10 min.). The nanocomposite, thus formed, was characterized by LRTEM, HRTEM, STEM and EDX. Samples for TEM were prepared by putting 1-2 drops of dispersed sample on a copper TEM grid followed by drying.

5.5. References

[1] (a) G. M. Whitesides, B. Grzybowski, *Science* **2002**, *295*, 2418. (b) D. V. Talapin, J.-S. Lee, M. V. Kovalenko, E. V. Shevchenko. *Chem. Rev*. **2010**, *110*, 389.

[2] A. M. Kalsin, M. Fialkowski, M. Paszewski, S. K. Smoukov, K. J. M. Bishop, B. A. Grzybowski, *Science* **2006**, *312*, 420.

[3] P. C. Ohara, D. V. Leff, J. R. Heath, W. M. Gelbart, *Phys. Rev. Lett*. **1995**, *75*, 3466.

[4] R. Klajn, K. J. M. Bishop, B. A. Grzybowski, *Proc. Natl. Acad. Sci. USA* **2007**, *104*, 10305.

[5] E. V. Shevchenko, D. V. Talapin, N. A. Kotov, S. O_Brien, C. B. Murray, *Nature* **2006**, *439*, 55.

[6] (a) A. P. Alivisatos, K. P. Johnsson, X. Peng, T. E. Wilson, C. J. Loweth, M. P. Bruchez, P. G. Schultz, *Nature* **1996**, *382*, 609. (b) C. A. Mirkin, R. L. Letsinger, R. C. Mucic, J. J. Storhoff, *Nature* **1996**, *382*, 607.

[7] (a) E. Katz, I. Willner, *Angew. Chem*. **2004**, *116*, 6166; *Angew. Chem. Int. Ed.* **2004**, *43*, 6042. (b) M. H. Hu, L. P. Qian, R. P. Brinas, E. S. Lymar, J. F. Hainfeld, *Angew. Chem*. **2007**, *119*, 5203; *Angew. Chem. Int. Ed*. **2007**, *46*, 5111.

[8] (a) J. P. Novak, D. L. Feldheim, *J. Am. Chem. Soc*. **2000**, *122*, 3979. (b) G. A. DeVries, M. Brunnbauer, Y. Hu, A. M. Jackson, B. Long, B. T. Neltner, O. Uzun, B. H. Wunsh, F. Stellacci, *Science* **2007**, *315*, 358.

[9] (a) K. K. Caswell, J. N. Wilson, U. H. F. Bunz, C. J. Murphy, *J. Am. Chem. Soc.* **2003**, *125*, 13914. (b) R. Sardar, J. S. Shumaker-Parry, *Nano Lett*. **2008**, *8*, 731.

[10] (a) E. Ramirez, S. Jansat, K. Philippot, P. Lecante, M. Gomez, A. M. Masdeu-Bulto, B. Chaudret, *Organomet. Chem*. **2004**, *689*, 4601.

[11] (a) M. Brust, M. Walker, D. Bethell, D. J. Schiffrin, R. Whyman, R. *J. Chem. Soc. Chem. Commun.* **1994**, 801. (b) M. Bartz, J. Küther, G. Nelles, N. Weber, R. Seshadri, W. Tremel, *J. Mater. Chem.* **1999**, *9*, 1121.

[12] (a) B. O'Regan, M. Grätzel, *Nature*, **1991**, *353*, 737. (b) H. Jiang, K.-S. Moon, Y. Li, C. P. Wong, *Chem. Mater*. **2006,** *18*, 2969.

[13] (a) A. Subbiah, D. Pyle, A. Rowland, J. Huang, R. A. Narayanan, P. Thiyagarajan, J. Zon, A. Clearfield, *J. Am. Chem. Soc*. **2005**, *127*, 10826. (b) N. Adden, L. J. Gamble, D. G. Castner, A. Hoffmann, G. Gross, H. Menzel, *Langmuir* **2006**, *22*, 8197.

[14] (a) J. H. Waite, M. L. Tanzer, *Science* **1981**, *212*, 1038. (b) W. A. Armstrong, P. K. Mascharak, R. H. Holm, *J. Am. Chem. Soc.* **1982**, *104*, 4373. (c) C. Xu, K. Xu, H. Gu, R. Zheng, H. Liu, X. Zhang, Z. Guo, B. Xu, *J. Am. Chem. Soc.*, **2004**, *126*, 9938. (d) M. N. Tahir, M. Eberhardt, P. Theato, S. Faiß, A. Janshoff, T. Gorelik, U. Kolb, W. Tremel, *Angew. Chem.* **2006**, *118*, 922; *Angew. Chem. Int. Ed.* **2006**, *45*, 908.

[15] M. Bartz, J. Küther, G. Nelles, N. Weber, R. Seshadri, W. Tremel, *J. Mater. Chem.* **1999**, *9*, 1121.

[16] (a) L. Margulis, G. Salitra, R. Tenne, M. Talianker, *Nature* **1993**, *365***,** 113. (b) A. Yella, E. Mugnaioli, M. Panthöfer, H. A. Therese, U. Kolb, W. Tremel, *Angew. Chem.* **2009**, *121*, 6546; *Angew. Chem. Int. Ed.* **2009**, *48*, 6426.

[17] (a) Y. Feldman, E. Wasserman, D. J. Srolovitz, R. Tenne, *Science* **1995**, *267***,** 222. (b) R. Tenne, M. Homyonfer, Y. Feldman, *Chem. Mater*. **1998**, *10*, 3225. (c) W. Tremel, *Angew. Chem.* **1999**, *111*, 2311; *Angew. Chem. Int. Ed.* **1999**, *38*, 2175. (d) M. Nath, C. N. R. Rao, *J. Am. Chem. Soc.* **2001**, *123*, 4841. (e) R. Tenne, *Nature Nanotechnol*. **2006**, *1*, 103.

[18] (a) Y. R. Hacohen, E. Grunbaum, R. Tenne, J. Sloan, J. L. Hutchison, *Nature* **1998**, *365***,** 336. (b) A. Q. Zhu, T. Sekine, Y. H. Li, W. X. Wang, M. Y. Fay, H. Edwards, P. D. Brown, N. Fleischer, R. Tenne, *Adv. Mater.* **2005,** *17*, 1500. (c) I. Kaplan-Ashiri, S. R. Cohen, K. Gartsman, R. Rosentsveig, V. Ivanovskaya, T. Heine, G. Seifert, H. D. Wagner, R. Tenne, *Proc. Natl. Acad. Sci*. *USA* **2006**, *103*, 523.

[19] (a) L. Scheffler, R. Rosentzveig, A. Margolin, R. Popovitz-Biro, G. Seifert, S. R. Cohen, R. Tenne, *Phys. Chem. Chem. Phys*. **2002**, *4*, 2095. (b) M. Nath, S. Kar, A. K. Raychaudhuri, C. N. R. Rao, *Chem. Phys. Lett.* **2003**, *368*, 690.

[20] (a) F. Hulliger, *Structural Chemistry of the Layer-Type Phases, Ed.:* F. Levy, Reidel, 1976. (b) A. Katz, M. Redlich, L. Rapoport, H. D. Wagner, R. Tenne, *Tribol. Lett*. **2006**, *21*, 135. (c) J. Tannous, F. Dassenoy, B. Vacher, T. Le Mogne, A. Bruhacs, W. Tremel, *Tribol. Lett.* **2011**, *41*, 55.

[21] A. Hirsch, O. Vostrowsky, *Top. Curr. Chem*. **2005**, *245*, 193.

[22] (a) M. N. Tahir, M. Eberhardt, N. Zink, H. A. Therese, U. Kolb, P. Theato, W. Tremel, W. *Angew. Chem*. **2006**, *118*, 4927; *Angew. Chem. Int. Ed.* **2006**, *45*, 4809. (b) M. N. Tahir, A. Yella, J. K. Sahoo, F. Natalio, U. Kolb, F. Jochum, P. Theato, W. Tremel, *Isr. J. Chem.* **2010**, *50*, 500. (c) J. K. Sahoo, M. N. Tahir, A. Yella, R. Branscheid, U. Kolb, W. Tremel, *Langmuir*, **2011**, *27*, 385.

[23] J. K. Sahoo, M. N. Tahir, A. Yella, T. D. Schladt, E. Mugnaioli, U. Kolb, W. Tremel, *Angew. Chem.* **2010**, *120*, 7741; *Angew. Chem. Int. Ed*. **2010**, *49*, 7578.

[24] (a) R. G. Pearson, *J. Am. Chem.Soc.* **1963**, *85*, 3533. (b) R. G. Pearson, *J. Chem. Educ.* **1968**, *45*, 581. (c) R. G. Pearson, *J. Chem. Educ.* **1968**, *45*, 643. (d) R. G. Parr, R. G. Pearson, *J Am. Chem. Soc.* **1983**, *105*, 7512. (e) R. G. Pearson, *Chemical Hardness. Applications from Molecules to Solids*, Wiley-VCH, Weinheim 1997.

[25] H. A. Therese, J. Li, U. Kolb, W. Tremel, *Solid State Sci.* **2005**, *7*, 67.

[26] C. Wang, H. Daimon, S. Sun, *Nano Lett*. **2009**, *9*, 1493.

[27] (a) T. D. Schladt, K. Schneider, M. I. Shukoor, F. Natalio, M. N. Tahir, S. Weber, L. M. Schreiber, H. C. Schröder, W. E. G. Müller, W. Tremel, *J. Mater. Chem.* **2010**, *20*, 8297. (b) M. N. Tahir, P. Theato, P. Oberle, G. Melnyk, U. Kolb, M. Stepputat, W. Tremel, *Langmuir* **2006**, *22*, 5209.

[28] J. K. Sahoo, M. N. Tahir, A. Yella, T. D. Schladt, S. Pfeiffer, B. Nakhjavan, E. Mugnaioli, U. Kolb, W. Tremel, *Chem. Mater.* **2011**, dx.doi.org/10.1021/cm201178n.

[29] B. Radisavljevic, A. Radenovic, J. Brivio, V. Giacometti, A. Kis, *Nature Nanotechnol*. **2011**, *6*, 147.

6. Rational Assembly and Selective Dual Functionalization of Au@MnO Nanoflowers onto TiO_2 Nanowires

Running Title: Dual Functionalization

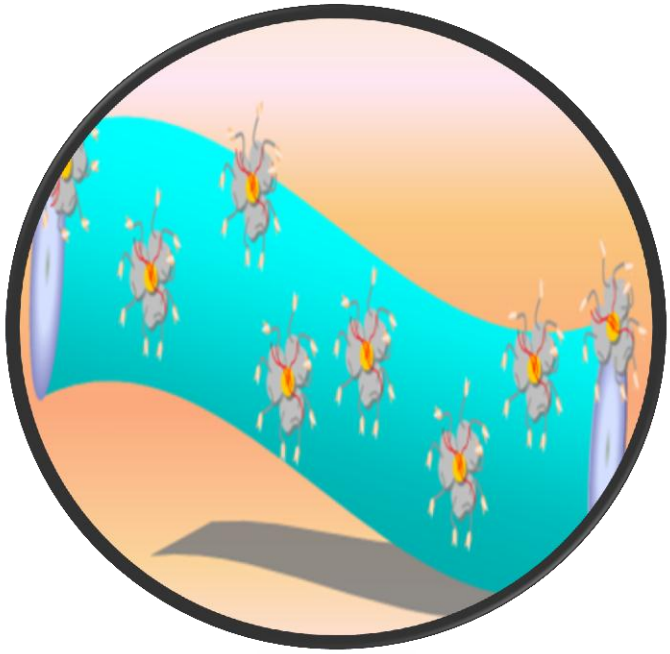

Jugal Kishore Sahoo[a], Muhammad Nawaz Tahir[a], Mohammad Ibrahim Shukoor[a], Thomas D Schladt[a], Filipe Natalio[a], Enrico Mugnaoli[b], Ute Kolb[b] and Wolfgang Tremel[a]

[a]Institute for Inorganic and Analytical Chemistry

[b]Institute for Physical Chemistry,

Johannes Gutenberg-Universität, Mainz, Germany.

Manuscript under preparation

6.1. Introduction

In present era of nanotechnology, the nanostructures involing assemblies of different nanodomains are getting more popular than individual nanoparticles [1] due to their multifunctional compartments which can be used to perform different applications. Therefore, the synthesis hybrid nanoparticles or assembly of different nanostructures with specific electronic, magnetic or optical properties to synthsize multicomponent composites can change and even enhance the properties of the individual constituents. These hybrid nanocomposites incorporate may involve two or more types of nanomaterial which can either effectively combine the properties of assembling materials [2], or can lead to novel functionalities that are independent of the individual components and may be tailored to fit a specific application. Such multifunctional, multicomponent nanocomposite materials can lead to applications that provide opportunities to achieve far-reaching challenges such as solar energy conversion, [3] biological sensors, [4] mechanical and optical devices, [5] catalysis, [6] and multimodal imaging in nanomedicine [7].

To achieve such multifunctional nanostructures, the first challenge is to assemble the nanomaterials into a complex hierarchical or supramolecular system and such assemblies can be obtained by conjugating the surfaces of nanoparticles with multifunctional ligands. These multifunctional ligands contain different functionalities which can be used to anchor the surfaces of nanoparticles and offering reactive head groups to construct supramolecular assemblies [8, 9]. Here we report immobilization of Au@MnO nanoflowers onto TiO_2 nanowires by using a versatile polymeric ligand and subsequent dual functionalization of the nanocomposite. The multifunctional polymeric ligand contains two functional group: a) a robust anchor group based on dopamine which can adhere to many metal oxide nanoparticles (e.g. TiO_2, Fe_2O_3, MnO etc) [10], b) a PEG chain tailoring the solubility and with an amine head group which can be used for further binding the metal nanoparticles. The architecture of the polymeric ligand is important as it provides the basis for comprehensive toolbox to build supramolecular architecture of organic-inorganic hybrid nanostructures. Moreover, this strategy of polymeric ligand functionalization of nanomaterial offers the possibility to introduce various functional molecules to tailor different applications.

TiO_2 particles with dimensions less than 100 nm are particularly attractive because being a wide band gap semiconductor material is a potential candidate for applications in different fields such as solar cell, [11] photo catalysis, [12] and sensors, [13] and the degradation of environmental hazardous chemicals [14]. On the other hand, Au@MnO nanoflowers, consists of two individually addressable Au and MnO domain, offers two functional surface for attachment of different kind of molecules, thereby increasing both diagonstics and therapeutic potentials [15].

Here we have used a versatile polymeric ligand as a mean to conjugate different nanomaterials to form nanocomposite. The modification strategy is based on the chelating affinity of catecholate ligand present on the polymer to metal oxide nanostructures. Furthermore, the primary amine group, attached to the multidentate polymer as an additional functional moiety, can be successfully utilized to conjugate Au@MnO nanoflowers onto the nanowires. The nanocomposite, thus formed, can be selectively dual functionalized utilizing the uniqueness of the different surfaces, where the metal (Au) core of the nanoflower can be surface activated using thiol tagged oligomer for specific bioconjugation through gold-thiol interaction [16], the free amine present on the TiO_2 nanowires can further be functionalized with a green flourophore 4-chloro, 7-nitro benzofurazan, (NBD-Cl) for optical detection [17].

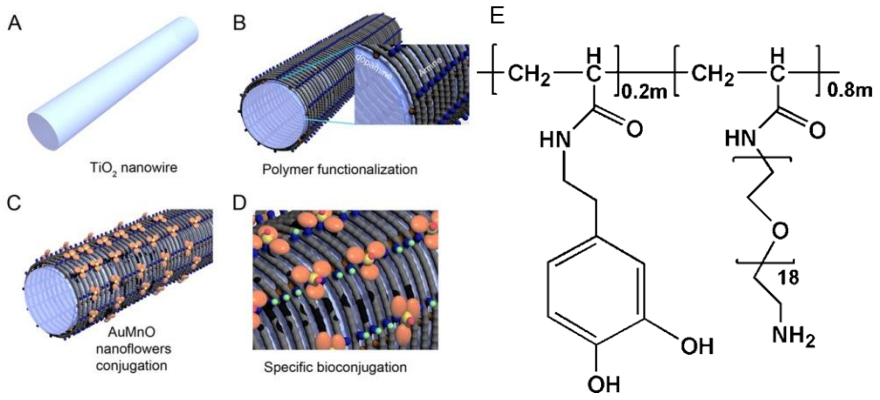

Scheme 6.1: *(a) Representative TiO_2 nanowires (b) Surface functionalization of nanowires with a multidentate polymer where blue sphere represents NH_2 functional group and orange sphere denotes catechol group on the polymer (c) Au@MnO nanoflowers conjugation onto the polymer functionalized TiO_2 nanowire through gold-NH_2 interaction (d) Specific dual functionalization of the nanocomposite where green fluorescent sphere denotes NBD dye attached to free amine of polymer bound TiO_2 nanowires where red fluorescent sphere represents Texas Red from the oligomer (e) Representative polymeric ligand.*

6.2. Results and Discussion

Synthesis and Characterization of Metal Oxide and Metal Chalcogenide Nanoparticles

As basic components to build the magnetic nanohybrids, Au@MnO heterodimer nanoparticles and TiO_2 nanowires were synthesized. The TiO_2 nanowires were prepared as described previously using hydrothermal synthesis [18]. Briefly, titanium iso-propoxide was added hydrolysed slowly in teflon vessel in ethanol under moist conditions, followed by the addition of 25 ml of 10M NaOH and hydrothermal treatment for 20 hours at 160 °C resulted in TiO_2 nanowires.

Figure 6.1a shows a representative transmission electron microscopy (TEM) image of the TiO_2 nanowires. The Au@MnO heterodimers were synthesized using solution synthesis at high temperature [19]. Figure 6.1b shows the transmission electron microscopy image of the nanoflower shape Au@MnO heterodimer nanopartilces. Typically, 1 mM of manganese (II) acetylacetonate and 0.05 mM of gold (III) acetate were added to a mixture of phenyl ether, oleic acid and oleylamine under argon. The resulting solution was rapidly heated to reflux (259-261°C) with approx. 20-25°C min-1 and kept at this temperature for 60 minutes before cooling to room temperature followed by washing under centrifugation. The nanoflowers were soluble in toluene and stored at 4 °C. TiO_2 nanowires were functionalized with polymeric ligand (Scheme 6.1) in DMF at 60 °C by a reported procedure. The functionalized TiO2 nanowires were well dispersed in various polar and non polar solvents such as water, ethanol, toluene etc.

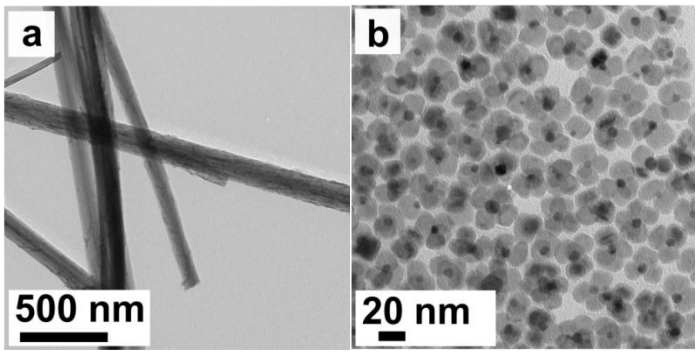

Figure 6.1. *TEM images of the as-synthesized TiO_2 nanowires (a), Au@MnO nanoflowers (b)*

For the synthesis of nanocomposite, (as shown in scheme 6.1) the surface of nanowire was modified by a versatile polymeric ligand that contains dopamine as chelating ligand which

binds to TiO_2 nanowire surface. The polymeric ligand contains amine as an additional functionality which was utilized for the assembly of Au@MnO nanoflowers onto the nanowire. The assembly of nanoflowers onto TiO_2 nanowires were produced by mixing a dispersion of the polymeric ligand functionalized TiO_2 nanowires and solution of nanoflower shape Au@MnO heterodimer nanoparticles in toluene under mechanical shaking. During this process, the nanoflowers were attached onto the nanowires surface *via* gold amine interaction [20].

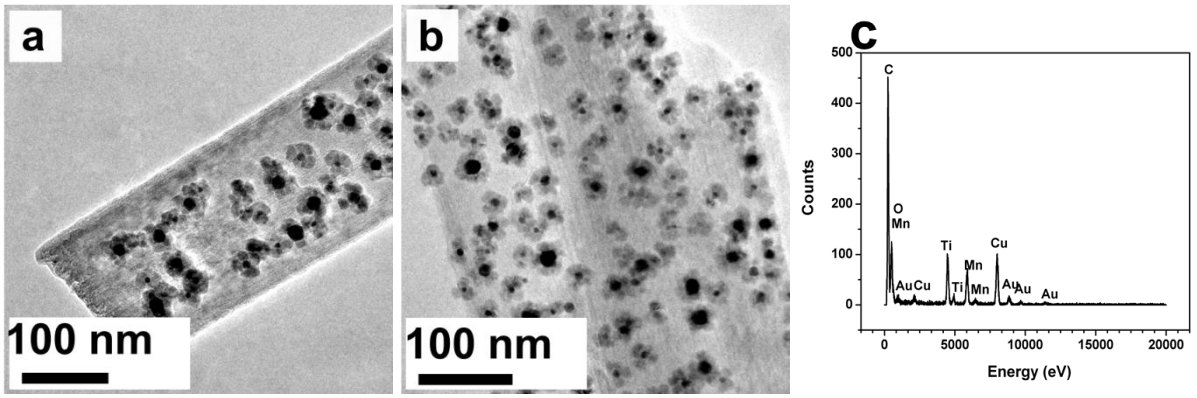

Figure 6.2. *High resolution TEM images of the nanocomposites. (a) A single TiO_2 nanowire bound with Au@MnO nanoflowers (b) Au@MnO nanoflowers bound to a couple of nanowires (c) EDX spectrum indicating the presence of Ti, Au, Mn, O with respective elementary signal.*

An overview TEM images of are Au@MnO heterodimer assembly onto TiO_2 nanowires is shown in Figure 6.2a which shows almost all the nanowires are uniformly covered with nanoflowers. Figure 6.2b shows a single nanowire decorated with nanoflowers. Figure 6.2c shows the EDX spectrum that confirms the presence of Ti, Au, Mn, and O in the nanocmposite. The signal for 'Cu' and 'C' come from the copper coated carbon grids used as a substrate for visualisation.

Furthermore, we investigated the addressability of both surface. The remaining amine groups onto the surfaces of TiO_2 nanowires were coupled with a flourophore (4-chloro, 7-nitro benzofurazan). Selective functionalization of the gold domain was achieved by incubating an acqueous solution of TiO_2@Au@MnO nanocomposite with thiol modified 24-mers customised oligonucleotide tagged with texas red through gold-thiol interaction [21]. Excess reagents were removed by repeated centrifugation. The oligonucleotide conjugated nanocomposite is stable in various acquesous solution (deionised water, PBS buffer) for several days.

The whole immobilization was monitored by UV-Vis spectroscopy and confocal microscopy. Figure 6.3d shows UV-Vis spectroscopy of TiO_2@Au@MnO nanocmposite bound by polymer. The absorption peak at 560 nm denotes gold core of the nanoflowers, whereas absorption at 280 nm is due to the presence of dopamine on the polymeric ligand. The immobilization of the flourophore (NBD: green, Texas red: red) was visualised in a confocal microscope. The green fluorescence was observed when the laser was excited at 514 nm whereas the red fluorescence was observed when the laser was excited at 543 nm. Both the fluorescence signals were co-localised (Figure 4c). Fig 6.3a shows the NBD bound TiO_2 nanowire whereas Figure 6.3b shows the oligomer bound Au core of the nanocomposite at the same place. Figure 6.3c (inset) shows a magnified image of a single nanowire coated with nanoflower, where the nanowire fluoresces green because of NBD dye, the nanoflowers looks red because of oligomer attached Au core.

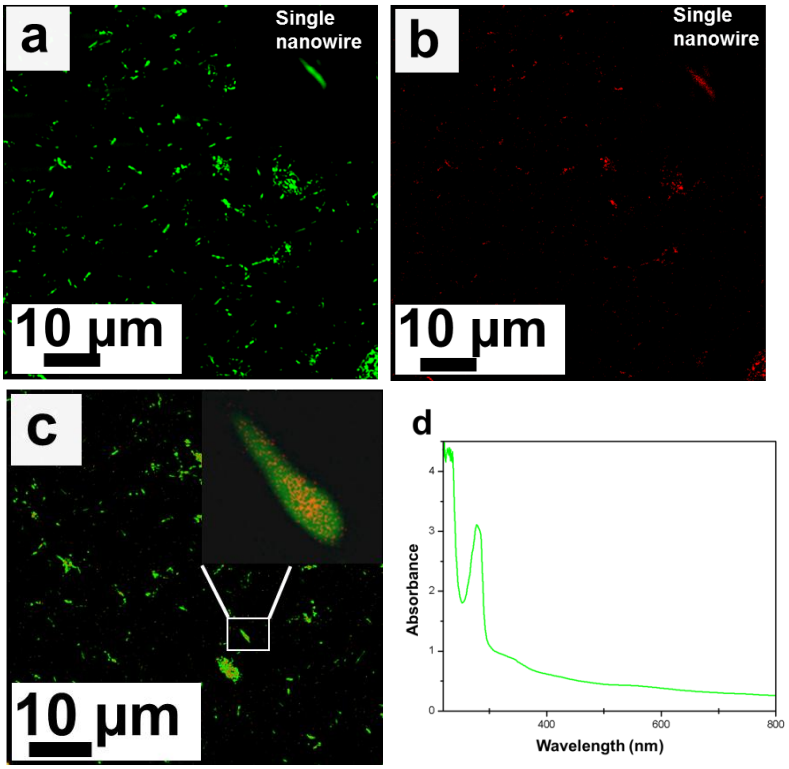

Figure 6.3. *Representative confocal laser scanning microscopic images collected at λ_{ex}=514 nm (a)Green fluorescence showing NBD immobilized TiO_2 nanowires (b) Red fluorescence showing SH-SS DNA-Texas Red bound Au core of Au@MnO nanoflowers bound on TiO_2 nanowires. (c) Co-localisation of both fluorescent signal indicating that Au@MnO nanoflowers are bound to TiO_2 nanowires and both surface can be selective dual functionalized with flourophore. Fig.c inset shows a single nanowire bound with the nanoflower, where green signal refers to the nanowire and red corresponds to Au core of*

Au@MnO nanoflowers. (d) UV-VIS spectrum of Au@MnO bound TiO_2 nanowire. The peak at 560 nm denotes absorbance due to gold core of the nanoflowers whereas peak at 280 nm signifies the presence of dopamine.

6.3. Summary and Conclusion

In summary, we have used simple established chemical route to achieve the functionalization of TiO_2 nanowire with Au@MnO magnetic nanoparticles and been able to bring three different unique surfaces to one platform. The modification strategy is based on the chelating affinity of dopamine to metal oxide nanostructure, as well as the affinity of amine functionality to bind to gold domain of nanoflowers. The surface bound nanoflowers are still amenable to functionalization with anchor groups such as thiol that readily binds gold surface. We have selectively conjugated a thiol tagged single stranded DNA that has texas red at 5' end for optical visualization. The free amine group present on the polymer can further be bound to green flourophore (NBD-Cl).

The functionalization of nanowires opens several new fields for this class of materials which have been pursued actively during the past few years for the related oxide materials. Similar functionalization strategy can be used for attachment of different metal oxide nanostructures (MnO, Fe_2O_3, Fe_3O_4). Janus nanostructures (Pt-Fe_3O_4, Au-Fe_3O_4, Au-MnO), electronically active components (metal and semiconductor nanoparticles) chalcogenide nanotubes for the attachment of electronically active components (metal and semiconductors nanoparticles) onto nanowires and nanotubes to construct different unique nanoarchitectures and can further be studied the change and behaviour of different intrinsic properties (magnetic, optical, electronic, catalytic) of the nanocomposites.

6.4.Experimental Section.

Methods and Materials.

Manganese (II) acetylacetonate (97%, ABCR), gold (III) acetate (>99.9%, Alfa Aesar), oleic acid (90%, Aldrich), oleylamine (80-90%, Acros), phenyl ether (>99%, Sigma Aldrich),3-Hydroxy tyramine hydrochloride (98%, Aldrich), 4-chloro-7-nitro benzofurazan, (NBD) (98%, Aldrich), Titanium isopropoxide (ACROS) used as received without further purification. Solvents such as ethanol (99.8%, Roth), toluene (>99%, Sigma-Aldrich), hexane

(p.A., Fisher), DCM (p.A., Fisher), DMF (extra dry, >99.8%, Acros), diethyl ether (p.A. Fisher) were purchased technical grade and used as received without further purification.

Apparatus. The morphology and composition of the product obtained after functionalization was examined in transmission electron microscope (TEM). Low-resolution TEM images were recorded on a Philips EM420 microscope operating at an acceleration voltage of 120 kV. High resolution electron microscope (HRTEM, FEI Tecnai F30 ST operated at an extraction voltage of 300 kV, equipped with EDX and also the product was characterized by ultraviolet-visible (UV-Vis) spectroscopy, and confocal laser scanning microscopy (CLSM) (Leica TCS SL, Leica Microsystems, Bensheim, Germany).

Synthesis of Au@MnO nanoflowers. Au@MnO nanoflowers were synthesized following a reported procedure [19]. All reactions were carried out using standard Schlenk conditions. 1 mM of manganese (II) acetylacetonate and 0.05 mM of gold (III) acetate were added to a mixture of phenylether (12mL), oleic acid (1 mL) and oleylamine (2 mL) under argon. The mixture was degassed at 50°C (10-2mbar) for 1 hour and repeatedly backfilled with argon to remove any traces of air and moisture. The resulting solution was rapidly heated to reflux (259-261°C) with approx. 20-25°C min-1 and kept at this temperature for 60 minutes before cooling to room temperature. The product was precipitated by addition of excess ethanol and collected by centrifugation. The nanoparticles were repeatedly washed by dissolving them in toluene, precipitating them with ethanol and centrifugation. Finally, the product was dissolved in toluene, flushed with argon and stored in a refrigerator.

Synthesis of TiO_2 nanowires. TiO_2 nanowires were synthesized using a reported procedure [18]. In a typical experiment, 1 g of Titanium isopropoxide (ACROS) was taken in a teflon vessel and 6 ml of analytical grade Ethanol were added into it. The teflon vessel was kept in desiccator. The precipitation of TiO_2 was initiated under moist atmosphere induced by placing a petri dish filled with water at the bottom of the desiccator. The diffusion experiment was stopped after 12 hrs, followed by the addition of 25 ml of 10 M NaOH aqueous solution. Then the reaction vessel was sealed into a stainless steel hydrothermal bomb, which was placed in an oven maintained at 160 °C for 20 hrs. After the autoclave was naturally cooled to room temperature, the obtained sample was filtered and repeatedly washed with 0.1 M HNO_3, 1 N HCl and deionized water. The obtained nanowires were characterized by using low resolution TEM. Samples for the TEM was prepared by putting a drop of the diluted sample on carbon coated copper grid, followed by drying.

Functionalization of TiO_2 nanowire with multi-dentate polymer ligand. TiO_2 NW's were functionalized with polymer ligand using a reported procedure. Typically in a RB flask, 10 mg of the nanowires were dispersed in 10 ml of DMF under a ultrasonication bath for 15 min, followed by degassing. In another vial, polymeric ligand (20 mg) was dissolved in 5 ml of DMF and was added to the dispersed nanowire solution dropwise under constant stirring at 60 °C. After the ligand was added, the reaction was allowed to stir overnight at 60 °C. The unbound polymer was washed away with centrifugation (9000 rpm, 10 min) after the completion of the reaction. The functionalized nanowires were repeatedly centrifuged to get rid of any unbound polymer and then were dispersed in toluene.

Binding of Au@MnO nanoflowers onto TiO_2 nanowires. In a typical experiment 4 ml (1mg/ml) of polymer bound TiO_2 nanowire was sonicated in a centrifuge vial in toluene. During sonication, 8 mg of Au@MnO nanoflowers (in toluene) was dropped inside the nanowire. The whole solution was allowed to sonicate further for 5 mins before it was put to shaker to react for 4 hrs at RT. After the completion of reaction, the unbound nanoflowers were washed away by centrifuging the sample at 9000 rpm for 10 min thrice in toluene. Finally Au@MnO bound TiO_2 nanocomposite was characterized morphologically by TEM/HRTEM and EDAX. Samples for TEM were prepared by putting 1-2 drops of dispersed sample on a copper TEM grid followed by drying.

Conjugation of NBD dye to free NH_2 groups of polymer functionalized TiO_2 @ Au-MnO nanocomposite.

In a typical experiment, 4 mg (1mg/ml) of the nanocomposite was dispersed in DMF in an ultrasonication bath. To the dispersed solution 4-chloro, 7-nitro benzofurazan (NBD-Cl) solution (10 mg/2 ml) was added drop wise and was further sonicated for 5 mins. The reaction was put to shaker at room temperature for 6 hrs. After the reaction got over, the unbound NBD-Cl was washed away by centrifugation at 9000 rpm for 10 min. The binding of the flourophore to the nanowire was visualized under confocal laser scanning microscope. Samples for the confocal microscopy were prepared by dropping 20 microliter of the sample in a glass slide followed by drying.

Selective Functionalization of Au domain of Au@MnO nanoflower bound TiO_2 using Texas Red-ODN-SH.

For functionalization of the Au core, a 24-mers customized oligonucleotide with the following composition: TTTTTTTTTTTTTTTTTTTTTTTT-SH containing Texas red at the 5'end and a thiol group on the 3'end (Texas Red ODN-SH, Sigma Aldrich) was used. A stock

solution with a concentration of 75 mM was prepared in Tris-EDTA buffer (pH 7.5) and aliquots were kept at –20ºC. For oligonucleotide functionalization, NBD-polymer modified TiO_2@Au-MnO nanoflowers (2 mg/ml) were incubated with a 10 mM solution of Texas Red-ODN-SH as described elsewhere.[30] After shaking for 24 h at 20°C, the sample was treated with phosphate buffer (10 mM, pH 7.0) containing NaCl (0.1 M) followed by a centrifugation step (15 min at 10000*x*rpm, room temperature) to remove unbound oligonucleotides. Following removal of the supernatant, the nanoparticles were washed twice with phosphate buffer (10 mM, pH 7.0) +NaCl (0.1 M), re-centrifuged (15 min,10000*x*rpm, room temperature) and re-dispersed in the same phosphate buffer solution. The fluorescence analysis of the multi-fluorescent labeled nanoparticles was performed with a Confocal laser scanning microscope (Leica TCS SL, Leica Microsystems, Bensheim, Germany) equipped with He/Ne Laser excited at 488 nm for green fluorescence and 543 nm for red fluorescence visualisation. The images were co-localized using the software Analysis (Olympus, USA).

6.5. References

[1] (a) P. D. Cozzoli, T. Pellegrino, L. Manna, *Chem. Soc. Rev*. 2006, *35*, 1195. (b) H. Zeng, S. Sun, *Adv. Funct. Mater*. **2008**, *18*, 391. (c) J. A. McGuire, J. Joo, J. M. Pietryga, R. Schaller, V. I. Klimov, *Acc. Chem. Res.* **2008**, *41*, 1810.

[2] (a) V. Subramanian, E. E. Wolf, P. V. Kamat, *J. Phys. Chem. B* **2003**, *107*, 7479. (b) T. Mokari, E. Rothenberg, I. Popov, R. Costi, U. Banin, *Science* **2004**, *304*, 1787. (c) T. Mokari, C. G. Sztrum, A. Salant, E. Rabani, U. Banin, *Nat. Mater*. **2005**, *4*, 855. (d) J. Yang, H. I. Elim, Q. Zhang, J. Y. Lee, W. Ji, *J. Am. Chem. Soc*. **2006**, *128*, 11921.

[3] A. Rizzo, C. Nobile, M. Mazzeo, M. De Giorgi, A. Fiore, L. Carbone, R. Cingolani, L. Manna, G. Gigli, *ACS Nano* **2009**, *3*, 1506.

[4] (a) P. K. Sudeep, S. T. S. Joseph, K. G. Thomas, *J. Am. Chem. Soc.* **2005**, *127*, 6516. (b) X. Huang, I. H. El-Sayed, W. Qian, M. A. El-Sayed, *J. Am. Chem. Soc.* **2006**, *128*, 2115.

[5] (a) M. Thomalla, H. Tributsch, *J. Phys. Chem. B* **2006**, *110*, 12167. (b) J.-P. Salvetat, J.-M. Bonard, N. H. Thomson, A. J. Kulik, L. Forrö, W. Benoit, L. Zuppiroli, *Appl. Phys. A* **1999**, *69*, 255.

[6] (a) Q. Liu, Z. Yan, N. L. Henderson, J. C. Bauer, D. W. Goodman, J. D. Batteas, R. E. Schaak, *J. Am. Chem. Soc*. **2009**, *131*, 5720. (b) B. Lim, M. Jiang, P. H. C. Camargo, E. C. Cho, J. Tao, X. Lu, Y. Zhu, Y. Xia, *Science* **2009**, *324*, 1302.

[7] (a) M. Liong, J.Lu, M. Kovochich, T. Xia, S. G. Ruehum, A. E. Nel, F. Tamanoi, J. I. Zink, *ACS Nano* **2008**, *2*, 889. (b) L. Y. Wang, J. W. Bai, Y. J. Li, Y. Huang, *Angew.Chem*. **2008**, *120*, 2473; *Angew.Chem. Int. Ed*. **2008**, *47*, 2439. (c) C.-K. Kim, P. Ghosh, V. M. Rotello, *Nanoscale* **2009**, *1*, 61.

[8] (a) J. K. Sahoo, M. N. Tahir, A. Yella, R. Branscheid, U. Kolb, W. Tremel, *Langmuir* **2011**, *27*, 385.

[9] M. N. Tahir, M. Eberhardt, P. Theato, S. Faiß, A. Janshoff, T. Gorelik, U. Kolb, W. Tremel, *Angew. Chem. Int. Ed*. **2006**, *45*, 908.

[10] N. M. Dimitrijevic, Z. V. Saponjic, B. M. Rabatic, T. Rajh, *J. Am.Chem. Soc*. **2005**, *127*, 1344.

[11] A. Hagfeldt, M. Gratzel, *Acc. Chem. Res*. **2000**, *33*, 269.

[12] S. Hore, E. Palomares, H. Smit, N. J. Bakker, P. Comte, P. Liska, K. R. Thampi, J. M. Karoon, A. Hinsh, J. R. Durrant, *J. Mater. Chem*. **2005**, *15*, 412.

[13] E. Palomares, R. Vilar, A. Green, J. R. Durrant, *Adv. Funct. Mater*. **2004**, *14*, 111.

[14] (a) J. H. Schattka, D. G. Shchukin, J. G. Jia, M. Antonietti, R. A. Carusa, *Chem. Mater*. **2002**, *14*, 5103. b) L. X. Chen, T. Rajh, Z. Y. Wang, M. C. Thurnauer, *J. Phys. Chem. B* **1997**, *101*, 10688.

[15] C. Xu, J. Xie, D. Ho, C. Wang, N. Kohler, E. G. Walsh, J. R. Morgan, Y. E. Chin, S. H. Sun, *Angew. Chem.***2008,** *120*, 179; *Angew. Chem. Int. Ed*. **2008**, *47*, 173.

[16] F. Zhang, M. W. A. Skoda, R. M. J. Jacobs, S. Zorn, R. A. Martin, C. M. Martin, G. F. Clark, G. Goerigk, F. Schreiber, *J. Phys. Chem. A* **2007**, *111*, 12229. (b) E. C. Dreaden, S. C. Mwakwari, Q. H. Sodji, A. K. Oyelere, M. A. El-Sayed, *Bioconjugate Chem.* **2009,** *20,* 2247.

[17] M. N. Tahir, N. Zink, M. Eberhardt, H. A. Therese, U. Kolb, P. Theato, W. Tremel, *Angew. Chem. Int. Ed*. **2006**, *45*, 4809.

[18] M. N. Tahir, M. Eberhardt, P. Theato, S. Faiß, A. Janshoff, T. Gorelik, U. Kolb, W. Tremel, *Angew. Chem. Int. Ed*. **2006**, *45*, 908.

[19] T. D. Schladt, M. I. Shukoor, K. Schneider, M. N. Tahir, F. Natalio, I. Ament, J. Becker, F. D. Jochum, S. Weber, O. Köhler, P. Theato, L. M. Schreiber, C. Sönnichsen, H. C. Schröder, W. E. G. Müller, W. Tremel. *Angew. Chem. Int. Ed*. **2010**, *49*, 3976.

[20] H. Wang, D. W. Brandl, F. Le, P. Nordlander, N. J. Halas, *Nano Lett*. **2006**, *6*, 827.

[21] M. Cardenas, J. Barauskas, K. Schillen, J. L. Brennan, M. Brust, T. Nylander, *Langmuir* **2006**, *22*, 3294.

7. Biocompatible Amine Functionalized ZrO_2 Nanoparticles as Multi Color Luminescent Agents

Running Title: Luminiscent ZrO_2

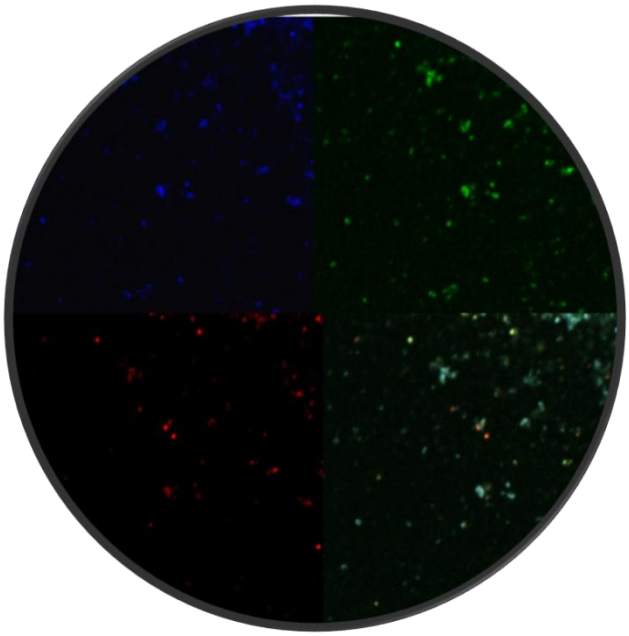

Jugal Kishore Sahoo[a], Filipe Natalio[a], Muhammad Nawaz Tahir[a], Anubha Kashyap[b], Dennis Strand[b], Wolfgang Tremel[a].

[a]Institut für Anorganische Chemie und Analytische Chemie

[b]Medizinische Klinik I, Universitätsmedizin

Johannes Gutenberg-Universität, Mainz, Germany.

Manuscript under preparation

7.1. Introduction

Fluorescent nanoparticles with tailored surfaces are used in many different fields of imaging and diagnosis. The inorganic fluorescent nanomaterials used in last couple of years consist of fluorescent semiconductor quantum dots (QDs) and have been widely explored because of their broad absorption, narrow photoluminescence (PL), and high photostability [1]. The QDs are more photostable and offers a wide range of emission colors based on size and compositions. They also provide the opportunity to separate the short lived fluorescent signal due to the presence of different self signailing moieties in cells due to the fact that QDs have long fluorescence lifetime. But the major concern to use these QDs as recognition materials in cells is their cytotoxicity and it limits them to be used in biological systems [1,3]. Therefore, there is an ever growing need to explore nanoprobes with exceptionally well fluorescent peoperties and should be biocompatible.

Recently a new dye free metal oxide nanoparticles (SiO_2) without metal activator was prepared by condensation of alkoxy-silane in presence of organic acids [4]. Alternate procedure for synthesizing luminescent silica nanoparticles have also been reported [5]. In comparison to other luminescent materials (QDs), silica nanoparticles are found to be more photostable, biocompatible and less toxic [6]. A novel low temperature wet chemical method to produce photoluminiscent silica has been reported [7-8] which confers intrinsic luminescence after functionalization depending on the coupled ligand. The emergence of silica as an alternative multiphoton fluorescent material to rather toxic Q-dots offers new high performance, photo stability, biocompatibility and low toxicity and leaves open window for other metal oxide nanoparticles.

Multi-photon fluorescent nanomaterials have attracted much attention recently for their broad range of applications including improved biological sensors and bioimaging [9-10]. Multi-photon microscopy enables imaging of different fluorofores with less overall photobleaching and photodamage than conventional imaging techniques [11]. Hence current research interests are oriented towards finding novel nanomaterials which lumineses less than two photon microscopy. Until now, the best performing two photon fluorescent materials are quantum dots (QDs) [12-14], and metallic nanoparticles [15-18]. These fluorescent nanomaterials have been studied both *in vitro* and *in vivo*. Recently carbon dots (C-dots) [19-20] and silicon [21] have emerged as an alternative to quantum dots. However the toxicity and more expensive

heavy metal based semiconductor quantum dots have propelled the researchers to find a more benign, eco-friendly alternative.

Here we report a novel wet chemical synthetic strategy for topological tailoring of ZrO_2 nanoparticles which confers photoluminescence without introducing any dye molecule onto the surface. These functionalized zirconia nanoparticles exhibit strong photoluminescence and photostability and are biocompatible. Moreover, these fluorescing nanoparticles can be imaged using multiphoton microscopy.

7.2. Results and Discussion

Synthesis and amine functionalization of ZrO_2 nanoparticles

ZrO_2 nanoparticles (np's) were synthesized using a hydrothermal route [22]. Briefly, zirconium isopropoxide isopropanol complex (Aldrich, 99.9%) was added into teflon reaction cup, and 30 mL of benzyl alcohol under constant shaking at high speed until the whole zirconium isoproxide became soluble. The cup was then inserted into a 50ml stainless steel autoclave and heated to 210 °C. After 72 h the vessel was allowed to cool down and then opened to retrieve a white turbid suspension. The product was isolated as a white powder by centrifugation or simple decantation, washing with tetrahydrofuran (THF), and drying in vacuo resulted in white crystalline powder of ZrO_2 nanoparticles with size around 4 nm. A representative low resolution TEM image of as synthesized ZrO_2 np's is shown in Figure 7.1a, which shows that the zirconia np's are monodisperse and are approximately 4-5 nm in diameter. ZrO_2 np's were surface functionalized has schematically demonstrated in Scheme 7.1.

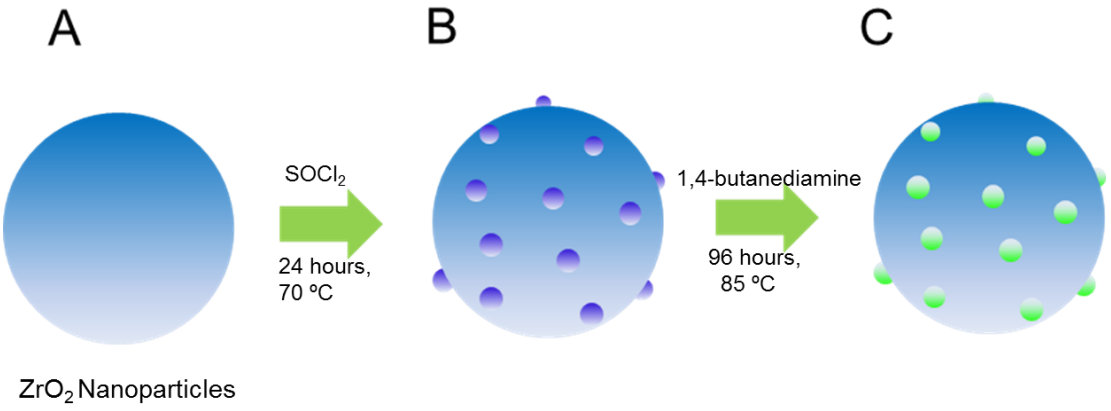

Scheme 7.1. *Schematic representation of amination of ZrO_2 nanoparticles. (a) ZrO_2 nanoparticles; (b) after treatment with $SOCl_2$ that replaces the surface hydroxyl group by*

chlorine (nucleophilic attack); (c) The highly reactive intermediate can easily be replaced by amine.

In a typical functionalization procedure, ZrO_2 np's were surface treated with excess of $SOCl_2$ for 24 h at 70 ºC in order to replace the surface hydroxyl groups by chlorine [23]. After repeated washing in dry THF to remove excess of $SOCl_2$, the highly reactive Cl-substituted intermediate ZrO_2 np's were allowed to react with N-Boc-1,4-butanediamine for 96 h at 85 ºC so as to allow a nucleophilic substitution for surface chlorine atom with primary amine functionality. After extensive washing (removal of unreacted ligand), the Boc (Di-tert-butyl dicarbonate) group present in the side chain was deprotected by using a solution of HCl (0.1M) in methanol and stirring it for 2 h at room temperature (RT) . TEM image of ZrO_2 np's after functionalization with 1, 4-butanediamine (Figure 7.1 b) shows that the nanoparticles retain their shape, size and monodispersity. This is confirmed by DLS measurements (Figure 7.1c) where a narrow size distribution can be observed and it ranges from 4-60nm with maximum at 16 nm.

The functionalized ZrO_2 np's offer a free surface primary amine which renders these fluorsecnt probes soluble in water soluble [24] and the successful Boc deprotection was confirmed by means of FT-IR (ATR). Figure 7.1d shows clearly the free amine frequencies (3500-3300 cm^{-1}) making these nanoparticles suitable for binding biomolecules for further biomedical applications.

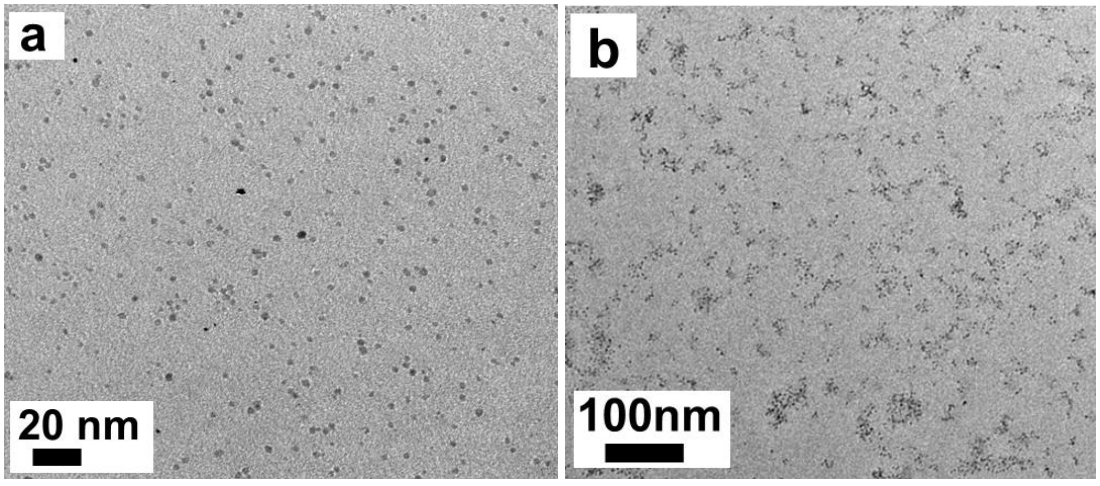

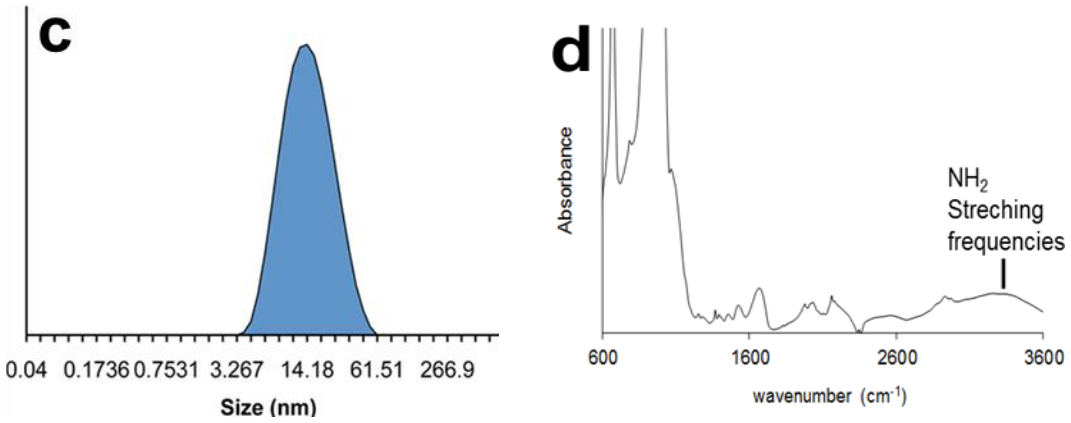

***Figure 7.1**. (a) Electron microscopy images of as synthesized ZrO_2 nanoparticles (np). (b) ZrO_2 np's after functionalization, (c) Dynamic light scattering data of functionalized ZrO_2. (d) FT-IR ATR spectra of functionalized ZrO_2 nanoparticles. The free amine groups corresponding frequencies are shown by arrows.*

Interestingly, after amine functionalization, these ZrO_2 np's display strong photoluminiscence with emission band at 420 nm when excited at 280 nm and red shifted to 450 nm on increasing excitation wavelength to 360 nm (blue line, Figure 7.2 a). Under a UV-lamp at (λ_{ex}, 366 nm) a strong blue photoluminiscence is observed with naked eye (Figure 7.2 a (inset). However, the dependence of band shift with excitation wavelength observed in Figure 7.2a is still not well understood.

ZrO_2 np's are known to display a blue photoluminescence with emission wavelength at 376 nm, however the mechanism is not well understood. Indeed this is true for excitation wavelengths like 240nm-270nm which coreesponds to bandgap excitation. In our case after functionalization the maximum emission was observed for excitation wavelength 360nm which is higher than the bandgap of cubic ZrO_2. Figure 7.2b represents the fluorescent spectroscopic data of unfunctionalized ZrO_2 np's at different excitation wavelength where only at small excitation wavelengths a clear emission is observed, which correspond to band gap emission. This data indicate that the np's have an additional photoluminescence at a higher wavelength upon functionalization.

This data potentially discovered a new luminescent material in metal oxide nanoparticles apart from C-dots, Q-dots and metal nanoparticles and more recently silica nanoparticles.

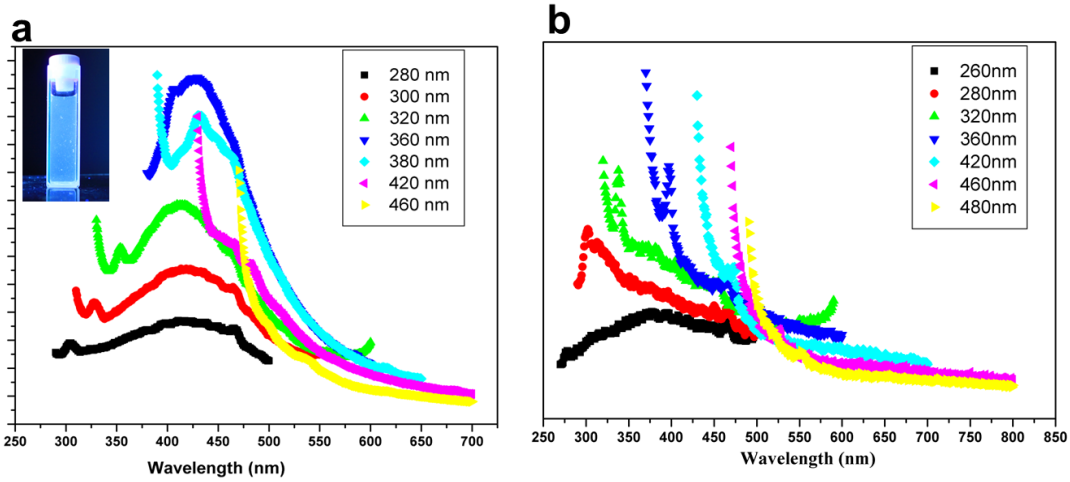

Figure 7.2. *Photoluminescence spectra of ZrO_2 np's (a) amine functionalized and unfunctionalized ZrO_2 (b). Inset (a) Digital photograph of the solution under UV excitation (λ_{ex} = 366 nm) showing a strong blue signal.*

To confirm it further, the amine functionalized ZrO_2 np's were analyzed using one and two-photon microscopy. Typically a small volume of aqueous solution of functionalized nanoparticles was dropped on a glass slide to measure the photoluminescence. The amine functionalized ZrO_2 np's were found to display strong blue, green and red luminescence when excited at different wavelengths. In order to study the photostability of these np's, two different areas of the sample were selected. In one area, (Region 1) the laser power in all the three channels (T1, T2 and T3) (Figure 7.3) was increased up to 20% of the original laser power (for 80 s) and in the second area (Region 2) the laser power was left in its original configuration in all the three channels (T1, T2 and T3) . Figure 7.3e shows the stability of these nanoparticles and the decay of the emitted luminescence was observed only when when exposed to a higher power of the laser. On the other hand, the control performed in parallel shows that these nanoparticles are highly photostable, i.e., the emitted luminescence remains constant throughout the exposition time which makes them suitable for biological application due to use of low laser power during imaging, thus preventing it from bleaching. The one photon luminescent images are shown in Figure 7.3 a-d where Figure 7.3 a, b and c correspond to blue, green and red luminescence respectively. Figure 7.3 d represents the co-localized image of the blue, green and red luminescence.

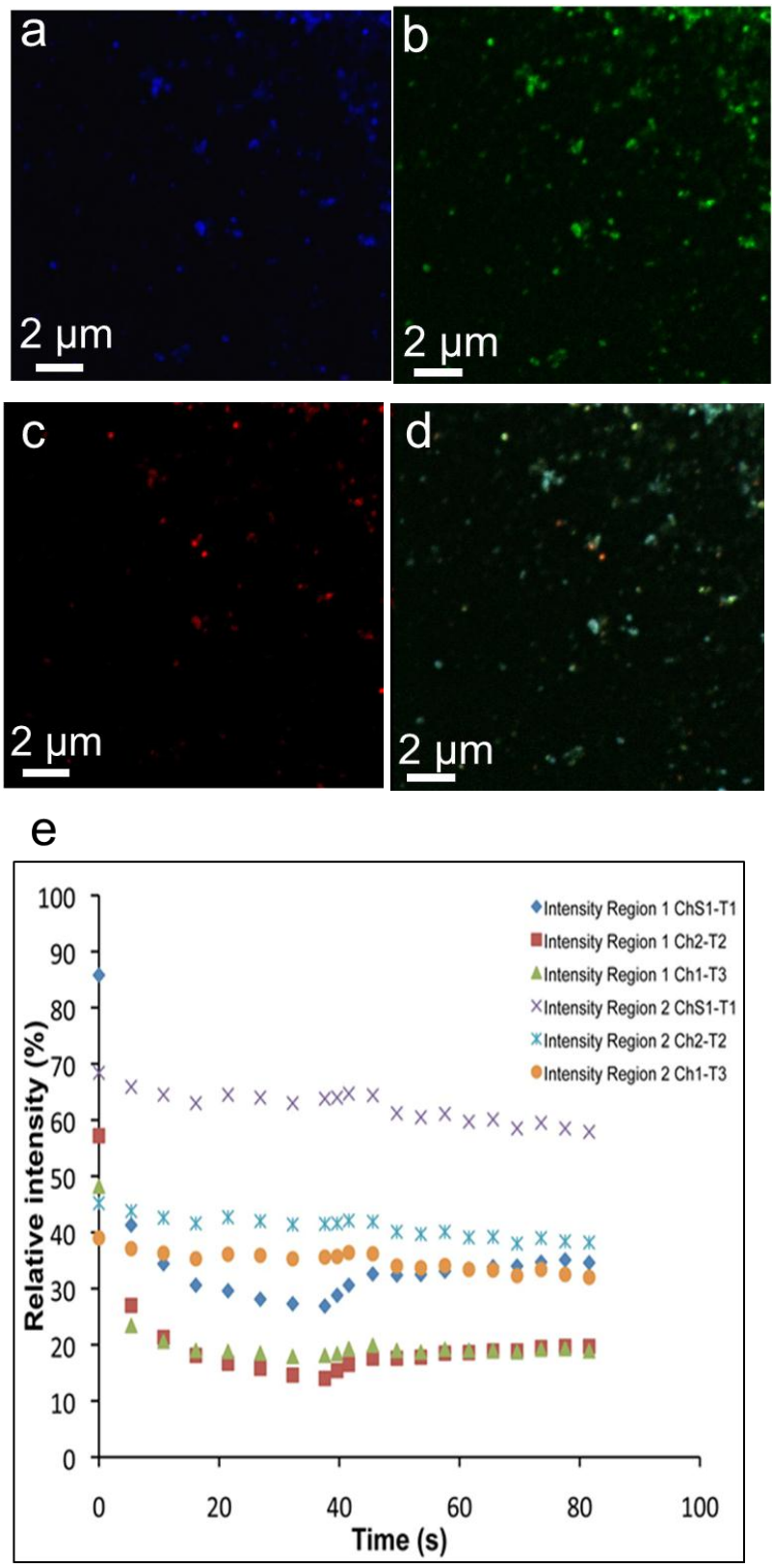

Figure 7.3. *One photon luminescence image of amine functionalized ZrO_2 acquired different wavelengths showing emission in blue (a) green (b) red (c) region. (d) shows co-localized image of blue, green and red region. (e) photo stability measurement of the sample when*

exposing the sample to an increased laser power (region 1) using the three different channels simultaneously (T1, T2, T3). A clear decay is clearly observed in all the channels meaning that these np's are luminescent. As control, the sample was exposed in a different area to initial laser power (Region 2). No decay is observed indicating that these np's are highly photostable.

A potential biomedical use of these functionalized nanoparticles is targeted drug delivery. Therefore, the cytotoxic behavior of the ZrO_2 np's was studied for primary mouse hepatocytes (pMHs). It is known that upon introduction of nanoparticles into the blood stream, if they are not properly functionalized to target a specific cell type, they will be removed by urine or, in case of not complete clearance, get trapped in certain organs such as liver. For this purpose, the biocompatibility/biomedical potential applications of the ZrO_2 np's were assayed by means of cell viability analysis by co-incubating the nanoparticles with (pMHs). A cell viability assay (for 24, 48 and 72 h, 37ºC) revealed that the nanoparticles were not cytotoxic, i.e. that in concentrations of 50, 100 and 200 μg/mL the percentage of cell survival was almost more than 90% under all concentrations incubated to cells even after 72 h.

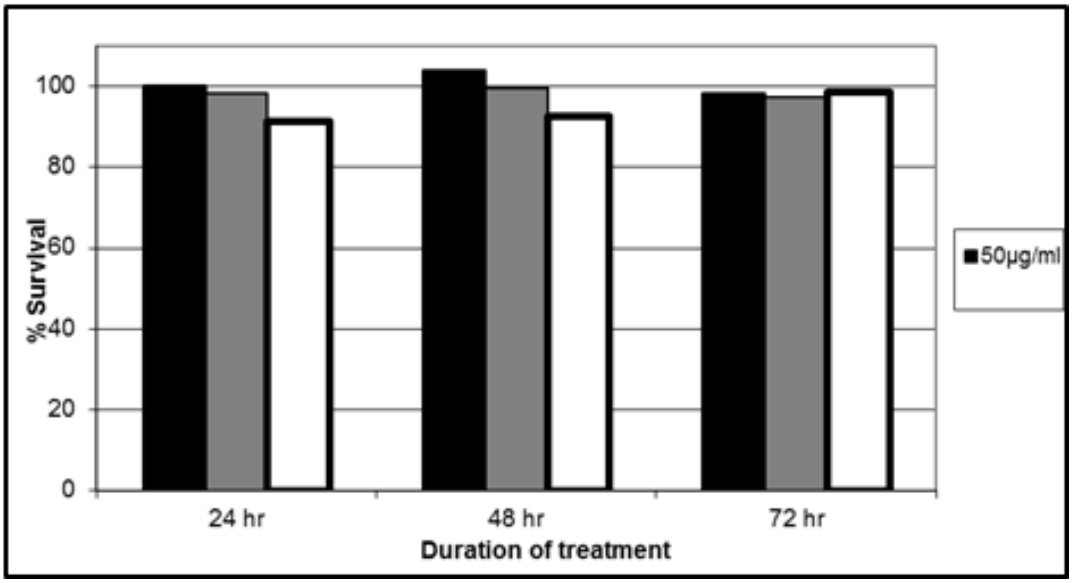

Figure 7.4. *ZrO_2 nanoparticles functionalized with 2A in different concentrations (50, 100 and 200 μg/mL) were co-incubated with primary mouse hepatocytes (mPHs) for 24, 48 and 72 h at 37ºC. After incubation period, the cells were washed and assayed for viability using cell titer qbo (ProOmega). No cytoxicity was observed for any of the concentrations used.*

7.3. Summary and Conclusion

In summary, we have described a facile, novel and versatile synthetic method to prepare water soluble photoluminescent ZrO_2 nanoparticles. The nanoparticles retain their morphology and monodispersity even after functionalization. The functionalized ZrO_2 nanoparticles showed multi-color luminiscence in using 1-photon microscopy. The facile synthesis, the long-term aqueous stability, and the extreme robustness of the photophysical properties make the zirconia nanoparticle, an excellent candidate for biomedical applications and for *in vivo* and *in vitro* studies.

7.4. Experimental Section

Materials and Methods

N-Boc-1,4-butanediamine (Sigma-Aldrich), thionyl chloride ($SOCl_2$) (Sigma-Aldrich) were purchased and used as received without further purification. Solvents such as, THF, DMF, were purchased technical grade and used as received.

Synthesis of ZrO_2 Nanoparticles

ZrO_2 nanoparticles were synthesized by adding 3.33 g of zirconium isopropoxide isopropanol complex (Aldrich, 99.9%) into tefelon reaction cup, and 30 mL of benzyl alcohol under constant shaking at high speed until the whole zirconium isoproxide became soluble. The cup was then inserted into a 50ml stainless steel autoclave and heated to 210 °C. After 72 hours the vessel was allowed to cool down and then opened to retrieve a white turbid suspension. The product was isolated as a white powder by centrifugation or simple decantation, washing with tetrahydrofuran (THF), and drying in vacuo resulted in white crystalline powder of ZrO2 nanoparticles with size around 4 nm.

ZrO_2 nanoparticles functionalization. ZrO_2 nanoparticles were surface modified using different approaches. The surface of the zirconia nanoparticles were modified using a modified procedure as previously described [17]. Typically 15 mL of $SOCl_2$ and 5 ml of anhydrous DMF was added to 60 mg of zirconia nanoparticles and was allowed to react at 70 ºC for 24 h. After the reaction got over, the product was allowed to cool down to room temperature and was washed with centrifugation (9000 rpm, 15 min). The yellow supernant

was discarded and the functionalized nanoparticles were washed with dry THF again with centrifugation (9000 rpm, 15 mins) and dried under nitrogen atmosphere. Typically 600 mg of N-Boc-1,4-butanediamine were added to Cl-functionalized zirconia nanoparticles and left to react for 96 h at 85 ºC under constant stirring. After the reaction got over, Boc group was deprotected in 0.1M HCl in methanol for 2 hours at room temperature. The deprotected sample was centrifuged 2 times (9000 rpm, 10 min) in methanol.

Characterization

TEM analysis and characterization of the products. Transmission electron microscopy (TEM) was carried out on a Philips EM420 instrument with a twin lens. Samples for TEM measurements were prepared from ethanolic suspensions of the samples. Three drops of the ultrasonicated suspension were administered on a Cu grid coated with FORMVAR polymer and an amorphous carbon layer.

Cell culture and cytotoxic assay. Primary mouse hepatocytes (pMHs) were obtained by culturing as reported [21]. RPMI media supplemented with supernatant of X6310-GM-CSF cells for 8 days. To perform cytotoxic assay, $2x10^4$ pMHs were cultured in 96 well plate and *t*M-dots were added at given concentrations (50, 100 and 200 μg/mL). After 24, 48, 72 h at 37ºC/5% CO_2, cell viability was determined by CellTiter-Glo viability assay kit (Promega) according to manufacturer instruction and measured in Saffire-ELISA reader (Tecan, Salzburg, Austria).

7.5. References

[1]S. Ohkuma, B. Poole, *Proc. Natl. Acad. Sci. USA* **1978**, *75*, 3327.

[2]J. W. Lichtman, J. A. Conchello, *Nature Method.* **2005**, *2*, 910.

[3] M. Chalfie, Y. Tu, G. Euskircher, W. W. Ward, D. C. Prasher, *Science* **1994**, *263*, 802.

[4] W. H. Green, K. P. Le, J. Grey, T. T. Au, M. J. Sailor, *Science* **1997**, *276*, 1826.

[5] A. M. Jakob, T. A. Schmedake, *Chem. Mater.* **2006**, *18*, 3173.

[6] M. Ghiazza, M. Polimeni, I. Fenoglio, E. Gazzano, D. Ghigo, and B. Fubini, *Chem. Res. Toxicol.* **2010**, *23*, 620.

[7] F. Natalio, M. Haase, T. Basché, K. Koynov, W. Tremel, submitted.

[8] F. Natalio, A. Kashyap, D. Strand, W. Tremel, submitted.

[9] W. R. Zipfel, R. M. Williams, W. W. Webb, *Nat. Biotechnol.* **2003**, *21*, 1369.

[10] C. Xu, W. Zipfel, J. B. Shear, R. M. Williams, W. W. Webb, *Proc. Natl. Acad. Sci.* **1996**, *93*, 10763.

[11] L. M. Maestro, E. M. Rodriguez, F. S. Rodriguez, M. C. Iglesias-de la Cruz, A. Juarranz, R. Naccache, F. Vetrone, D. Jaque, J. A. Capobianco, J. G. Sole, *Nano Lett.* **2010**, *10*, 5109.

[12] W. C. W. Chan, S. Nie, *Science* **1998**, *281*, 2016.

[13] X. Michalet, F. F. Pinaud, L. A. Bentolila, J. M. Tsay, S. Doose, J. J. Li, G. Sundaresan, A. M. Wu, S. S. Gambhir, S. Weiss, *Science* **2005**, *307*, 538.

[14] D. R. Larson, W. R. Zipfel, R. M. Williams, S. W. Clark, M. P. Bruchez, F. W. Wise, W. W. Webb, *Science* **2003**, *300*, 1434.

[15] H. F. Wang, T. B. Huff, D. A. Zweifel, W. He, P. S. Low and A. Wei, J. X. Cheng, P*roc. Natl. Acad. Sci. USA* **2005**, *102*, 15752.

[16] N. J. Durr, T. Larson, D. K. Smith, B. A. Korgel, K. Sokolov, A. Ben-Yakar, *Nano Lett*. **2007**, *7*, 941.

[17] C. Sönnichsen , A. P. Alivisatos, *Nano Lett*. **2005**, *5*, 301.

[18] J. Park, A. Estrada, K. Sharp, K. Sang, J. A. Schwartz, D. K. Smith, C. Coleman, J. D. Payne, B. A. Korgel, A. k. Dunn, J. W. Tunnel, *Opt. Express* **2008**, *16*, 1590.

[19] L Cao, X. Wang, M. J. Meziani, F. Lu, H. Wang, P. G. Luo, Y. Lin, B. A. Harruff, L. M. Veca, D. Murray, S.-Y. Xie, Y.-P. Sun, *J. Am. Chem. Soc*. **2007**, *129*, 11318.

[20] Y.-P. Sun, B. Zhou, Y. Lin, W. Wang, K. A. S. Fernando, P. Pathak, M. J. Meziani, B. A. Harruff, X. Wang, H. Wang, P. G. Luo, H. Yang, M. E. Kose, B. Chen, L. M. Veca, S.-Y. Xie, *J. Am. Chem. Soc*. **2006**, *128*, 7756.

[21] C. Tu, X. Ma, P. Pantazis, S. M. Kauzlarich, A.Y. Louie, *J. Am. Chem. Soc.* **2010**, *132*, 2016.

[22] S. Zhou, G. Garnweitner, M. Niederberger, M. Antonietti, *Langmuir* **2007**, *23*, 9178.

[23] S. A. M. Metwally, *J. Appl. Chem. and Biotech*. **1975**, *25*, 161.

[24] M. N. Tahir, P. Theato, P. Oberle, G. Melnyk, S. Faiss, U. Kolb, A. Janshoff, M. Stepputat, W. Tremel, *Langmuir* **2006**, *22*, 5209.

[25] P-J. Chen, T. Moore, S. Nesnow, *Toxicology in Vitro* **2008**, *22*, 1476.

8. Conclusions and Outlook.

The present doctoral thesis encloses novel methodologies for the synthesis and design of nanoarchitectures. The design is based on the 'bottom up' approach of nanotechnology using surface functionalization as a toolbox. Novel nanocomposites are produced by mimicking organic molecule, inorganic nanoparticles on the same platform. These nanocomposites could further be used as raw materials for the development of innovative devices or structures for the benefit of society in the long run.

We have successfully used the principles of coordination chemistry to achieve the reversible functionalization of highly inert chalcogenide WS_2 nanotubes with metal oxide (MnO) nanoparticles. The modification strategy is based on the chalcophilic affinity of Mn^{2+}, as described by the Pearson HSAB concept. The surface-bound nanoparticles are still amenable to functionalization with anchor ligands such as dopamine. As the chelating dopamine ligand is a much more potent ligand for surfaces of 3d metals than the sulfur atoms of the chalcogenide nanoparticles, MnO nanoparticles can be detached from the chalcogenide surfaces at slightly elevated temperature. The remaining chalcogenide particles can be the functionalized again with fresh metal oxide nanoparticles. The "self-assembled" hybrid architecture can incorporate various different selective nanoparticle-substrate interactions based on well-known surface chemistries, and it may be generalized for various layered chalcogenide nanoparticles and transition metal and main group oxides. This assembly technique offers benefits for low-cost and low-waste manufacturing, and such methods are becoming increasingly important in the development of green nanofabrication strategies.

A step further, the Pearson hardness of the different metal cations was used as a basis for the binding of many metal oxides other than MnO to the chalcogenide surface. It has been found out that the density of binding of different metal oxide nanoparticles in completely dependent on their hardness of the corresponding metal cations. Pearson soft metals like Au bind heavily and irreversibly. Pearson borderline metals like MnO, Fe_3O_4 bind reversibly whereas Pearson hard metals like TiO_2, Fe_2O_3 don't bind at all.

We have also demonstrated that the hierarchical assembly of $Pt@Fe_3O_4$ Janus particles onto WS_2 nanotubes is dictated by the principles of Pearson´s HSAB concept, i.e. Pt compared to Fe_3O_4 is the preferred binding site because of its Pearson hardness. This binding preference can be inverted by camouflaging the Pt domain with an organic ligand.

In the realm of inorganic coordination chemistry, we have demonstrated functionalization

protocol for layered metal chalcogenide nanostructures (IF-ReS_2) exploiting the Fe^{2+}-TerPy coordination chemistry. This strategy described in this work can be generalized for all layered chalcogenide nanoparticles. In addition, the TerPy "anchor group" might be replaced by a range of related ligands like bispyridine (bipy) or 1, 10-phenanthroline (phen), which have similar coordination chemistry with iron. In accordance with this strategy, the terpyridine anchor group can be modified with some hydrophilic group (PEG) which confers solubility of these otherwise inert nanostructures in water and other polar solvents. In similar fashion, long alkyl hydrophobic chain can be impregnated into terpyridine group which improved solubility in non-polar solvents like hexane, toluene etc.

We have used simple established chemical routes to achieve the functionalization of TiO_2 nanowires with Au@MnO magnetic nanoparticles and been able to bring three different unique surfaces to one platform. We have used a versatile polymeric ligand that has dopamine and free amine groups on its side chain. The modification strategy is based on the chelating affinity of dopamine to metal oxide nanostructure, as well as the affinity of amine functionality to bind to gold domain of Au@MnO nanoflowers. The surface bound nanoflowers are still amenable to functionalization with anchor groups such as thiol that readily binds gold surface. We have selectively conjugated a thiol tagged single stranded DNA that has texas red at 5' end for optical visualization. The free amine groups present on the polymer backbone can further be used to bind green flourophore (NBD-Cl).

The functionalization of nanowires opens several new fields for this class of materials which have been pursued actively during the past few years for the related oxide materials. The functionalization strategies explored in this thesis, can be used for attachment of different metal oxide nanostructures (MnO, Fe_2O_3, and Fe_3O_4). Janus nanostructures (Pt-Fe_3O_4, Au-Fe_3O_4, Au-MnO), electronically active components (metal and semiconductor nanoparticles) chalcogenide nanotubes for the attachment of electronically active components (metal and semiconductors nanoparticles) onto nanowires and nanotubes to construct different unique nanoarchitectures and can further be studied the change and behaviour of different intrinsic properties (magnetic, optical, electronic, catalytic) of the nanocomposites.

We have also successfully synthesized a new biocompartible fluorescent material which shows luminescent behaviour without incorporation of any dye molecule. A novel wet chemical synthetic methodology was performed for topological tailoring of ZrO_2 nanoparticles. The nanoparticles were first chlorinated by $SoCl_2$ by substituting the surface hydroxyl groups, which subsequently were nucleophilic substituted by primary amine groups.

These amine functionalized ZrO_2 nanoparticles develop fluorescence behavior as observed in fluorescence spectroscopy and one photon microscopy. The nanoparticles retained its morphology after functionalization and were highly stable in water. They show no toxicity effect, unlike quantum dots, as observed in cytotoxicity test (MTT), which propelled for further biological studies both *in vitro* and *in vivo*. The ease and versatility of synthesis, biocompatibility, and high performance and long photophysical stability, and no toxicity make these luminescent ZrO_2 nanoparticles a perfect candidate that could demonstrate its potential in different bio-medical applications in future.

The functionalization of WS_2 nanotubes opens several new fields for this class of materials which have been pursued actively during the past few years for the related carbon nanotubes and various oxide materials: (i) the functionalization of chalcogenide nanotubes, nanowires and nanoparticles for the attachment of electronically active components (metal and semiconductors nanoparticles, light harvesting ligands for solar cell applications) to the sidewalls of the tubes, (ii) dispersion of nanotubes, e.g. for the integration in composites, which is of interest because of their exceptional mechanical properties. (iii) Furthermore, it allows the fabrication of thin films by surface binding of chalcogenide particles to oxide surfaces, which might allow their use as lubricants on seemingly incompatible ceramic materials.

9. Methods and Instrumentations.

9.1. Confocal Laser Scanning Microscopy.

Confocal laser scanning microscopy (CLSM or LSCM) is a technique for obtaining high resolution optical images with depth selectivity [1]. The key feature of confocal microscopy is its ability to acquire in-focus images from selected depths, a process known as *optical sectioning*. Images are acquired point-by-point and reconstructed with a computer, allowing three-dimensional reconstructions of topologically complex objects. The principle for this special kind of microscopy was developed by Marvin Minsky in 1953, but it took another thirty years and the development of lasers as near-ideal point light sources for confocal microscopy to become a standard technique toward the end of the 1980s. In a typical laser scanning confocal microscope (Figure 9.1.1) a laser beam passes a light source aperture and then is focused by an objective lens into a small (ideally diffraction-limited) focal volume within a fluorescent specimen.

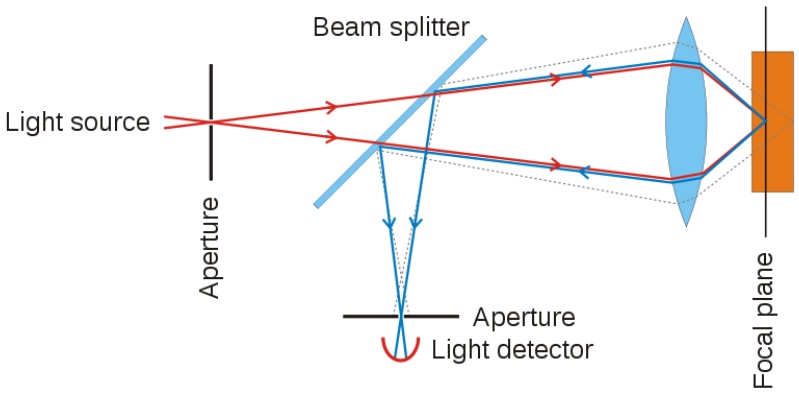

Figure 9.1.1. *Schematic illustration of the principle of CLSM [1].*

Confocal microscopy provides the capacity for direct, noninvasive, serial optical sectioning of intact, thick, living specimens with a minimum of sample preparation as well as a marginal improvement in lateral resolution.

In this doctorate work, the confocal laser scanning microscope used was an inverted laser scanning microscope, equipped with He/Ne Laser (Leica TCS SL, Leica Microsystems, Bensheim, Germany).

9.2. Transmission Electron Microscopy.

Transmission electron microscopy is a microscopic technique where a beam of electron is transmitted through a ultrathin specimen, and interacts with the sample as it passes through. An image is formed as the electrons interact with the materials in the sample, which can be focused, magnified on an imaging device, which can be detected and stored by a sensor such as CCD camera. When electrons are accelerated upto high energy levels (few hundred KeV) and focused on materials, they can scatter or backscatter elastically or inelastically, or produce many interactions, sources of different signals such as X-rays, Auger electrons or light (Figure 9.2.1). Some of them are used in transmission electron microscopy (TEM).

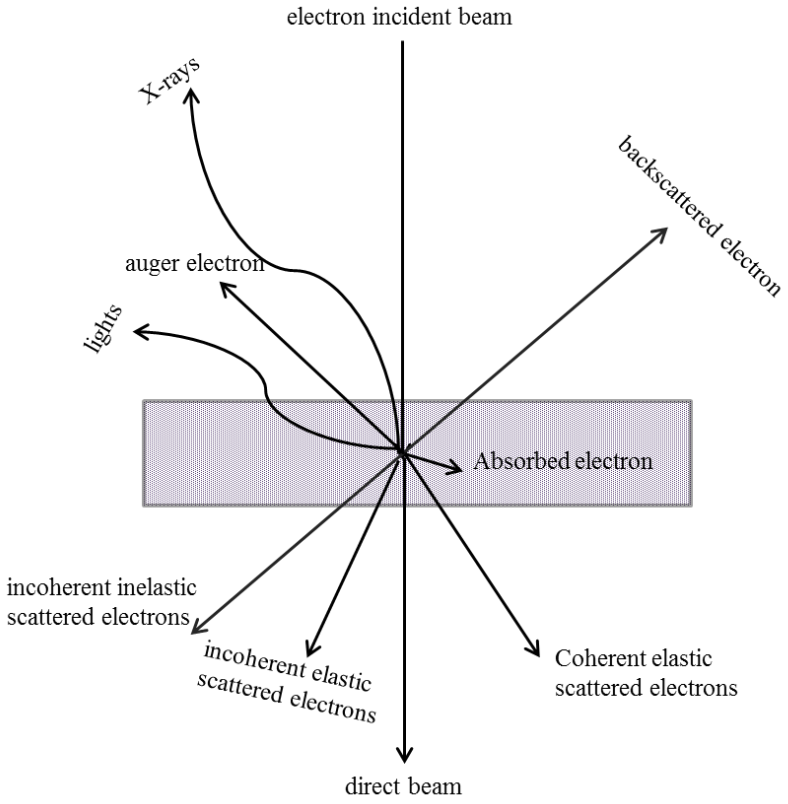

Figure 9.2.1. *Interactions between electrons and material.*

A Transmission electron microscope consists of different component for its working (Figure 9.2.2). It includes a vacuum system, an electron generation source, electromagnetic lenses, and electrostatic plates [2]. A standard TEM is evacuated to low pressure (10^{-4} Pa) to increase mean free path of electron gas interaction. The mean free path is increased at low pressure

because of low collision frequency between electrons and gas atoms. High-voltage TEMs require ultra high vacuums on the range of 10^{-7} to 10^{-9} Pa to prevent generation of an electrical arc, particularly at the TEM cathode.

Typically in TEM, electron guns are fitted in order to generate electrons when heated up. Normally the electron guns are of tungsten because of its high melting point and of (LaB6) because of its low work function. The electron generator source must be heated up for themionic emission of electron beam. Electromagnetic lenses are designed to act in a manner so as to emulate optical lense. Lenses may operate electrostatically or magnetically, hence known as electromagnetic lenses. Most of the electron lense for TEM utilise electromagnetic coil to generate a convex lens. The components include the yoke, the magnetic coil, the poles, the polepiece, and the external control circuitry. The coil which produced magnetic field is located inside the yoke. Aperatures are annular metallic plate. They consists of a metallic disc, thick enough to prevent electrons passing through, whirlst allowing axial electrons. Apertures are either a fixed aperture within the column, such as at the condensor lens, or are a movable aperture, which can be inserted or withdrawn from the beam path, or moved in the plane perpendicular to the beam path. TEM utilises the information contained in the transmitted electron, after interaction with the sample to form an image. The observed intensity of the image can be approximately proportional to time average amplitude of electron wave function.

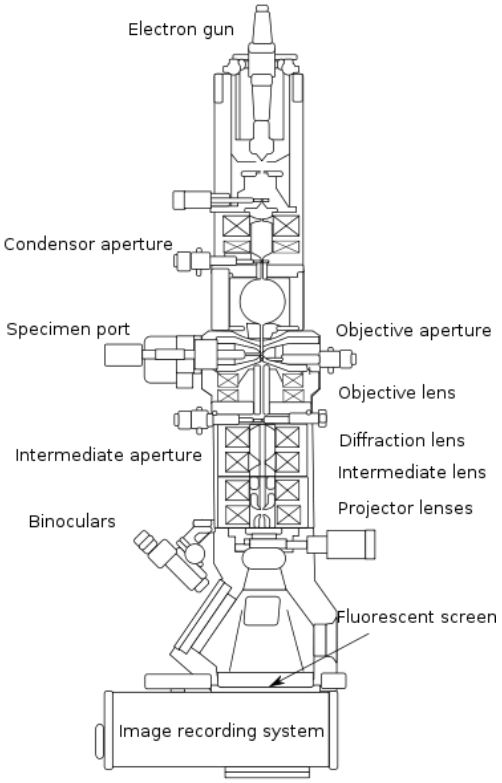

Figure 9.2.2. *Layout of basic components of a TEM [2].*

In this doctoral work, TEM was carried out on a Philips EM420 instrument with a twin lens and a Philips CM12 with a twin lens at an acceleration voltage of 120 kV. High resolution images were taken with a Philips FEI TECNAI F30 ST electron microscope (field-emission gun, 300 kV extraction voltage) equipped with an Oxford EDX (energy-dispersive X-ray) spectrometer with a Si/Li detector and an ultrathin window for elemental analysis. Samples for TEM measurements were prepared from ethanolic suspensions of the samples. Three drops of the ultrasonicated suspension were administered on a Cu grid coated with FORMVAR polymer and an amorphous carbon layer.

9.3. Scanning Electron Microscopy.

Scanning electron microscopy (SEM) images a sample by scanning it in high energy beam of electrons. The electrons interact with the sample which is collected as an image that gives information about the size and shape of materials in nano and micro scale and gives its surface composition and other properties. The first SEM image was taken by Max Knoll in 1935 of silicon steel. Studies on the physical working principle and the interaction between electron and surface of the sample were performed by Manfred Von Ardenne in 1937. The first commercial SEM was broght into market in 1965.

9.3.1. Working Principle.

Typically, In a SEM, electrons are generated and emitted from an electron gun fitted with a tungsten filament cathode. Tungsten, owing to its low cost, high melting point, and low vapour pressure, is used as electron gun as it has to be heated up for electron generation. The electron beam has an energy range of 0.5 keV-40 keV. After the electron generation from the electron gun, the electron beam is focused by one or two condenser lenses to a spot of 0.4 nm-5 nm diameter. The electron beam passes through pairs of scanning coil or deflector plates in the electron column, which deflect the beam in x and y axes for scanning over a rectangular area of sample surface. The schematic illustration of a SEM is provided in Figure 9.3.1.

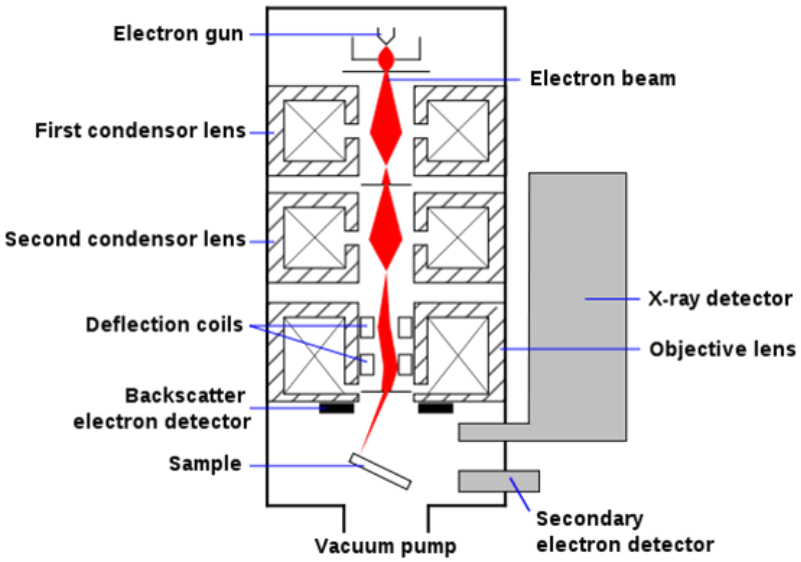

Figure 9.3.1. *Schematic diagram of a Scanning Electron Microscope [3].*

The electrons loose energy by random scattering and absorption once it interacts with the sample surface, within 'interaction volume' which ranges from 100 nm-5 µm. The dimension of the interaction volume depends on electron's landing energy, atomic number of specimen and specimen's density [3]. The interaction between electron beam and sample surface results in reflection of high elergy electron by elastic scattering, electromagnetic radiation and emission of secondary electrons by inelastic scattering, which can be detected by detectors. The beam current absorbed by the sample can be detected and can further be used for image creation. The resulting image is a distribution map of the intensity of the signal being emitted from the scanned area of specimen. The image is digitally captured and displayed on a computer monitor which gives information about the sample, its morphology.

9.4. Atomic Force Microscopy.

Atomic force microscopy (AFM) or scanning force microscopy is a very high resolution type scanning probe microscopy whose resolution is 1000 times better than the optical diffraction limit [4]. AFM is one of the pioneering characterization tools for measuring, manipulating, and visualizing matter at nano and micro regime. Atomic force microscopy was developed by Binnig, Quate and Gerber in 1986. However the first commercial AFM was developed in

1989. AFM consists of a cantilever at its end that is used to scan the surface of the material as shown in Figure 9.4.1. Generally the cantilever is composed of silicon or silicon nitride, with a radius of curvature on the order of nanometer. When the tip of cantilever is brought closer to the sample surface, force between the tip and sample lead to deflection of the cantilever according to Hooke's law, which states that stress is proportional to strain. Mainly there are three different types of interaction between the tip and sample surfaces, i.e., contact mode, tapping mode and non-contact mode.

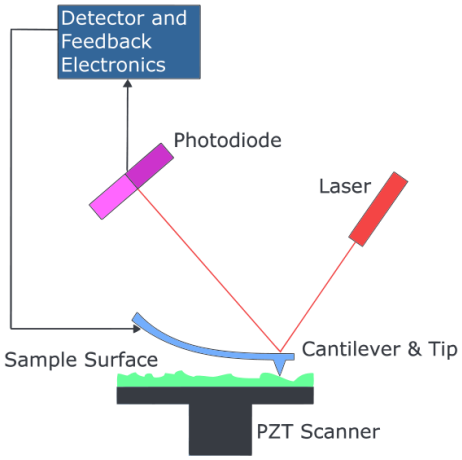

Figure 9.4.1. *Schematic diagram of Atomic Force Microscope [4].*

In contact mode, the force between the tip of cantilever and material surface remain constant. This mode of operation is called contact mode, because the tip and the surface remain so close to each other that intermolecular repulsive force become positive and cause strong lateral force on the sample. In tapping mode, the cantilever is allowed to oscillate at its resonant frequency. This mode is used for soft sample like lipid bilayer or visualizing single polymer molecule. Tapping mode lessens the damage made to the sample and to the tip, as it taps the surface for a very short time. In non contact mode, the cantilever oscillates much above the sample surface that, there is no lateral force which means it's not in the repulsive domain of intermolecular force.

In addition to the study of surface profile at higher resolution, AFM is very useful in studying nanomechanics and time resolved investigations. In contrast to other electron microscope, which need vaccum and proper environment for operation, AFM can be operated in typical ambient conditions which makes it suitable characterization technique for biological sample and living organism.

9.5. References.

[1] http://en.wikipedia.org/wiki/Confocal_laser_scanning_microscopy.

[2] http://en.wikipedia.org/wiki/Transmission_electron_microscopy

[3] http://en.wikipedia.org/wiki/Scanning_electron_microscope

[4] http://en.wikipedia.org/wiki/Atomic_force_microscopy

10. Appendix

10.1. List of figures

(d) or the tip (e) of a WS_2 nanotube, (f) EDX spectrum of the MnO@NT-WS_2 composite.

Figure 2.2. UV-VIS absorption spectrum of (a) as synthesized WS_2 nanotubes (red line), (b) MnO@NT-WS_2 nanoparticles functionalized with dopamine-NBD, (b) Confocal laser scanning microscopy image of WS_2 nanotubes coated with dopamine-NBD, the inset shows a single nanotube.

Figure 3.1. (a) TEM overview and (b) HRTEM images of functionalized IF-ReS_2 nanoparticles, (c) EDX spectrum of the area marked by the circle in (b).

Figure 3.2. UV-VIS spectra of TerPy-NBD functionalized IF-ReS_2 (orange line), unfunctionalized IF-ReS_2 (black line), and pure ligand TerPy-NBD (5) (green line), (b) CLSM image of TerPy-NBD functionalized IF-ReS_2, (c) FT-IR spectrum of TerPy-amine functionalized IF-ReS_2 (black line), the unfunctionalized IF-ReS_2 (green line) and the pure TerPy-amine (red line).

Figure 3.3. Distribution of IF-ReS_2 in water-hexane before and after PEGylation, (b) UV-VIS spectra of TerPy-PEG (3) functionalized IF-ReS2 (red line), unfunctionalized IF-ReS_2 (black line), and pure ligand (TerPy-PEG), (c) stable dispersions of IF-ReS_2 in DMSO (1), DMF (2), THF (3) and CHCl3 (4) from left to right. The solubility corresponds to the polarity of the solvents.

Figure 3.4. Stable dispersion of IF-ReS_2 in hexane (1), cyclohexane (2), 1, 4-dioxane (3) and toluene (4) (from left to right).

Figure 4.1. Electron microscopy images of as synthesized nanoparticles, (a) IF-MoS_2, (b) Fe_2O_3, (c) MnO, (d) Fe_3O_4, (e) ZnO, (f) TiO_2, (g) Au.

Figure 4.2. (a) TEM overview and (b) HRTEM image of MnO coated IF-MoS_2 nanoparticles, (c) EDX spectrum showing the presence of Mo, S as well as Mn and O. The Cu signal is due to the Cu Tem grid.

Figure 4.3. (a) TEM overview and (b) HRTEM image of Fe_3O_4 nanoparticles bound onto IF-MoS_2 particles, (c) EDX spectrum showing the presence of Mo, S as well as Fe and O. The Cu signal is due to the Cu Tem grid.

Figure 4.4. (a) TEm image of IF-MoS_2 after mixing with (a) Fe_2O_3 nanoparticles, (b) TiO_2 nanoparticles confirming that hard cations like Fe (III) and Ti (IV) don't bind to layered metal chalcogenide surfaces.

Figure 4.5. Digital image of surface bound Fe_3O_4 (IF-MoS2@Fe_3O_4) and unbound Fe_2O_3 nanoparticles. The magnetic nanoparticles are attracted by the permanent

magnet. Whereas the sample containing the surface bound magnetite nanoparticles (left) becomes transparent through the attraction by the magnet, the unbound IF-MoS_2 particles remain dispersed leaving a turbid sample (right).

Figure 4.6. (a) TEM micrograph of IF-MoS_2 nanoparticles with a monolayer of surface bound ZnO particles, (b) IF-MoS_2 nanoparticles after detachment of the ZnO particles or (c) Fe_3O_4 particles with catecholate ligands.

Figure 4.7. TEM images of (a) Au nanoparticles functionalized IF-MoS_2 (b) after addition of 1-hexadecanethiol to Au@IF-MoS_2, which confirms the irreversible binding of gold nanoparticles onto IF-MoS_2.

Figure 5.1. TEM images of (a) NT-WS_2 and (b) Pt@Fe_3O_4 JPs. The HRTEM image in (b) shows the Pt and Fe_3O_4 of a single Pt@Fe_3O_4 JP.

Figure 5.2. (a) TEM, (b) HRTEM and (c) STEM images of pt@Fe_3O_4 JPs chemisorbed on NT-WS_2. (a) Overview TEM image of a WS_2 nanotube having a monolayer with nearly full coverage of Pt@Fe_3O_4 JPs. (b) HRTEM image showing the binding of the Pt face of a single Pt@Fe_3O_4 JP to the surface of NT-WS_2. (c) STEM image showing the quantitative binding of the Pt Janus faces onto NT-WS2. The histogram in the inset shows the binding ratio of Pt and Fe_3O_4 domain (70:30), average from 60 individual particles.

Figure 5.3. (a) TEM image of Pt@Fe_3O_4 JP whose Pt domain was masked with an organic ligand of immobilization on NT-WS_2 (b) HRTEM image showing binding of the Fe_3O_4 magnetite face of the JP to NT-WS_2, (c) STEM image showing the preferred binding of the Fe_3O_4 faces to NT-WS_2. The histogram in the inset shows the binding ratio of Pt and Fe3O4 domain (90:10), average from 65 individual particles.

Figure 5.4. EDX spectrum showing the presence of tungsten (W), sulfur (S), platinum (Pt), iron (Fe). The presence of copper (Cu) and carbon (C) can be assigned to the carbon coated copper grid used for electron microscope.

Figure 6.1. TEM images of as-synthesized TiO_2 nanowires (a), Au@MnO nanoflowers (b).

Figure 6.2. High resolution TEM images of the nanocomposites. (a) a single TiO_2 nanowire bound with Au@MnO nanoflowers (b) Au@MnO nanoflowers bound to a couple of nanowires (c) EDX spectrum indicating the presence of Ti, Au, Mn, O with respective elementary signal.

Figure 6.3. Representative confocal laser scanning microscopic images collected at λ_{ex}=514 nm (a) green fluorescence showing NBD immobilized TiO_2 nanowires (b) Red fluorescence showing SH-SS DNA-Texas Red bound Au core of Au@MnO nanoflowers bound on TiO_2 nanowires. (c) Co-localization of both fluorescent signal indicating that Au@MnO nanoflowers are bound to TiO_2 nanowires and both surface can be selectively dual functionalized with fluorophore. Fig.c inset shows a single nanowire bound with the nanoflower, where green signal refers to the nanowire and red corresponds to Au core of Au@MnO nanoflowers. (d) UV-VIS spectrum of Au@MnO bound TiO_2 nanowire. The peak at 560 nm denotes absorbance due to gold core of the nanoflowers whereas peak at 280 nm signifies the presence of dopamine.

Figure 7.1. (a) Electron microscopy images of as synthesized ZrO_2 nanoparticles. (b) ZrO_2 np's after functionalization. (c) Dynamic light scattering data of functionalized ZrO_2. (d) FT-IR ATR spectra of functionalized ZrO_2 nanoparticles. The free amine groups corresponding frequencies are shown by arrows.

Figure 7.2. Photoluminescence spectra of ZrO_2 np's (a) amine functionalized and unfunctionalized ZrO_2 (b). Inset(a) digital photograph of the solution under UV excitation (λ_{ex} = 366 nm)showing a strong blue signal.

Figure 7.3. One photon luminescence image of amine functionalized ZrO_2 acquired different wavelengths showing emission in blue (a) green (b) red (c) region. (d) shows co-localized image of blue, green and red region. (e) photo stability measurement of the sample when exposing the sample to an increased laser power (region 1) using the three different channels simultaneously (T1, T2, T3). A clear decay is clearly observed in all the channels meaning that these np's are luminescent. As control, the sample was exposed in a different area to initial laser power (Region 2). No decay is observed indicating that these np's are highly photostable.

Figure 7.4. ZrO_2 nanoparticles functionalized with 2A in different concentrations (50, 100 and 200 μg/mL) were co-incubated with primary mouse hepatocytes (mPHs) for 24, 48 and 72 h at 37ºC. After incubation period, the cells were washed and assayed for viability using cell titer qbo (proOmega). No cytotoxicity was observed for any of the concentrations used.

Figure 9.1.1. Schematic illustration of the principle of CLSM.

10.2. List of schemes and tables

group that replaces chlorine (nucleophilic substitution). (c) The highly reactive intermediate can easily be replaced by amine.

Table 4.1. Pearson hardness of transition metal species used for the assembly of metal oxide or metal particles on chalcogenide nanoparticles.

10.3. Abbreviations.

LTMC	Layered Transition Metal Chalcogenide
NT	Nanotube
IF	Inorganic Fullerenes
MQ_2	Metal Dichalcogenide
NTA	Nitrilotriacetic Acid
HSAB	Hard Soft Acid Base
MWNT	Multi Walled Carbon Nanotube
MOCVD	Metal-Organic Chemical Vapour Deposition
TerPy	Terpyridine
EG	Ethylene Glycol
PEG	Poly Ethylene Glycol
JPs	Janus Nanoparticles
SS DNA	Single Stranded DNA

10.4. Supplementary Informations.

^{1}H NMR Spectroscopy.

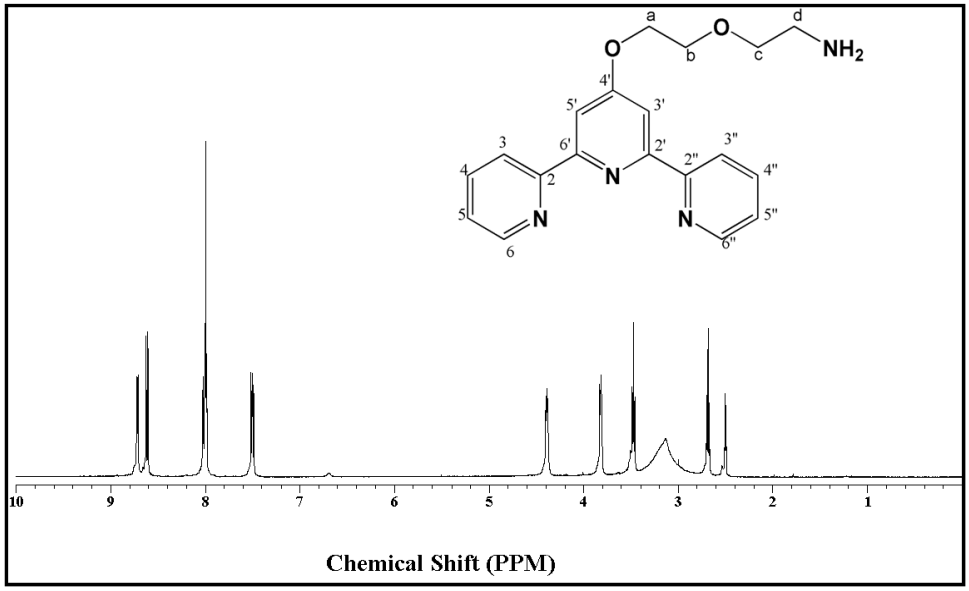

Appendix A1. *^{1}H NMR of 1-amino-5-(2, 2': 6', 2''-terpyrid-4'-yl-oxy) pentane.*

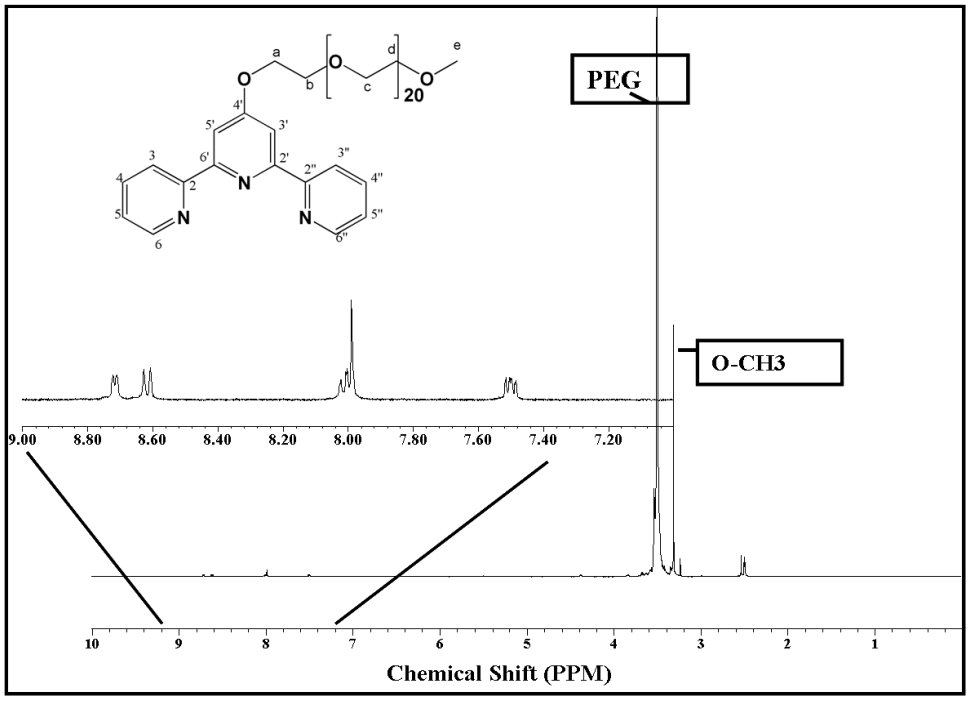

Appendix A2. *^{1}H NMR of 1-(2, 2': 6', 2''-terpyrid-4'-yl-oxy)polyethylene glycol 1000 monomethyl ether.*

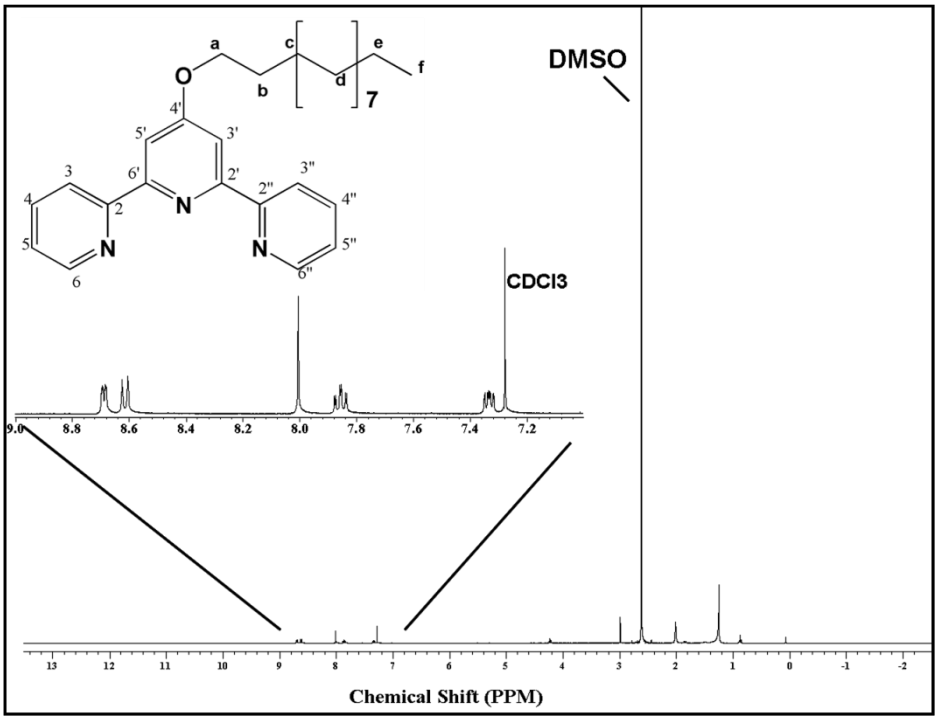

Appendix A3*. ^{1}H NMR of 1-(2, 2': 6', 2''-terpyrid-4'-yl-oxy) Octadecane.*

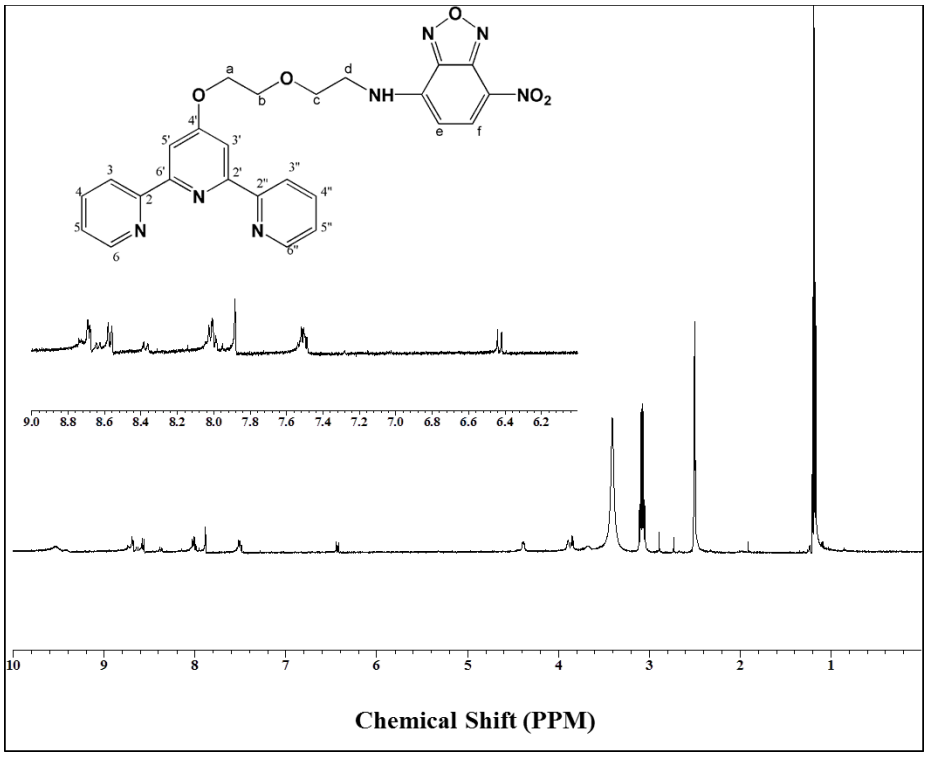

Appendix A4. *^{1}H NMR of terpyridine-NBD complex.*

FD-MS spectroscopy.

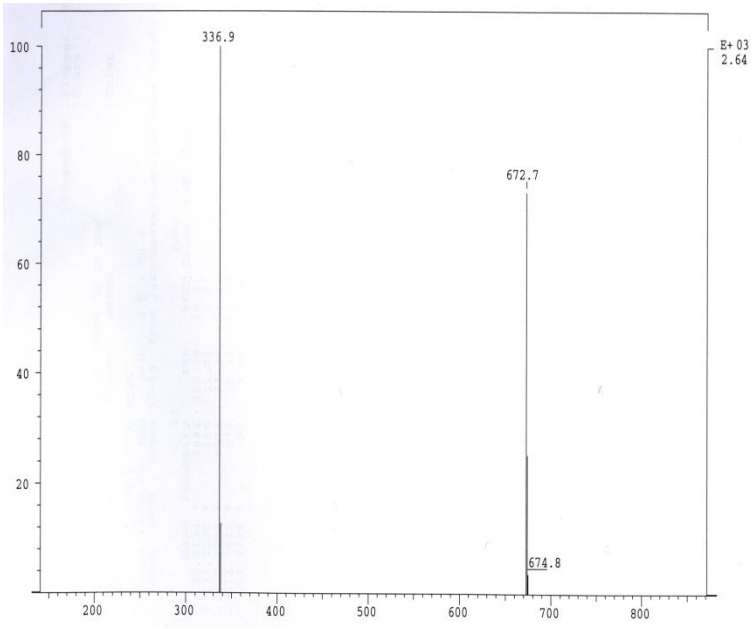

Appendix A5. *FD-MS Spectrum of 1-amino-5-(2, 2': 6', 2''-terpyrid-4'-yl-oxy) pentane*

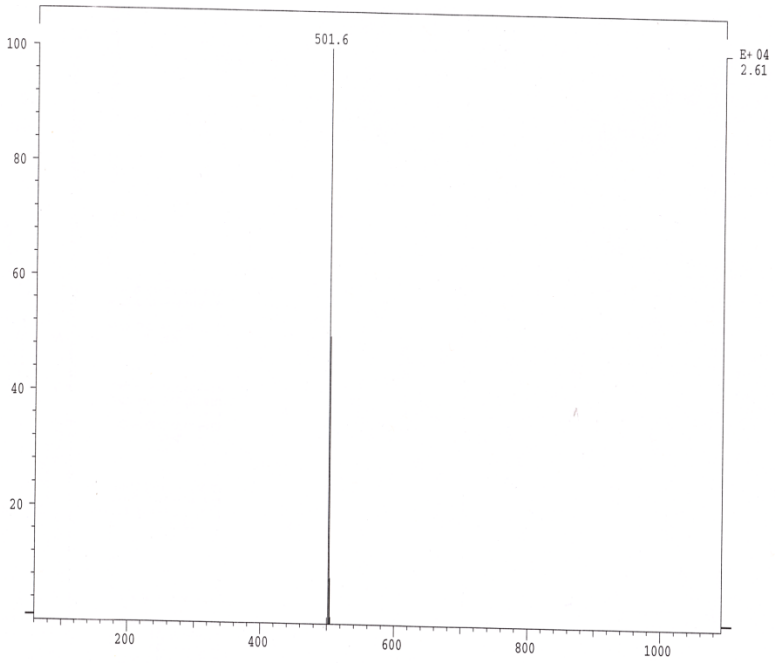

Appendix A6. *FD-MS Spectrum of 1-(2, 2': 6', 2''-terpyrid-4'-yl-oxy) Octadecane*

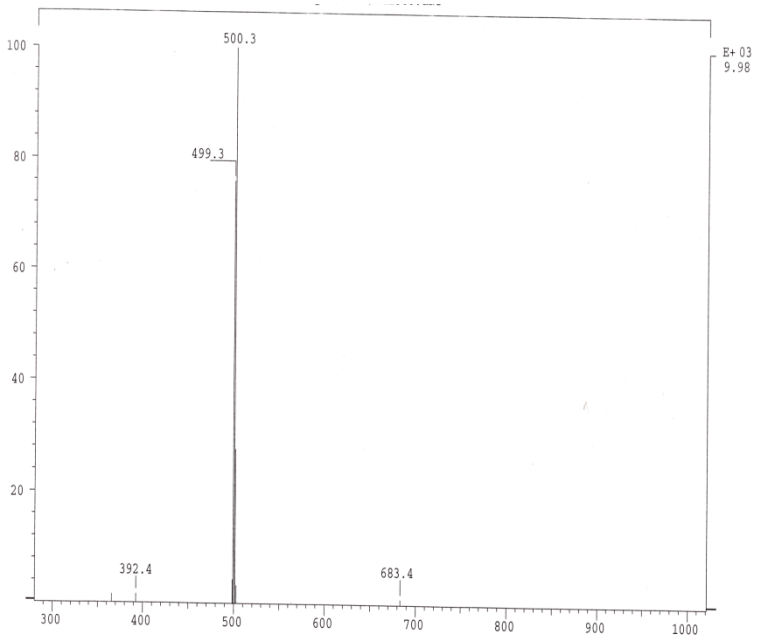

Appendix A7. *FD-MS Spectrum of terpyridine-NBD complex.*

X-Ray Diffraction.

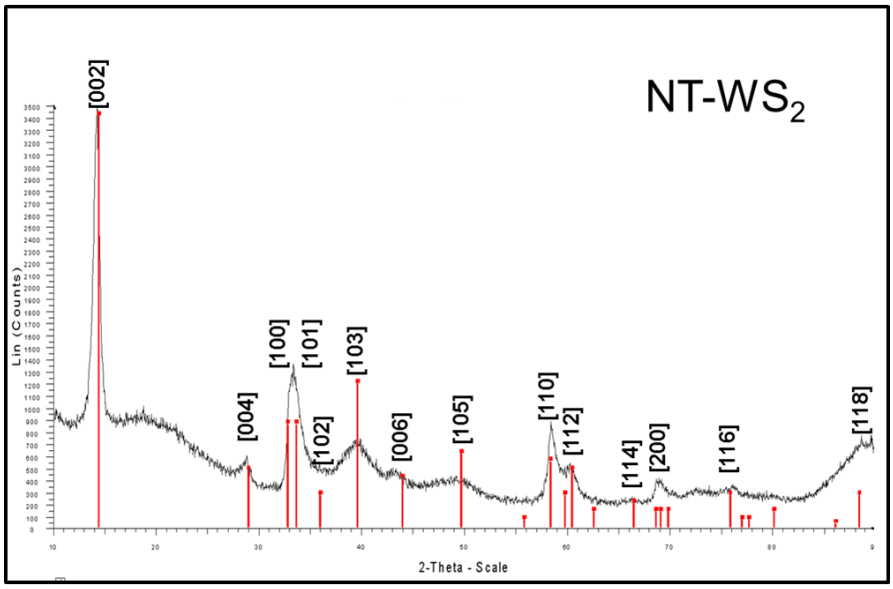

***Appendix A8**. Powder X-Ray Diffraction of NT-WS_2.*

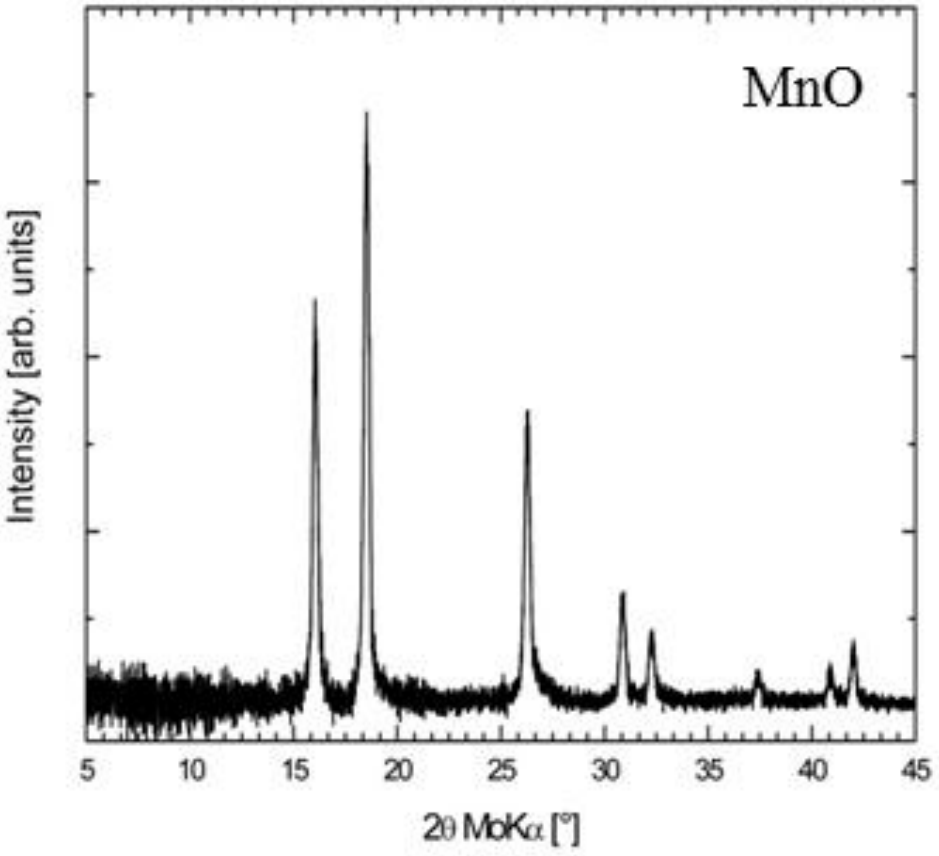

***Appendix A9**. Powder X-Ray Diffraction of MnO nanoparticles.*

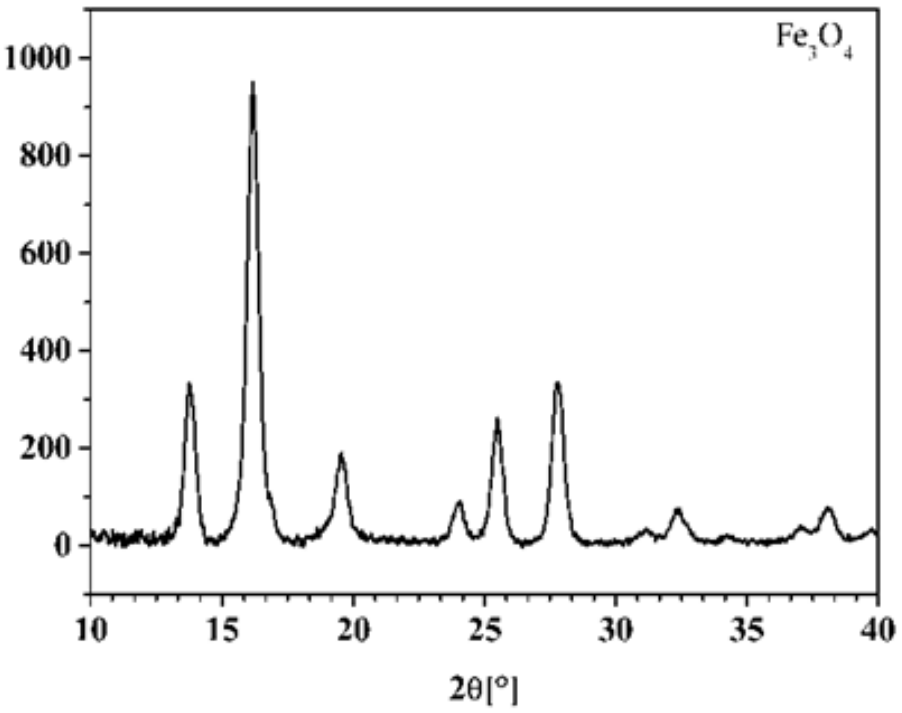

***Appendix A10**. Powder X-Ray Diffraction of Fe_3O_4 nanoparticles.*

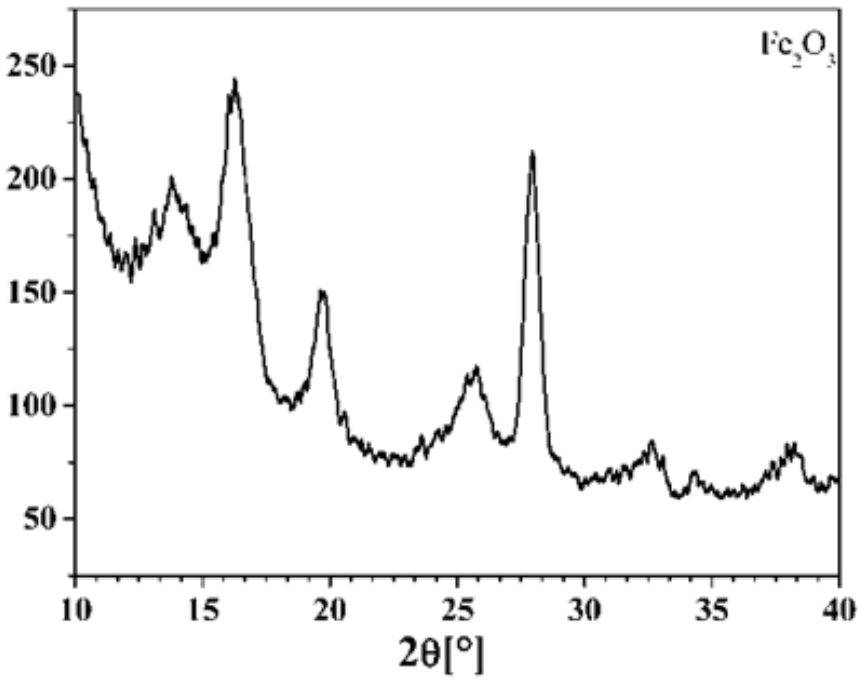

***Appendix A11**. Powder X-Ray Diffraction of Fe_2O_3 nanoparticles.*

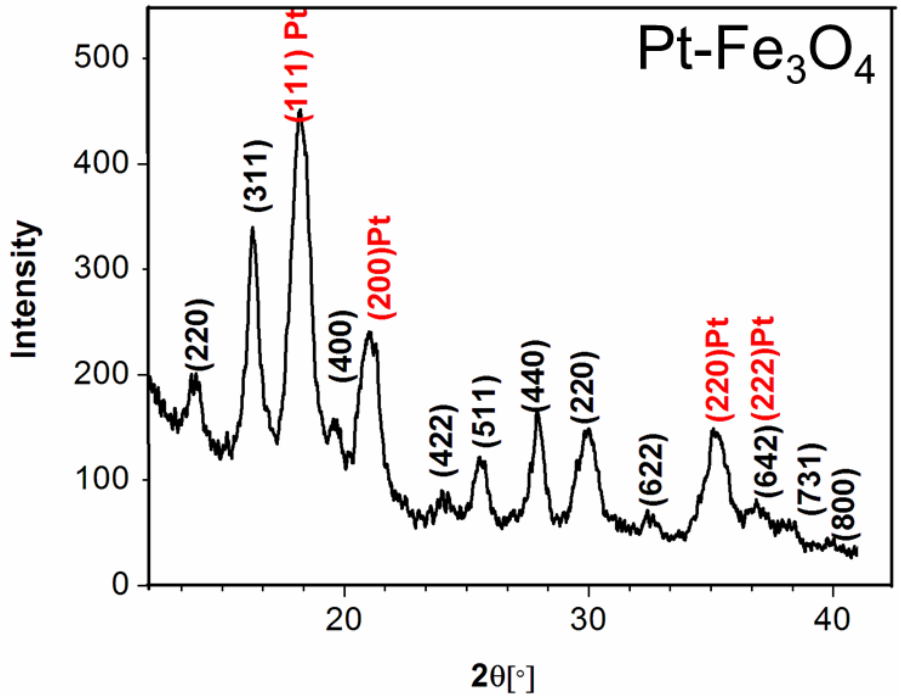

Appendix A11. *Powder X-Ray Diffraction of Pt-Fe_3O_4 nanoparticles*

Mean	0.2676 mg/L
Standard deviation	0.0118 mg/l
% RSD	4.41

Appendix A12. *Atomic absorption spectroscopic data confirming presence of Fe in terpy-NBD functionalized IF-ReS_2.*

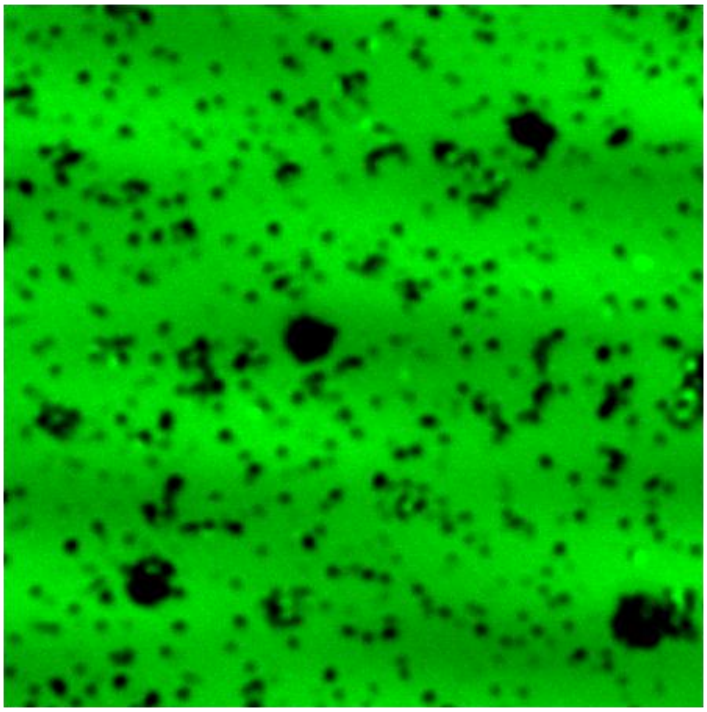

***Appendix A13**. CLSM image of unfunctionalized IF-ReS_2.*

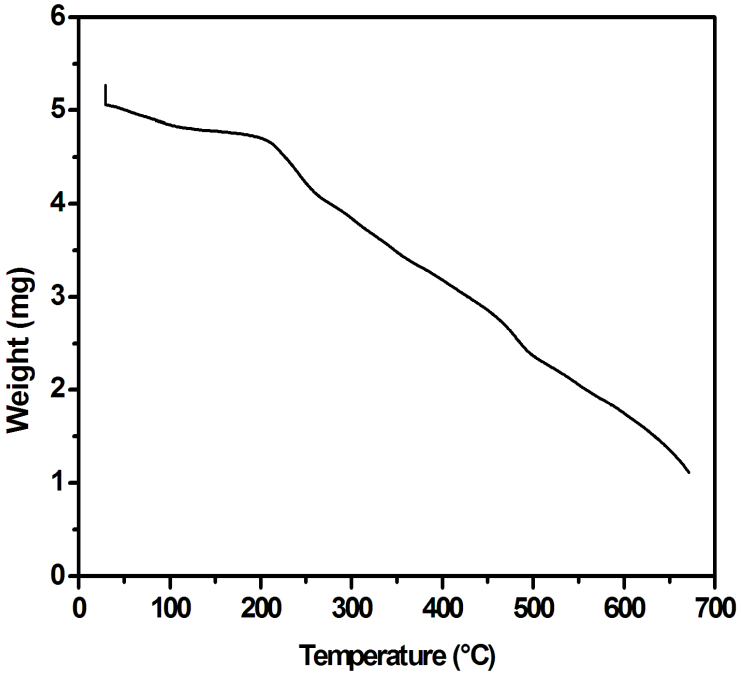

Appendix A14. *TGA curve for functionalized IF-ReS_2.*